de Vries, R., Jeyaraj, A.K., Salucci, F., Brown, A., Clarke, M.A., Ansell, P.J., Hoogreef, M., Zaghari, B., Liscouët-Hanke, S., Love, R.D., Ilak, M.,and Cinar, G. (2026). Conceptual Design of Electrified Aircraft: A Practical Guide for Engineering Students and Practitioners. In AIAA AVIATION 2026 Forum (p. 4690).

Conceptual Design of Electrified Aircraft: A Practical Guide for Engineering Students and Practitioners

Reynard de Vries *1, Andrew K. Jeyaraj †2, Francesco Salucci‡3, Arthur Brown§4, Matthew A. Clarke¶5, Phillip J. Ansell‖5, Maurice F.M. Hoogreef **6, Bahareh Zaghari††7, Susan Liscouët-Hanke ‡‡8, Robert Love§§9, Milos Ilak ¶¶10, and Gokcin Cinar ***11

[1] *Elysian Aircraft, Hoofddorp, 2132MS, The Netherlands*
[2] *MDA Space, Montreal, Quebec, H9X 3R2, Canada*
[3] *Argonne National Laboratory, Lemont, IL, 60439, USA*
[4] *Massachusetts Institute of Technology, Cambridge, MA, 02139, USA*
[5] *University of Illinois, Urbana-Champaign, Urbana, IL, 61820, USA*
[6] *Delft University of Technology, Delft, 2629HS, The Netherlands*
[7] *University of Southampton, Southampton, SO171BJ, UK*
[8] *Concordia University, Montreal, Quebec, H3G 1M8, Canada*
[9] *AirMorph LLC, Ramona, CA, 92065, USA*
[10] *RTX Technology Research Center, East Hartford, CT, 06118, USA*
[11] *University of Michigan, Ann Arbor, MI, 48109, USA*

Aircraft conceptual design traditionally relies on well-established handbooks and empirical methods developed for conventional fuel-based propulsion systems. However, the growing emphasis on sustainable aviation and the rapid development of hybrid-electric and fully-electric aircraft have introduced new challenges to this early stage of design. Existing literature and educational resources often lack accessible, structured guidance for beginners seeking to apply appropriate methods to electrified aircraft design. This paper presents a practical guide for the conceptual design and sizing of electrified aircraft, aimed at students and new practitioners. The work consolidates a range of low-fidelity methods from established handbooks and academic research, and includes references to higher-fidelity methods and industrial best practices. The paper includes an example of the sizing calculations for a hybrid-electric commuter aircraft, illustrating how to estimate parameters such as maximum take-off mass, wing area and installed power based on top-level aircraft requirements.

I. Introduction

Aircraft design is a complex and multidisciplinary endeavour comprising multiple design stages of increasing detail. Conceptual design is the first stage of aircraft design, where the configuration of the aircraft and its performance are established based on top-level requirements. The conceptual stage features significant design freedom but is beset by lower fidelity in the analyses that are performed and the assumptions that are made. However, over the last 50 years, a large body of knowledge on design methods and best practices, in addition to empirical data on aerodynamics, weight correlations and other useful design tools, has come to the disposal of the modern aircraft designer. Handbooks such as those by Roskam [1], Raymer [2], Torenbeek [3, 4], Nicolai [5], and Gudmundsson [6] provide most of the necessary information required for the conceptual design of different types of aircraft. Therefore, from the perspective of both a

*Chief Engineer, AIAA Senior Member.
†Systems Engineer, Fault Detection, Isolation and Recovery, AIAA Member.
‡Aerospace Research Engineer, Vehicle and Mobility Systems, TAPS, AIAA Member.
§Postdoctoral Associate, Department of Aeronautics and Astronautics, AIAA Professional Member.
¶Assistant Professor, Department of Aerospace Engineering, University of Illinois, Urbana-Champaign, AIAA Professional Member.
‖Associate Professor, Department of Aerospace Engineering, University of Illinois, Urbana-Champaign, AIAA Associate Fellow.
**Assistant Professor, Flight Performance and Propulsion, Faculty of Aerospace Engineering, AIAA Senior Member.
††Assistant Professor, Faculty of Engineering and Physical Sciences, AIAA member.
‡‡Associate Professor, Department of Mechanical, Industrial and Aerospace Engineering, AIAA Member
§§Chief Technical Officer, AIAA Senior Member
¶¶Senior Manager, Research, RTX Technology Research Center, AIAA Senior Member
***Assistant Professor, Department of Aerospace Engineering, University of Michigan, AIAA Senior Member

new practitioner of aircraft design and an engineering student taking an aircraft design course, the existing body of literature proves to be sufficient for most purposes.

The drive towards more sustainable aviation has intensified efforts to electrify aircraft propulsion systems. Electrified aircraft* are now an active area of development in both academia and industry, for both civil and military applications. Electrified aircraft design introduces additional complexity in managing overall aircraft weight, battery sizing, integrating powertrain systems, and managing thermal considerations. The electrification of the propulsion system also opens the design space to a wide range of powertrain architectures and propulsor arrangements that are not practical with conventional fuel-based systems, introducing additional parameters and design choices. Furthermore, other considerations, such as safety, become increasingly apparent and influence decisions in conceptual design to further reduce certification risks later in the aircraft development process. Hence, from the perspective of a student or a new practitioner, designing hybrid/electric aircraft can often be confusing. It can also be challenging to navigate the literature to find methods that are applicable to the configuration they are interested in. While there are *hundreds* (if not thousands) of papers describing hybrid/electric aircraft concepts, models, and methods at different levels of fidelity (see e.g. [7]), it can be challenging to find the right approach to start designing such aircraft from scratch.

This paper presents a selection of practical approaches in line with the expectations and level of expertise of a student or an engineering practitioner starting out in electric aircraft design. The main objective of the paper is not to tell the reader what a good hybrid/electric aircraft design is, nor to explain what the main trade-offs are, but to provide the reader with tools that can be used to size the hybrid/electric aircraft for a given set of inputs. The reader is assumed to have a background in aerospace engineering (e.g. basic principles of flight are not covered here) and some basic familiarity with the conceptual design of conventional aircraft. The paper covers methods found in handbooks and in academic papers, as well as best practices from industry. Where possible, references are provided for more detailed models and analyses in case the designer wants to improve the level of fidelity or understanding beyond what is presented explicitly in this paper. At the end, each step of the sizing process is demonstrated using a design example. However, describing the conceptual design of electrified aircraft comprehensively would require writing a book akin to the handbooks mentioned above, and thus, this white paper attempts to limit the level of detail to the bare minimum required to obtain a first estimate of basic top-level aircraft parameters such as maximum take-off mass, wing area, and installed power. It should also be noted that only a very limited number of manned hybrid/electric aircraft have been flown so far, let alone been certified. Therefore, the content of this paper represents a best effort by the authors based on publicly available data and their experience in the research and development of hybrid/electric aircraft and their subsystems, but there is an inherent uncertainty in the methods, which can only be quantified as more hybrid/electric aircraft enter service and data becomes available.

A. Scope

To restrict the length and complexity of this paper, its scope is limited to subsonic "conventional take-off and landing" (CTOL) tube-and-wing aircraft, with a focus on (passenger) transport aircraft. Other configurations, such as blended wing bodies, non-transport military aircraft, vertical take-off and landing aircraft, and supersonic aircraft, are not considered within the scope of this work. In terms of powertrain or propulsion-system architectures, this paper is applicable to conventional (i.e. only fuel), serial hybrid, parallel hybrid, turboelectric, and fully-electric configurations. This includes aircraft with single and multiple propulsors, including "distributed propulsion" configurations. More advanced architectures with two or more sets of propulsors—for example, partial turboelectric powertrains or "series/parallel partial hybrids" with one set of propellers on the wing and another on the tail—are not addressed here, though references are provided. Hydrogen-based propulsion systems, including fuel cell systems, are also excluded, but may be included in future work.

Within the realm of "typical" tube-and-wing aircraft, multiple categories exist. When performing the conceptual design of an aircraft, the designer often will encounter different classifications in different sources. Even within this paper, which takes data from earlier sources, different tables may list different aircraft categories. It is up to the designer to select the category that is most appropriate in each case. To provide some guidance in this matter, Table 1 provides an overview of the categories of aircraft that are within the scope of this document, along with their typical characteristics. Note that "General aviation" is often encountered as a category for reference data or models and is therefore adopted here, but this actually defines how the aircraft is operated (i.e. no scheduled commercial transport or military use),

*In this paper, "electrified aircraft" refers to any aircraft where electricity is used in the storage or transmission of energy used for *propulsion*. This includes fully-electric and hybrid-electric aircraft, and the term is used interchangeably with "hybrid/electric aircraft" throughout the paper. This does *not* include "more electric aircraft" (MEA) which only use fuel as energy source and only use electricity for non-propulsive systems.

and not what its physical characteristics are. Also note that all aircraft certified under FAA Part 23/EASA CS-23 are defined as "normal category" since 2017, without formally distinguishing the commuter class anymore. In the absence of data specifically for the commuter class, either general aviation or regional turboprop data can be the most suitable, depending on the case.

Table 1 Categories of aircraft that are in the scope of this paper, including their most common characteristics.

Aircraft category	Cert. basis	MTOM [lb]	Prop. system	N^o engines	Landing gear	N^o aisles
Commercial jet[1]	Part/CS-25	>19000	Turbofan	≥2	Retractable	≥1
Regional turboprop[2]	Part/CS-25	>19000	Turboprop	≥2	Retr. or fixed	1
Business jet	Part/CS-23 or 25	<19000 or >19000	Turbofan	≥1	Retr. or fixed	1
Commuter aircraft	Part/CS-23	>12500 and <19000	Turboprop	2	Retr. or fixed	1
General aviation[3]	Part/CS-23	<12500	Piston	1 or 2	Retr. or fixed	1 or none
Small general av.[4]	Part/CS-23	<12500	Piston	1	Retr. or fixed	none
Military transport	Military	>12500 (typically)	Turboprop or fan	≥2	Retr. or fixed	N/A

[1] Sometimes also called civil jet, high-subsonic jet, or transport jet.
[2] Sometimes also called large turboprop or twin turboprop.
[3] Here we include twin engine pistons, small twin engines.
[4] Here we include small single engines and agricultural aircraft.

II. Overview of the Conceptual Aircraft Design Process

The aircraft design process consists of three main design phases: conceptual design, preliminary design and detail design. The first stage, conceptual design, typically includes an analysis of the business case and market needs, establishing top-level aircraft requirements (TLARs), evaluating different aircraft concepts, and translating aircraft parameters such as maximum take-off mass (MTOM) and fuel consumption into operating costs or emissions. The process of creating an aircraft concept and calculating its main "physical" properties (wing area, MTOM, etc.) based on top-level requirements is known as *aircraft sizing*. This paper describes the sizing process followed to evaluate a given aircraft configuration; in practice, the designer would typically evaluate different candidates, perform trade studies, and select the winning concept not only based on physical properties, but also based on metrics like operating costs, noise, or emissions. The typical steps followed in an aircraft sizing process are shown in Fig. 1. Note that this is just one of many possible approaches. The process is identical for electrified aircraft as for conventional aircraft. The main differences lie within the analysis methods in individual disciplines such as weights, aerodynamics and propulsion, and in dealing with new design choices such as the type of powertrain architecture or the so-called degree of hybridization.

The design process begins with the elicitation of requirements [1, p. 3], [6, p. 4], [3, p. 5]. These can be in the form of a request for proposals [1, p. 3], a mission specification issued by the potential customer or agency that will operate the aircraft [1] or by the identification of needs by an aircraft manufacturer and the continuous interaction between the manufacturer and potential customer [2, p. 3]. The activities in conceptual design help determine if the requirements can be met with a feasible aircraft design [5, p. 24]. As a result, it is also expected that requirements will be challenged and negotiated based on the trade studies performed in conceptual design.

The assessment of requirements is followed by the definition of one or more aircraft configurations to be evaluated. This includes qualitative or discrete design choices such as high or low wing, number of propulsors, type of propulsors, etc. Once that is done, the calculations start. First, an aerodynamic model is created. This is used to size the powertrain and the wing in "matching diagrams", as well as in the energy estimation. Once the energy required for the mission is known, the designer proceeds to estimate the mass of the different components of the aircraft. This can be done in different levels of detail; in Fig. 1, we show both a "Class I" and a "Class II" loop (see Sec. VI). In practice, the designer may opt to perform only the Class I loop or only the Class II loop. Since many component mass estimation methods, as well as the energy estimation step, require an initial guess of the MTOM of the aircraft, an iterative calculation is performed until the mass of the aircraft converges. Aside from the wing, in this paper, we do not address the geometrical sizing of other components, such as the tail (which requires a CG analysis) or fuselage, in detail, and therefore, a simplified drag polar is used, and no outer convergence loop on aerodynamics is required in this case.

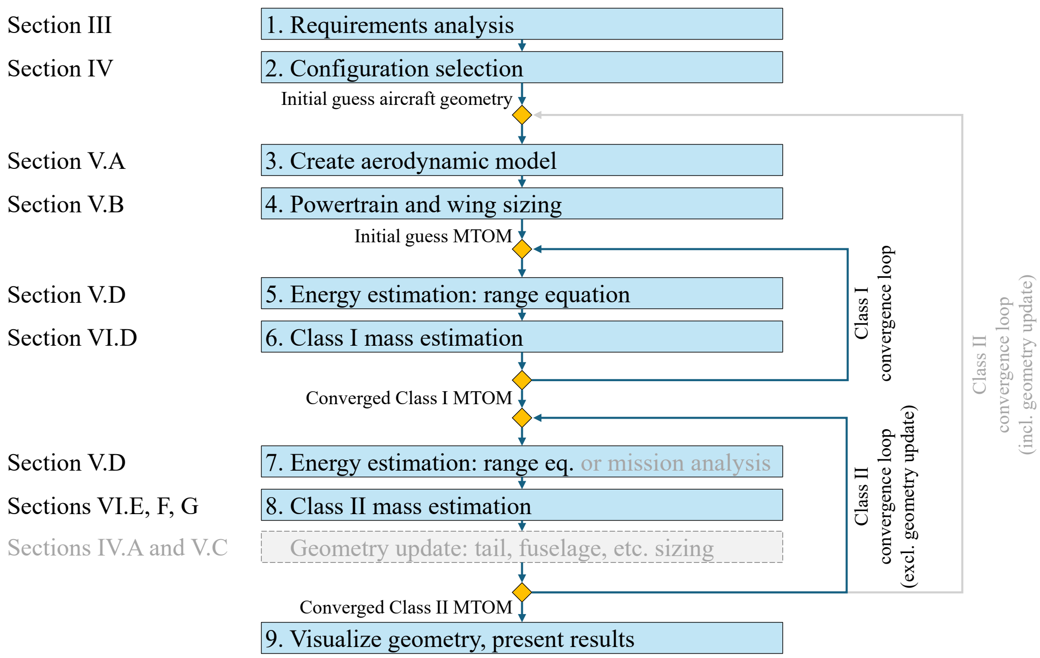

Fig. 1 Main steps of a typical initial aircraft sizing process, including the sections of this paper in which they are covered. The steps shown in grey are not covered in detail in this paper.

III. Analysis of Top-Level Aircraft Requirements

Requirements can be classified into several types based on their source. Some requirements that are derived from market analysis, from aviation infrastructure needs such as the aerodrome reference code [8, p. 38], or from noise emission standards [9, p. 57][9, p. 51].Other requirements stem from a safety and certification perspective. In the case of civil aircraft, these are prescribed by airworthiness authorities such as the Federal Aviation Administration (FAA) or the European Union Aviation Safety Agency (EASA). For example, for most passenger and cargo aircraft, certification requirements are defined in 14 CFR Part 23 [10] or Part 25 [11] based on the aircraft type, weight and the number of passengers, in the case of the FAA. The European counterpart to these rules is EASA's CS-23 and CS-25 certification specifications. Part 23 regulations are applicable to aircraft that carry up to 19 passengers or which have an MTOM of up to 19000 lbs [12]. Commercial fixed-wing aircraft designed to carry more than 19 passengers or which have an MTOM greater than 19000 lbs are typically certified under Part 25 regulations. The designer must analyze the requirements to determine if they are sound, challenge them if necessary (see Nicolai [5], Sec. 1.3.6 for further reading), and ensure that all key requirements that can be handled in conceptual design are incorporated into the aircraft configuration selection and sizing process.

For the design of electrified aircraft, in particular in the CS-25/Part 25 category, one additional complication is that the regulations and means of compliance are still under development. Therefore, it is not always clear beforehand what safety requirements need to be imposed for the design of the hybrid/electric powertrain. For additional information, the reader can check documents such as EASA's Special Condition E-19 [13] or Ref. [14] on loss of power control. Alternatively, the reader can investigate the standards that are being developed in organizations such as ASTM, EUROCAE, or SAE (see e.g. Refs. [15–18]). However, these new regulations are not very prescriptive, and the standards typically focus on subsystems/sub-components, and therefore the main requirements for conceptual design of the aircraft as a whole still stem from the "traditional" certification specifications mentioned in the previous paragraph.

In the context of a university-level aircraft design project, the requirements are usually specified or have to be derived from a problem statement or statement of need for an aircraft. In some cases, a Request for Proposal (RFP) may also be issued, providing information about specific requirements or a target market for the aircraft. In either case, the student is encouraged to investigate the target market and ascertain the typical routes, the aircraft servicing these routes and identify the long-term potential of an aircraft designed to meet the requirements in the RFP.

The student is also encouraged to investigate potential technology choices that may enable the designed aircraft to meet and exceed requirements while avoiding the pitfall of incorporating a particular technology choice solely for the sake of novelty [3, p. 11]. Typical “top-level aircraft requirements” (TLAR) that can be defined in a design process include:

- **Performance requirements**, either specified by the customer and business needs (payload mass, payload volume, range, cruise speed, take-off distance, etc.) or derived from the applicable safety regulations (climb rate with one engine inoperative (OEI), minimum loiter time, etc.). These requirements typically affect the required wing size, tail size, installed power, and fuel and battery mass.
- **Operational requirements**, such as gate span compatibility, cargo bay accessibility, number and position of exits, turnaround time, maintenance requirements, passenger comfort, etc. Again, these can be specified by the customer and the choice of airports at which the aircraft should operate, or by safety regulations. These requirements typically affect the fuselage size and layout, and the choice of the overall aircraft configuration.
- **Economic requirements**, such as operating costs per available seat-kilometer (CASK) or seat-mile, production costs, maintenance costs, etc. Practically all characteristics of the aircraft, including its maximum take-off mass (MTOM), energy consumption, part count, type of propulsion system, and so on, affect the total operating costs of the aircraft, which is one of the main drivers for the customer to choose one aircraft over another.
- **Environmental requirements**, such as in-flight CO_2 emissions, local NO_x emissions at the airport, or life cycle emissions, as well as community/external noise requirements. The requirements can in turn again affect the operating costs and business case of the aircraft through emission- or noise-based charges or community acceptance.

The process of defining and assessing requirements is the same for hybrid & electric aircraft as for conventional aircraft, though additional requirements may appear, such as maximum battery charging time (affecting turnaround time) or minimum battery cycle life (affecting operating costs). In some cases, the requirements are the same as for a conventional aircraft, but the impact on the hybrid-electric aircraft is very different. For example, an electric aircraft with distributed propulsion may easily meet OEI climb performance requirements due to its high number of engines and the absence of a power lapse with altitude, but may struggle to meet range requirements if powered only by batteries. Furthermore, while electrified propulsion can unlock significant performance benefits, the choice of whether or not to use an electrified powertrain in the first place is often determined by economic and environmental requirements, and not necessarily by the performance requirements themselves. Therefore, while this paper focuses on the physical design of the aircraft, in order to make a good trade-off between different aircraft concepts with different technologies, the designer must take the assessment one step further than what is presented in this paper and include preliminary economic and environmental assessments.

IV. Configuration Selection

The very first step after defining the requirements is to make a list of existing *reference aircraft* which could potentially meet the requirements. These aircraft will serve as benchmarks during the design process, both to calibrate or verify numbers and as potential competitors that the new aircraft must present an advantage over. Then, before making any calculations or estimations of the performance, mass, or dimensions of the new aircraft, it is important to decide how the aircraft will fulfill its functional requirements. Since this paper focuses on transport aircraft, the requirement is typically to transport a certain payload (passengers and/or cargo) over a certain distance at a certain speed. This means that a decision needs to be made on what the aircraft will look like in order to house the payload safely and meet the other performance requirements. This section describes some of the configurational choices that can be made and how they affect performance. As is the case with many aspects in aircraft design, this is a trade-off process, and the entire design synthesis (iterative) process must be repeated for every design solution (configuration) being compared.

While there is no clear-cut distinction between what is considered a “configuration choice” and what is considered a design parameter of the aircraft, the former typically refers to discrete choices affecting the overall topology of the aircraft (for example, a T-tail vs. a V-tail), while the latter refers to continuous variables (for example, the wing aspect ratio). In the following paragraphs, we briefly describe the main configuration choices of a tube-and-wing aircraft, where the use of electrified propulsion adds new degrees of freedom in terms of propulsion system architecture and placement. Tables 2 and 3 give an overview of some of these choices. Before making any calculations, the designer should choose one of the options and make a rough first-hand sketch of the aircraft, including the position of the main components of the propulsion system. After sizing is performed, the sketch of the aircraft is updated with dimensions until a full 3D CAD model of the aircraft is created.

A. Fuselage

For passenger transport aircraft, a cabin (pressurized or unpressurized) must be provided for a comfortable and safe environment. Such cabins are traditionally integrated in (near-) cylindrical fuselages if pressurization is required—typically when the cruise altitude exceeds 8000 ft, so that the crew and passengers can breathe without the need for supplemental oxygen. In addition to the cross-section shape, the designer must determine the general layout and dimensions of the fuselage (usually in terms of desired slenderness ratio, between length and diameter—a trade-off between aerodynamics and structures). The layout determination is a detailed design exercise in itself, and is primarily driven by the volume of cargo, location of the cargo holds, the number of seats, number of seats abreast, the seat pitch, the length of the flight deck, and additional space required for doors/hatches, galleys, and other systems. For electrified aircraft, the same process can be followed as for conventional aircraft, though additional volume needs to be allocated to powertrain components such as batteries or turbogenerators, if they are placed inside the fuselage. In both cases, special attention must be paid to safety requirements (e.g. ensuring passenger safety during a crash landing) and the impact of batteries on the center of gravity of the aircraft.

Table 2 Examples of configuration choices for tube-and-wing aircraft with electrified propulsion.

Fuselage	Wing	Tail
Cross-section	Vertical position	Lifting surface type
Circular	High wing	Wing + tail
Double-bubble	Low wing	Canard
Square	Mid wing	Three-surface
Cabin/cargo hold layout	Wing planform	Tail type
N^o seats abreast	Rectangular	Low/conventional tail
N^o aisles	Trapezoidal	T-tail
Pressurization	Double trapz. (kink)	Cruciform
Pressurized	Other	V-tail
Unpressurized	Box wing	H-tail
etc.	Biplane	etc.
	Tandem wing	
	etc.	

Table 3 Examples of configuration choices for tube-and-wing aircraft with electrified propulsion (continued).

Landing gear	Powertrain architecture	Propulsor arrangement
Type/arrangement	Conventional (fuel based)	Type of propulsor
Tricycle	Piston engine	Propeller
Taildragger	Turbine engine	Fan
Bicycle & outrigger	Fully battery-electric	Placement
Skid/ski	Hybrid	Wing-mounted tractor
Main gear position	Series	Wing-mounted pusher
Fuselage-mounted	Parallel	Fuselage tractor
Wing-mounted	Turboelectric	Fuselage pusher (BLI*)
Nacelle-mounted	etc.	Over-the-wing
etc.		Tip-mounted
		Tail-mounted
		etc.

*BLI = boundary layer ingestion.

B. Wing

The main wing is the lifting surface of the aircraft and is essential to get the aircraft airborne (though lifting bodies also exist [19]). An important configurational choice is the vertical position of the wing (e.g. high, mid or low) with respect to the fuselage. This is typically driven by many different aspects: aerodynamic interactions between wing and fuselage, or wing and horizontal tail, as well as structural design and crashworthiness. Also, the accessibility to the fuselage is important in combination with the landing gear positioning and engine type and integration. For example, a low wing with large (propeller) engines may require a tall landing gear to prevent the propellers from striking the ground, meaning that an external staircase might be needed to access the aircraft. Depending on the type of operation envisioned for the aircraft, this may not be desirable. Moreover, both the wing vertical position and planform shape affect the aerodynamic performance, structural mass, and (lateral) stability of the aircraft. For electrified aircraft, the design process of the wing is the same as for conventional aircraft, although the optimum choice may be different. For example, a low-wing configuration is typically more compatible with an electric aircraft with many small, electrically-driven propellers than with two large propellers. If batteries are placed in the wing, it is important to verify that there is sufficient volume for the batteries, and to account for the (generally positive) effects of the batteries on wing structural mass due to relief of the bending moment [20, 21].

C. Landing Gear

The positioning of the landing gear is one of the most important elements that is often overlooked in early conceptual design. Important factors include the landing gear arrangement, the position and excursion of the center of gravity, ground clearance constraints (e.g. tip-back angle during take-off and maximum bank angle during landing), the type of runway, etc. For more information on landing gear choices and sizing, the reader is referred to traditional aircraft design handbooks and Ref. [22]. The use of electrified propulsion has no direct influence on the landing gear unless an electric taxi system is integrated, other than its impact on the aircraft center of gravity, engine position, and so on. Note that the maximum landing mass often influences landing gear mass, and in the case of fully-electric aircraft, it is equal to the maximum take-off mass.

D. Tail

The tail is required for the balance, stability and controllability of the aircraft. Typically, this includes a vertical and horizontal tail, both equipped with control surfaces (rudders and elevators, respectively), but also more unconventional designs, such as V-tails or canard configurations, are possible. Conventional configurations include the low tail (where the horizontal is mounted below the vertical on the fuselage), a cruciform tail (with the horizontal surface somewhere along the vertical surface) and a T-tail where the horizontal surface is on top of the vertical surface. The vertical position of the horizontal tail is often selected such that it is outside the wing wake at high angles of attack, to avoid deep stall. It is also important in relation to the vertical tail as the wake from the horizontal tail may blanket part of the rudder. For electrified aircraft, the use of an electrified powertrain in itself does not have a major impact on the tail, but the propulsor placement does. For example, in distributed electric propulsion (DEP) arrangements with many propellers on the wing, the effect of engine failure may be more or less severe for the vertical tail than for conventional aircraft, depending on the number and position of propellers. Moreover, the characteristics of the propeller slipstreams (location, strength, and direction) change and their impingement on the tail should be avoided, or at least be accounted for in the design process.

E. Propulsion System: Powertrain Architecture

In conventional tube-and-wing transport aircraft, defining the propulsion system boils down to two choices—the number of engines, and the type of engine: piston engine, turboprop, or turbofan. In that case, we implicitly choose the type of thermal engine (piston or turbine), the propulsor (propeller or fan), and the energy source (fuel) simultaneously. However, in the case of electrified propulsion systems, we need to make a distinction between the type and number of propulsors, the type and number of energy sources, the type and number of electric machines and/or thermal engines in the powertrain[†], and how these are all connected. A wide range of architectures can be considered (see e.g. Refs. [7, 23]) and—since it is a relatively new field—the literature uses varying terminologies and classifications.

Table 4 collects the main characteristics of the most common (hybrid) electric powertrain architectures. In addition to the tabulated potential benefits, the use of electrified propulsion systems can present other benefits such as reduced

[†]In this paper, the powertrain constitutes all components of the propulsion system, including energy sources (fuel/batteries), power distribution (e.g. busbars, cables), thermal engines, electric motors & generators, gearboxes, and the propulsors.

noise, lower maintenance costs, emission-free taxiing, increased redundancy, etc. Other important considerations that can drive the choice of the powertrain architecture are the location (and volume required) of the energy carrier, the positioning and integration of the propulsors, safety considerations, and supply chain maturity. For some configurations, the routing of cables through the aircraft becomes an important challenge to solve early in the design process.

Table 4 Simplified comparison of powertrain architectures.

Powertrain architecture	Energy carrier	Typically suitable for: ↑ aero-prop.	↑ thermal engine	↑ electrical energy	Maximum range
Conventional	Fuel				long
Fully electric	Battery	✓		✓	short
Parallel	Fuel+batt.		✓		mid/long
Series	Fuel+batt.	✓		✓	mid
Turboelectric	Fuel	✓			mid/long

Legend:
"↑ aero-prop." = using distributed propulsion to enhance aero-propulsive performance of aircraft
"↑ thermal engine" = using electric motors to down-size or improve efficiency of thermal engine
"↑ electrical energy" = using electricity as primary source of energy, enabling fully-electric flights

F. Propulsion system: Propulsor arrangement

In addition to the powertrain architecture, the designer must specify where propulsors are installed and how they are integrated. Most of today's aircraft feature one propulsor installed on the fuselage nose, two on the fuselage, or two or four propulsors installed on the wing. However, since electrical power can be distributed across multiple motors without significant mass, efficiency, or cost penalties, electrified aircraft can feature a much higher number of propulsors ("distributed electric propulsion") or propulsors placed at unconventional locations. Examples include tip-mounted propellers, over-the-wing propellers, or arrays of distributed electric fans. These more unconventional propulsor arrangements can have positive (and negative) impacts on aerodynamic efficiency, propulsor efficiency, ground clearance, component availability in the supply chain, noise, safety (redundancy), or reduced moments in case of component failure. The exact benefits and drawbacks of each solution depend on how the propulsion system is integrated and need to be assessed during the aircraft design process. The impact of some propulsor arrangements on aerodynamic and propulsive efficiency is notionally given in Sec. V.A.3.

V. Sizing: Aircraft Performance

Once a configuration has been chosen, the designer starts with "sizing" calculations to obtain a first estimate of the wing size, installed power, and the energy required to fly the mission. This information will later be used to estimate the mass of the aircraft. For these calculations, we need a simplified aerodynamic model of the aircraft. The following subsections describe A) the aerodynamic model, B) ways to estimate wing size and installed power based on top-level requirements using the aerodynamic model, C) how to estimate the tail size based on the wing size, and D) ways to estimate the energy required for the mission.

A. Aerodynamics

Aerodynamic parameters are crucial to both conceptual and detailed design activities. For initial sizing, modelling the aerodynamic performance of the aircraft basically boils down to two things: having a model that relates the drag (coefficient) of the aircraft to the lift (coefficient) of the aircraft, and having an estimate of the maximum lift coefficient in different flight conditions. For hybrid/electric aircraft, two additional contributions that are normally neglected for conventional aircraft may already need to be considered during the conceptual design phase: the changes in aerodynamic forces due to aero-propulsive interaction, and the drag of heat exchangers. This section describes different ways to obtain these numbers.

1. Drag estimation

Low Fidelity

A first estimate of the maximum lift-to-drag ratio of the aircraft can be obtained based on the wing aspect ratio and the so-called wetted-area-ratio, as shown in Appendix B. However, the most common way to establish a relationship between the lift coefficient C_L and the drag coefficient C_D is by means of a simple two-term drag polar. This is, in essence, a (symmetric) quadratic equation given by:

$$C_D = C_{D_0} + \frac{C_L^2}{\pi A e}, \tag{1}$$

where:

- C_D is the drag coefficient,
- C_{D_0} is the zero-lift drag coefficient,
- C_L is the lift coefficient,
- A is the aspect ratio, and
- e is the Oswald efficiency factor

The first and second terms of Eq. 1 represent the *profile* drag and *induced* drag of the aircraft, respectively. While the lift coefficient is determined by the flight condition ("lift equals weight") and the aspect ratio is a design choice, the zero-lift drag coefficient and Oswald factor need to be assumed at the start of the design process. For this, it is important to make a distinction between their "clean" values and their total values, which account for additional effects such as flap deflection or landing-gear deployment:

$$C_{D_0} = C_{D_0,\text{clean}} + \Delta C_{D_0,\text{flaps}} + \Delta C_{D_0,\text{LG}}, \tag{2}$$

$$e = e_{\text{clean}} + \Delta e_{\text{flaps}}. \tag{3}$$

Note that the landing gear generally has a negligible effect on the Oswald factor. Typical values of $C_{D_0,\text{clean}}$ and e_{clean} are shown in Table 5. Additional data on the Oswald factor of various transport-category aircraft can be found in Obert [24], Ch. 40, as a function of aspect ratio. To estimate the drag polars in low-speed conditions, when flaps and/or the landing gear are deployed, some initial values for $\Delta C_{D_0,\text{flaps}}$, $\Delta C_{D_0,\text{LG}}$, and Δe_{flaps} can be found in Roskam [1], Part I, Table 3.6. In cruise conditions, these terms can be set to zero.

Aircraft type	$C_{D_0,\text{clean}}$	e_{clean}
High-subsonic jet aircraft	0.014 - 0.020	0.75 - 0.85
Large turbopropeller aircraft	0.018 - 0.024	0.80 - 0.85
Twin-engine piston aircraft	0.022 - 0.028	0.75 - 0.80
Small single-engine aircraft		
- Retractable gear	0.020 - 0.030	0.75 - 0.80
- Fixed gear	0.025 - 0.040	0.65 - 0.75
Agricultural aircraft:		
- Spray system removed	0.060	0.65 - 0.75
- Spray system installed	0.070 - 0.080	0.65 - 0.75

Table 5 Range of C_{D_0} and Oswald factor for different aircraft types in clean configuration, from Torenbeek [3], pg. 149.

At the start of the design process, the designer should assume a value for C_{D0} and e based on Table 5. Then, as soon as the initial geometry of the aircraft is known (e.g. airfoil thickness-to-chord ratio, sweep angles, wing area, fuselage area, tail area, etc.), a more detailed component drag buildup can be used to estimate the zero-lift drag coefficient. For this, the drag buildup of Raymer [2], Sec. 12.5.2 is recommended. These methods can be used for induced drag and first estimates of zero-lift drag if a friction drag model is included. Another vortex-based method is the vortex particle method (VPM), though this typically requires a more complex discretization and can also be considered a high-fidelity method.

High Fidelity
For more accurate estimates, computational fluid dynamics (CFD) is often used. These methods can be used in three ways: incorporated directly in the aircraft sizing loop, using the results to create a surrogate model or look-up table which provides lift and drag as a function of other parameters, or to fit or calibrate the C_{D0} and e terms of the parabolic polar presented above. Aerodynamic models can also be based on experimental data from wind-tunnel tests or flight tests.

2. Maximum lift coefficient
Low Fidelity
The maximum lift coefficient $C_{L,\max}$ is a key parameter of the aircraft since it is used to determine the wing area, among other things. Typically, a distinction is made between the $C_{L,\max}$ value in clean configuration (i.e. with high-lift devices retracted), in take-off condition (e.g. flaps deflected 15 degrees), and in landing condition (e.g. flaps deflected 30 degrees). Roskam [1] presents typical values for different aircraft categories, an extract of which is shown in Table 6. The designer must assume a value in this range, taking into consideration what kind of high-lift devices are used, and validate the assumption at a later stage using higher-fidelity analyses.

Aircraft Type	$C_{L,\mathbf{max,clean}}$	$C_{L,\mathbf{max,TO}}$	$C_{L,\mathbf{max,L}}$
Small single engine props	1.3 – 1.9	1.3 – 1.9	1.6 – 2.3
Small twin engine props	1.2 – 1.8	1.4 – 2.0	1.6 – 2.5
Regional turboprops	1.5 – 1.9	1.7 – 2.1	1.9 – 3.3
Transport jets	1.2 – 1.8	1.6 – 2.2	1.8 – 2.8
Military transports	1.2 – 1.8	1.6 – 2.2	1.8 – 3.4

Table 6 Typical values for maximum lift coefficient in clean, take-off (TO), and landing (L) configurations. Values extracted from Roskam [1], Part I, Table 3.1.

Alternatively, if the 2D maximum lift coefficient of the wing airfoil ($c_{l,\max}$) is known based on empirical data or lower-order analyses, a simple estimation of the three-dimensional maximum lift coefficient is as follows (Raymer [2], pg. 419):

$$C_{L_{\max}} = 0.9 \cdot C_{l_{\max}} \cdot \cos\left(\Lambda_{0.25c}\right) \tag{4}$$

where $\Lambda_{0.25c}$ is the quarter-chord sweep angle. This equation is valid for clean wings with a high aspect ratio and a large airfoil leading edge radius. If this equation is used to calculate the clean $C_{L_{\max}}$, the increase in $C_{L_{\max}}$ due to high-lift devices (denoted as $\Delta C_{L_{\max}}$) can be estimated using a model from Raymer [2], pg. 430:

$$\Delta C_{L_{\max}} = 0.9 \cdot \Delta C_{l_{\max}} \cdot \left(\frac{S_{\text{flapped}}}{S_{\text{ref}}}\right) \cos\left(\Lambda_{\text{HL}}\right) \tag{5}$$

where $\Delta C_{l_{\max}}$ is the increase in the 2D maximum lift coefficient of the wing airfoil from high-lift devices (obtained from experimental data or from Table 12.2 of Ref. [2]), $\frac{S_{\text{flapped}}}{S_{\text{ref}}}$ is the ratio of the wing area with a high-lift device to that of the reference wing (defined in Fig. 12.21 of Ref. [2]) and Λ_{HL} is the sweep angle of the high-lift device's hinge line.

Medium-to-High Fidelity
Estimation of the maximum lift coefficient is challenging with low- and medium-fidelity methods since its value is highly sensitive to the geometry and operating conditions of the system. Therefore, an estimation of $C_{L,\max}$ typically requires higher-fidelity analyses such as CFD or wind-tunnel experiments. Even in those cases, results can present significant uncertainty depending on the numerical method used or the physical scale of the wind-tunnel experiment. Once such information becomes available, the designer can update the assumption of $C_{L,\max}$ in the various flight conditions.

3. Aero-propulsive interaction
The discussion thus far has ignored the contribution of both compressibility effects and aero-propulsive interaction effects. The scope of this paper is limited to subsonic aircraft, and therefore, we can neglect the compressibility effects

for now. However, the use of electrified propulsion systems enables new propulsor layouts that can enhance the aircraft's aerodynamic or propulsive performance. Therefore, it may be necessary to estimate the aeropropulsive interaction effects, i.e., the changes in lift and drag due to the presence of propellers or fans. These effects can be incorporated in the sizing process by adding additional terms to the lift and drag (Eq. 1) breakdown:

$$C_L = C_{L,\text{airframe}} + \Delta C_L, \tag{6}$$

$$C_D = C_{D_0} + \frac{C_L^2}{\pi A e} + \Delta C_D, \tag{7}$$

where $C_{L,\text{airframe}}$ is the lift of the aircraft at zero thrust, and ΔC_L and ΔC_D are the changes in lift and drag due to aero-propulsive interaction at non-zero thrust, respectively. These "delta terms" are highly dependent on the operating condition (thrust, rotational speed, lift, etc.) and geometry of the propeller or fan installation (position, size, inclination, etc.). Since lift now depends on thrust, the equations of motion of the aircraft ("lift equals weight" and "thrust equals drag") become coupled and need to be solved iteratively. For more information, see Ref. [23]. Note that this "delta term" approach is just one way of approaching the aero-propulsive interaction effects. For more detailed analyses, a more comprehensive force bookkeeping method is required.

Low Fidelity

Since ΔC_L and ΔC_D are so dependent on the operating condition and geometry of the system, there are no methods to estimate these terms which are both simple and generic. The same applies to the change in propulsor efficiency due to the presence of the airframe, $\Delta\eta_\text{p}$. Fig. 2 shows typical values for the changes in lift, drag, and propeller efficiency due to aero-propulsive interaction for several (unducted) propeller arrangements, based on literature and author experience. The designer can assume a range of values based on this figure, or conclude that the effect is negligible for the propeller arrangement they are considering. For more accurate values or different propulsor arrangements, the designer should find data or simplified correlations in literature for a geometry comparable to the one they want to assess—though such data is often scarce and geometry-specific. A semi-empirical method for leading-edge distributed propellers is given in Ref. [23].

	Cruise conditions			Take-off/climb conditions			
	ΔC_L	ΔC_D	$\Delta\eta_\text{p}$	ΔC_L	ΔC_D	$\Delta\eta_\text{p}$	**Notes**
Inboard wing tractor	0% ~ +10%	-10% ~ +10%	-5% ~ +5%	+20% ~ +100%	-10% ~ +10%	-5% ~ +5%	Assuming typical twin-turboprop configuration.
Tip-mounted tractor	0% ~ +5%	-10% ~ 0%	-5% ~ +5%	0% ~ +10%	-15% ~ -5%	-5% ~ +5%	Assuming low aspect-ratio wing (AR < 8). Benefits reduce with higher aspect ratios.
Tip-mounted pusher	~ 0%	-5% ~ 0%	0% ~ +10%	~ 0%	-10% ~ 0%	+5% ~ +15%	Assuming low aspect-ratio wing (AR < 8). Benefits reduce with higher aspect ratios.
Fuselage pusher (BLI)	~ 0%	~ 0%	+5% ~ +10%	~ 0%	~ 0%	+5% ~ +10%	$\Delta\eta_\text{p}$ for a well-designed BLI prop of radius comparable to BL thickness. In that case aircraft probably also needs other propellers for $T = D$
OTW, near trailing edge	0% ~ +10%	-10% ~ +5%	-10% ~ +5%	+5% ~ +15%	-10% ~ +5%	-10% ~ +5%	ΔC_L, ΔC_D values highly dependent on number/ extent of OTW propellers. Excludes drag of pylon & duct (if applicable) (!)
OTW, near mid-chord	0% ~ +5%	-15% ~ -40%	-30% ~ -5%	0% ~ +5%	-20% ~ -50%	-20% ~ -5%	ΔC_L, ΔC_D values highly dependent on number/ extent of OTW propellers. Excludes drag of pylon & duct (if applicable) (!)

Fig. 2 Typical ranges of changes in lift, drag, and propeller efficiency due to aero-propulsive interaction, as a percentage of uninstalled (i.e. bare airframe + separate isolated propeller) lift, drag and efficiency, respectively. "BLI" = boundary later ingestion; "OTW" = over-the-wing.

Note that there is no dedicated entry for distributed (electric) propulsion in Fig. 2. While the term "distributed propulsion" often refers to the use of an array of electrically-driven propellers installed on the wing (tractor configuration), in other interpretations it refers to the use of multiple propulsors installed anywhere on the airframe in such a way that it provides an aero-propulsive benefit. Therefore, the exact benefit or penalty of distributed propulsion again depends on the physical location at which the propulsors are installed.

Medium-to-High Fidelity
Getting a decent estimation for aero-propulsive effects requires moving to medium- (e.g. vortex methods) or high- (CFD, wind-tunnel) fidelity aerodynamic analyses. However, for this, the initial geometry of the aircraft needs to be known.

4. Heat exchanger drag
Low Fidelity
A dedicated thermal management system (TMS) is often required to cool electrical powertrain components such as batteries or electrical machines. In that case, the heat exchanger (and the associated ram air duct, if applicable) can lead to additional drag. Again, this drag contribution is highly dependent on the operating condition and geometry of the system. Reference [25] provides some values of drag per kW of heat rejected for different aircraft configurations with electrified propulsion, which can be used for initial estimates. Alternatively, for a commercial passenger transport aircraft with an actively-cooled electrified powertrain, one can assume a drag increase between 2 and 10 drag counts[‡] for the TMS. This is based on author experience and assumes a variable-area inlet and nozzle for the ram air duct to minimize (spillage) drag. Higher values may be obtained for aircraft with high heat loads (e.g. fuel-cell aircraft) or small aircraft with relatively large heat exchangers. Negative values are possible due to the Meredith effect; however, this is unlikely for fixed-wing aircraft with hybrid/electric powerplants operating at "typical" temperature levels.

Medium Fidelity
If the initial geometry of the heat exchanger and ram air duct is known, one can estimate the drag of the TMS using semi-empirical models and adding up the intake drag (e.g. Ref. [26]), the pressure recovery in the diffuser (e.g. Ref. [27], the pressure drop across the heat exchanger (e.g. Ref. [28]; accounting for heat exchanger inclination [29]), and the thrust produced by the nozzle (e.g. Ref. [30]).

High Fidelity
Getting an accurate estimation for heat exchanger and ram air duct drag again requires moving fairly soon to high-fidelity aerodynamic analyses (CFD, wind-tunnel). For this, the detailed geometry of the installation needs to be known.

5. Tips & Tricks

- Wing aspect ratio is one of the most important design parameters of the aircraft. When performing a clean-sheet design, always perform a trade study on the wing aspect ratio.
- Oswald factor is an empirical parameter that results from fitting a parabola to a drag polar. It is typically only accurate in a specific range of lift coefficients, and can be greater than 1. It should not be confused with the *span efficiency*, also often represented by the letter e, which accounts for the impact of a non-elliptical lift distribution along the wing on the induced drag and is always below 1. The Oswald factor is largely driven by the span efficiency but also accounts for additional effects such as the lift and drag produced by the fuselage.
- Drag values obtained from numerical methods (CFD, panel methods, etc.) generally do not include miscellaneous drag due to excrescences, leakages, etc., which can be noticeable and need to be added separately. Obert [24] (Chapter 40) provides some values for transport-category aircraft; other values can be found in the classic aircraft design handbooks.
- Aircraft with low passenger mass fractions, such as regional battery-electric or "heavy hybrid" aircraft, can present a low $S_{\text{wet}}/S_{\text{ref}}$ ratio as a result of a small fuselage relative to a large wing. This can lead to a significantly higher maximum lift-to-drag ratio than conventional aircraft [31].
- One of the key potential benefits of hybrid/electric (distributed) propulsion is that it opens the design space to new forms of propeller/fan integration, which enhance (or deteriorate!) the aerodynamic performance of the vehicle. Obtaining a good estimate of the benefits or drawbacks of an aircraft with distributed propulsion compared to a conventional aircraft, therefore, requires moving to a minimum level of aero-propulsive modelling fairly early in the design process.

[‡] A drag count is defined as drag coefficient multiplied by 10^4; i.e., an increase of 10 drag counts implies a drag coefficient increase of 0.001.

B. Powertrain and Wing Sizing

Sizing the powertrain involves the determination of the maximum installed power P or thrust T of the engine—defined here as the propulsor or thrust-generating system. Traditionally, this is done using constraint diagrams that define feasible design regions based on performance constraints such as stall speed, climb rate, take-off distance, etc. These diagrams, often referred to as *constraint diagrams*, *wing-loading diagrams*, *performance matching plots* or *Sizing Matrix Plots* (SMP), help identify acceptable combinations of wing area and engine power once aircraft weight is estimated. For hybrid-electric aircraft, sizing the powertrain is one of the most complex steps in the design process compared to conventional aircraft. There are several reasons for this. First, there are multiple components in the powertrain (batteries, gas turbines, motors, generators...) which can be responsible for a different share of the total power in different flight conditions, and can be connected in different ways. Second, power and energy storage become coupled, because the maximum power available from a battery depends on its state of charge. Third, different components respond differently to altitude and speed: thermal engines typically exhibit a power loss with altitude, while the maximum output of electric motors is practically independent of altitude. And fourth, in thrust-rated systems such as turbofans, empirical data such as weight correlations or efficiency values are thrust-based, while electrical components care about power, and not about thrust. This means that we have to translate thrust into power requirements and vice versa, which can be challenging, especially near zero speed.

As a result of these four characteristics of hybrid-electric powertrains, different components can be sized for different conditions, and SMPs must be developed for each component, ensuring that all meet the relevant performance requirements. The process includes identifying the applicable constraints, plotting them, defining the feasible design region, and selecting the design point in terms of wing loading W/S and power loading W/P or thrust-to-weight ratio T/W. The principles of the technique behind the SMP were originally developed in Ref. [1] and have since then been expanded and re-proposed by other authors, such as Refs. [2, 3, 6, 32]. More recently, several authors have adapted the SMP in different ways to account for hybrid-electric propulsion (see e.g. [23, 33]), but there is no universally adopted approach. In this paper, we present a variant of the work in Ref. [23], seeking a balance between the generality of the method and the complexity of its implementation. If the calculation of the SMPs is considered too complex for a first estimate of the aircraft sizing, the designer can skip this section and choose a wing loading (W/S) and power loading (W/P) or thrust-to-weight ratio (T/W) value based on the reference aircraft instead, and use that in the mass estimation. This will work as an initial guess for fully fuel-based aircraft and, to a lesser extent, for fully-electric aircraft, but will in most cases lead to unrealistic or highly suboptimal results for hybrid aircraft, which combine both fuel and electricity. Especially in those cases, constructing the SMPs is a key step to correctly size the aircraft.

1. Architectures & Component Efficiencies

Before constructing the SMPs for hybrid-electric aircraft, we must define how propulsive power is generated, distributed, and transformed within the powertrain. Unlike conventional aircraft, where a single propulsion device is typically sized based on thrust or power requirements, hybrid-electric systems involve multiple interconnected components that may contribute differently across flight phases. Sources such as [7, 34] provide a basis for the most common powertrain configurations, and Figure 3 illustrates a generic architecture that can be adapted to multiple powertrain architectures, specifically: conventional, fully electric, parallel hybrid, turboelectric and series hybrid. It includes two power branches: a fuel-burning pathway (top branch) coupled to the thermal engine, and a battery-electric pathway (bottom branch) supplying electrically driven propulsion. The main components are the fuel tank (F), thermal engine (TE), gearbox (GB), batteries (BAT), generator (GEN), electric motor (EM), and propulsor (P), which may be a propeller or a fan. If additional architectures need to be simulated, Appendix E presents a methodology for modelling alternative powerplant options—including a mixed parallel/series hybrid—without requiring architecture-specific formulations.

To identify how power is distributed throughout the selected architecture, it is useful to define the supplied power ratio (or *source hybridization ratio*)

$$\Phi = \frac{P_{\text{bat}}}{P_{\text{bat}} + P_{\text{f}}}, \tag{8}$$

where P_{bat} is the power supplied by the battery, which is equal to voltage times current, and P_{f} is the (chemical) "power" supplied by the fuel, which is equal to the mass flow rate times the heating value of the fuel. Note that this is just one of many definitions encountered in literature to define the "power split" or "hybridization ratio". For fully electric powertrains, the supplied power ratio is always equal to one, while for conventional fuel-based powertrains, it is always equal to zero. For hybrid powertrains, the supplied power ratio ranges from zero to one in normal operating conditions; negative values or values above one represent a case where the battery is recharging instead of discharging, or the

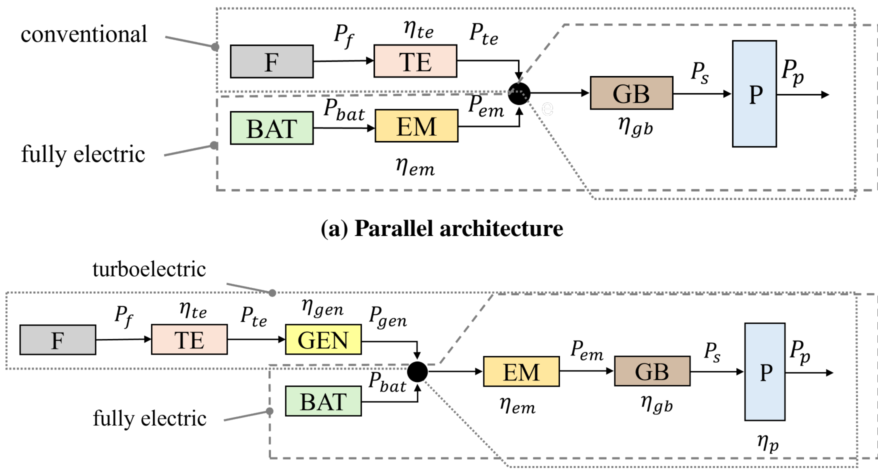

(a) Parallel architecture

(b) Series architecture

Fig. 3 Representations of powertrain architectures. Adapted from [34].

propulsor is acting as a windmill instead of producing thrust. These operating conditions are considered beyond the scope of this paper. The supplied power ratio $\Phi(t)$ may vary over the mission and can therefore be treated as a design or optimization variable for component sizing and energy management, for example, to minimize mass, fuel or energy use, or thermal load, subject to power and state-of-charge constraints.

To relate source power to propulsive power, each component in the architecture is assigned a conversion or transmission efficiency η_{comp}. By combining these efficiencies, the propulsive power P_{p} at the propeller or thrust-producing unit can be expressed in terms of the corresponding TE, EM, GEN, and battery power. Because these efficiencies may depend on flight phase or operating condition, the resulting power relations can also vary throughout the mission. Table 7 summarizes these relations for the architectures shown in Fig. 3, accounting for both component efficiencies and the supplied power ratio Φ. These equations assume the battery is discharging and that the propulsor is producing zero or positive thrust; in the case of negative thrust or battery recharging, the position of the efficiency factors in these equations would change.

Typical component efficiencies for hybrid-electric powertrains depend on technology maturity and operating point, but conceptual studies usually assume the values summarized in Table 8. These efficiencies are representative of current or near-term technology. The designer may assume a value within these ranges, look for values in literature, or estimate them using their own lower- or higher-fidelity methods. The table includes typical values for losses in the power distribution system that connects batteries with the electric motors and generators, which are not explicitly modelled and considered negligible in Fig. 3. This simplifying assumption is more accurate for "simple" powertrains (e.g. one battery pack connected to one motor), but the losses in the power distribution system can grow especially in case of complex powertrains with long cables, or if DC-DC converters are used to maintain a constant voltage level.

Table 7 Power relations for series and parallel hybrid architectures.

	Series	Parallel
Thermal engine	$P_{\text{te}} = \left[\eta_{\text{p}}\eta_{\text{gb}}\left(\frac{\Phi}{1-\Phi}\frac{\eta_{\text{em}}}{\eta_{\text{te}}} + \eta_{\text{gen}}\right)\right]^{-1} P_{\text{p}}$	$P_{\text{te}} = \left[\eta_{\text{p}}\eta_{\text{gb}}\left(\frac{\Phi}{1-\Phi}\frac{\eta_{\text{em}}}{\eta_{\text{te}}} + 1\right)\right]^{-1} P_{\text{p}}$
Electric motor	$P_{\text{em}} = \left[\eta_{\text{p}}\eta_{\text{gb}}\left(1 + \frac{1-\Phi}{\Phi}\frac{\eta_{\text{te}}\eta_{\text{gen}}}{\eta_{\text{em}}}\right)\right]^{-1} P_{\text{p}}$	$P_{\text{em}} = \left[\eta_{\text{p}}\eta_{\text{gb}}\left(1 + \frac{1-\Phi}{\Phi}\frac{\eta_{\text{te}}}{\eta_{\text{em}}}\right)\right]^{-1} P_{\text{p}}$
Battery	$P_{\text{bat}} = \left[\eta_{\text{p}}\eta_{\text{gb}}\left(\eta_{\text{em}} + \frac{1-\Phi}{\Phi}\eta_{\text{te}}\eta_{\text{gen}}\right)\right]^{-1} P_{\text{p}}$	$P_{\text{bat}} = \left[\eta_{\text{p}}\eta_{\text{gb}}\left(\eta_{\text{em}} + \frac{1-\Phi}{\Phi}\eta_{\text{te}}\right)\right]^{-1} P_{\text{p}}$

Tips & Tricks

- When designing an electrified aircraft with distributed propulsion, it is important to select realistic propeller/fan diameters, such that the resulting disk loading leads to reasonable propulsive-efficiency values. One simple way to include this sensitivity for propeller aircraft is to estimate the propulsive efficiency of the propellers in each flight condition using $\eta_p = 2k/(1+\sqrt{1+T_c})$, where $T_c = T/(q_\infty A_p)$ is the thrust coefficient, q_∞ is the freestream dynamic pressure, A_p is the propeller disk area, and k is a factor accounting for swirl and friction losses on the propeller blades (typically $k \sim 0.75 - 0.88$). Propellers optimized for high static thrust to enable VTOL or STOL will have reduced maximum efficiency for cruise or loiter. Variable-pitch (constant-speed) propellers mitigate most of the efficiency losses due to differing operating conditions, but some may remain due to a fixed twist and chord distribution. The appropriate propeller efficiency should be applied for each flight segment.

Table 8 Representative component efficiencies for hybrid-electric aircraft.

Component	Symbol	Typical Efficiency [−]
Electric generator	η_gen	0.92 – 0.97
Power electronics / converter (rectifier or inverter)	η_pm	0.97 – 0.99
Power distribution (cables, switches, etc.)	η_pd	0.97–0.99
Electric motor	η_em	0.92 – 0.97
Gearbox / mechanical transmission	η_gb	0.97 – 0.99
Propeller or fan (propulsive efficiency)	η_p	0.70 – 0.85
Thermal engine (piston)	η_te	0.25 – 0.35
Thermal engine (gas turbine)	η_te	0.30 – 0.50

2. Sizing for power-rated systems

For a power-based system – e.g. propeller aircraft – the performance constraints are analytical functions between power loading W/P and wing loading W/S to ensure compliance with the TLAR (e.g., stall speed, maximum speed, maximum climb gradient, takeoff distance, landing distance, etc.) and regulation requirements (e.g., balanced field length, one engine inoperative climb gradients, etc.). For a turbojet/turbofan aircraft, these constraints are usually functions between the thrust-to-weight ratio T/W and wing loading W/S. The constraints are generally formulated with *normalized* parameters (W/S, W/P, T/W) such that the result is independent of the actual aircraft "size" (i.e. weight). If any sizing constraint in the loading diagram is not formulated in a normalized way – e.g. using $P = f(S, W, ...)$ instead of $W/P = f(W/S, ...)$ – then this step of creating the SMP would have to be part of the mass convergence loop, sometimes requiring significant additional computational time. An example of a propulsive SMP, presented in both power loading and thrust-to-weight ratio formulations, is shown in Figure 4 where the green shaded area represents the feasible design region. In this section, we first focus on the process followed for power-rated systems, which is simpler since the electrical components are also sized in terms of power, and not thrust.

The process to find the sizing conditions for each powertrain component through the SMP, schematized in Fig. 5, involves:

1) **Formulate aircraft-level constraints (SMP):** Identify the performance and regulatory constraints relevant to the selected aircraft type, and express them analytically as functions of wing loading W/S and propulsive power loading W/P_p (or T/W) for each specific flight condition at a given speed, altitude, aircraft mass, etc. Identify the feasible design region that satisfies all constraints. Reference the sources in Table 9 or the examples in Appendix C.
2) **Normalize to maximum takeoff weight:** Express all power (or thrust) requirements relative to maximum takeoff weight W_TO to ensure consistency across constraints, yielding $W_\mathrm{TO}/P_\mathrm{p}$ (or T/W_TO) as a function of W_TO/S.
3) **Map to component-level requirements:** Select the powertrain architecture (e.g., conventional, fully electric, parallel hybrid, series hybrid, turboelectric) and define power split using the ratio Φ for each flight phase/constraint. Assign component efficiencies η_comp to form the efficiency chains (assumed constant per constraint). Propagate the aircraft-level *propulsive* power loading $W_\mathrm{TO}/P_\mathrm{p}$ through the architecture to obtain component-level constraints $W_\mathrm{TO}/P_\mathrm{comp}$. The resulting relations define the *component-level SMP*, from which component sizing (thermal engine, electric motor, generator, battery, etc.) is derived. Then, for each plot, the feasible design region and final design point can be found, yielding W_TO/S and $W_\mathrm{TO}/P_\mathrm{comp}$ (or T_i/W_TO) for each propulsion component.

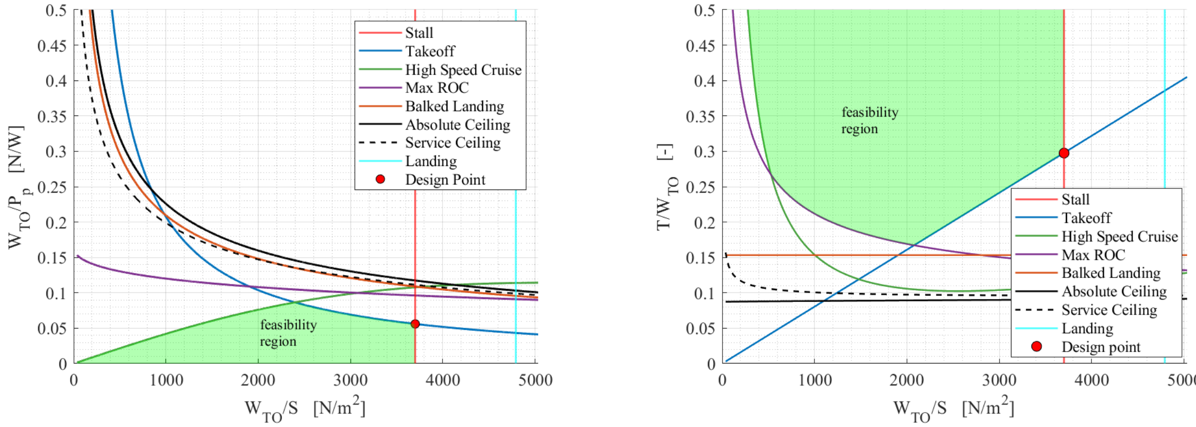

(a) W/P **formulation** **(b)** T/W **formulation**

Fig. 4 Examples of the propulsive SMP for power-rated (left) and thrust-rated (right) propulsion systems.

4) **Convert to sea-level static (SLS) conditions:** Translate power and thrust requirements to equivalent SLS values using appropriate lapse models—particularly for thermal power sources—to obtain comparable installed ratings (see Section V.B.4).

The following paragraphs describe these four steps respectively.

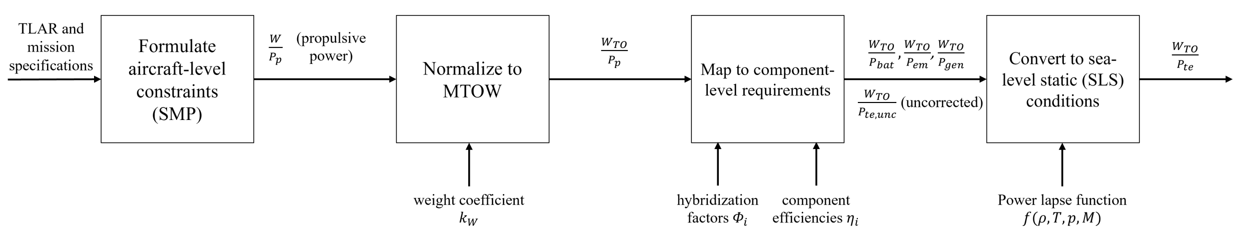

Fig. 5 Summary workflow to obtain component-level SMP.

Step 1. Formulate aircraft-level propulsive-power constraints (SMP): The first step in constructing the SMP is to express the relevant performance and regulatory requirements as analytical constraints on wing loading W/S and power loading W/P_p (or thrust-to-weight ratio T/W). Each constraint defines a line on the plot, delimiting the feasible design space. There are some aircraft parameters that may be necessary to build the SMP, depending on the types of constraints, but they can reasonably be calculated analytically or statistically assumed. Based on what parameters are necessary to assume, the SMP constraints can be categorized as follows:

- **Fixed flight speed and lift coefficient constraint**: when both V and C_L are fixed, only one wing loading satisfies the lift equation (e.g., stall speed, and landing distance).
- **Fixed flight speed constraint**: where W/S varies with C_L (e.g., maximum cruise speed, maximum rate of climb at a given speed, including OEI conditions).
- **Fixed lift coefficient constraint**: where V varies with W/S (e.g. climb gradient requirements)
- **Semi-empirical constraint**: during take-off, semi-empirical models (e.g., Take-Off Parameter, TOP).

Table 9 shows a list of the most common types of constraints with the relevant sources providing a detailed description of the equations involved, with some examples provided below in this section. In Appendix C, we present the flight-performance equations that are used to create the most common constraints of the SMP diagram. The designer should apply such equations for each value of wing loading in the interval of interest (e.g., 0 to 5000 N/m^2) for each performance constraint defined in the aircraft requirements. In these examples, aero-propulsive interaction effects are ignored. However, if these are significant, then the lift and drag terms need to be expanded (see Sec. V.A.3).

Table 9 Summary of constraint types, assumptions, and sources used in preliminary aircraft sizing.

Constraint	Type	Necessary assumptions	Roskam [1]	Raymer [2]	Torenbeek [4]	Torenbeek [3]	Sadraey [32]	Gudmundsson [6]
Stall speed	Fixed C_L and V	$C_{L,\mathrm{stall,LND}}$	3.1.1	5.3.2	9.3.1	5.4.4	4.3.2	3.2.2 Eqs. 3-7
Landing distance	Fixed C_L and V	V_{app} (usually linked to stall speed)	3.3.1 (prop), 3.3.2(jet)	5.3.5, 5.3.6	9.5	5.4.6	-	-
Takeoff distance	Semi-empirical	TOP, $C_{L,\mathrm{stall,TO}}$	3.2.1 (prop), 3.2.3 (jet)	5.3.3, 5.3.4	9.4	5.4.5	4.3.4.1 (jet), 4.3.4.2 (prop)	3.2.1 Eqs. 3-4
Max speed	Constant V	Drag polar (C_{D0} and K)	3.6	5.2.4 (T/W), 5.3.7 (best W/S)	9.2	5.4.1.b (prop), 5.4.1.a (jet)	4.3.3.1 (jet), 4.3.3.2 (prop)	3.2.1 Eqs. 3-5
Max rate of climb	Constant V	Drag polar (C_{D0} and K)	3.4.4.1 (prop), 3.4.9(jet)	5.3.11	-	5.4.3.b (prop), 5.4.3.a.2 (jet)	4.3.5.1 (jet), 4.3.5.2 (prop)	3.2.1 Eqs. 3-3
Max climb gradient	Constant C_L and V	Drag polar (C_{D0} and K)	3.4.4.2 (prop), 3.4.7(jet)	-	9.3.2, 9.3.3	5.4.3.a.1 (jet)	-	-
Maneuvering speed	Constant V	Drag polar (C_{D0} and K), n_{max}	3.5	5.3.9, 5.3.10	-	-	-	3.2.1 Eqs. 3-1, 3-2
Ceiling	Constant V	Engine power vs. altitude	3.4.10.2	5.3.12	-	-	4.3.6.1 (jet), 4.3.6.2 (prop)	3.2.1 Eqs. 3-6
OEI climb gradient	Constant C_L and V	Drag polar (C_{D0} and K)	3.4.4.2 (prop), 3.4.7(jet)	-	9.3.4	-	-	-
OEI rate of climb	Constant V	Drag polar (C_{D0} and K)	3.4.4.1 (prop), 3.4.7(jet)	-	-	-	-	-

Step 2. Normalize to takeoff weight: To enable a consistent comparison across all constraints, the derived power (or thrust) requirements are normalized with respect to the maximum takeoff weight W_{TO}. Hence, power loading becomes $W_{\mathrm{TO}}/P_{\mathrm{p}}$ (or thrust-to-weight ratio T/W_{TO}), and wing loading W_{TO}/S.

In practice, some performance constraints are evaluated at flight conditions that do not occur at maximum takeoff weight (e.g., maximum cruising speed, landing distance, balked landing, and certain OEI conditions). These must therefore be related back to takeoff weight through a representative coefficient

$$k_W = W_{\text{flight condition}}/W_{\mathrm{TO}} \tag{9}$$

which links the aircraft weight at the relevant condition to the takeoff weight. For conventional fuel-burning aircraft, k_W generally ranges between 0.5 and 0.9 depending on mission profile and aircraft type. For fully electric aircraft, where no fuel burn occurs, $k_W = 1$. For hybrid-electric configurations, the appropriate value is less well defined due to the combination of fuel burn and battery usage; assuming $k_W = 1$ in this case provides a conservative estimate of power requirements and is often a reasonable first-order assumption.

Step 3. Map to component-level requirements: Once the aircraft-level propulsive SMP has been obtained, it is propagated to the individual powertrain components using the architecture definitions introduced in Section V.B.1. The supplied power ratio Φ defines how propulsive power is split across the fuel-burning and battery-electric branches for the constraint under consideration, while the component efficiencies η_{comp} account for conversion and transmission losses. Using the architecture-specific relations summarized in Table 7, the aircraft-level loading $W_{\mathrm{TO}}/P_{\mathrm{p}}$ is converted into component-level loadings $W_{\mathrm{TO}}/P_{\mathrm{comp}}$. Repeating this procedure for each point (i.e. each wing-loading value) on each constraint yields a *component-level SMP* for each relevant component, from which the required installed sizes of the thermal engine, electric motor, generator, battery, and other power-producing units can be determined. Figure 6 illustrates an example of component-level SMPs obtained by propagating the propulsive SMP to the thermal engine, electric motor, and battery.

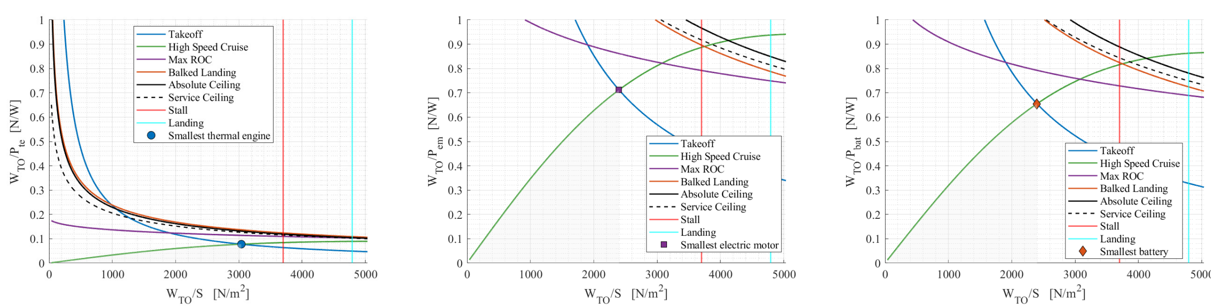

(a) Thermal engine **(b) Electric motor** **(c) Battery**

Fig. 6 Example component-level SMPs derived from the propulsive SMP. Each subplot shows the resulting power loading constraints for a specific propulsion component.

Step 4. Convert to sea-level static conditions (and max throttle): Some SMP requirements are defined at the specific flight conditions (e.g., altitude, speed, and Mach number). To enable consistent component sizing and comparison, these requirements are converted to equivalent sea-level static (SLS) conditions using appropriate power or thrust lapse models. In general, this conversion can be expressed as

$$\left(\frac{W_{\mathrm{TO}}}{P_{\mathrm{te}}}\right)_{\mathrm{SLS}} = f(\rho, p, T, M) \cdot \left(\frac{W_{\mathrm{TO}}}{P_{\mathrm{te}}}\right) \tag{10}$$

where the lapse function $f = f(\rho, p, T, M)$ accounts for the variation of available power (or thrust) with atmospheric and operating conditions. This correction primarily applies to thermal power-producing components (e.g., turbofans, turboshafts), whose performance degrades with altitude and flight speed. In contrast, electrically driven components (e.g., electric motors and batteries) exhibit a much weaker dependence on ambient conditions and are often assumed to deliver their rated power independently of altitude in conceptual design. The specific form of the lapse function depends on the component type and is discussed in detail in Sections V.B.4.

Finally, if the aircraft must be able to meet a specific performance constraint at a throttle (ψ) setting different from $\psi = 100\%$ (e.g. if you want a turbofan to cruise at 80% throttle to reduce maintenance costs), we must also correct the power of that specific constraint to the maximum continuous throttle[§]:

$$\psi = P/P_{\mathrm{max}} \tag{11}$$

which implies that

$$\left(\frac{W_{\mathrm{TO}}}{P_{\mathrm{te}}}\right)_{\mathrm{SLS,max}} = \left(\frac{W_{\mathrm{TO}}}{P_{\mathrm{te}}}\right)_{\mathrm{SLS}} \frac{1}{\psi} \tag{12}$$

If there is no reason why a constraint should be met at a lower throttle setting than 100%, there is no need to perform this correction and the additional subscripts can be dropped for simplicity.

Tips & tricks

- When creating the constraint diagram for a hybrid aircraft, always evaluate different hybridization strategies. In other words, "play around" with the supplied power ratio chosen per constraint. This can significantly impact the powertrain mass. For additional information, see Sec. VII.
- For fully-electric aircraft, the go-around can be an important sizing condition since it requires a high power setting and the battery is at a relatively low state-of-charge, meaning its maximum power output (maximum discharge rate) is lower than at take-off. To evaluate this, a battery discharge model must be incorporated.

3. Sizing for thrust-rated systems

As noted above, SMPs for turbofan- and turbojet-powered aircraft have historically been expressed in terms of thrust-to-weight ratio (T/W_{TO}). This convention arises because engine weight correlations are typically parameterized by thrust, while fuel efficiency is traditionally represented through thrust-specific fuel consumption (TSFC). An example of the SMP formulation for thrust-based propulsion systems is shown in Figure 4(b). In this representation, the design space (green shaded region) is at the top of the chart, resulting from the intersection of all constraints, and a design point can be chosen in that region.

For hybrid-electric propulsion systems, however, the sizing of electrical components is inherently power-based. As a result, a consistent transformation from thrust-based to power-based quantities is required. This conversion may usually be performed using

$$P_{\mathrm{p}} = TV \tag{13}$$

where P_{p} is the propulsive power and V is the true airspeed. Accordingly, thrust-based constraints can be recast in terms of power loading as

$$\frac{W}{P_{\mathrm{p}}} = \frac{1}{V\,(T/W)}, \tag{14}$$

using a representative flight speed for each mission segment. For takeoff conditions, this conversion is not directly applicable because the velocity approaches zero, leading to a singularity. To enable an approximate conversion, a

[§]Assumed to be equal to take-off throttle for simplicity.

characteristic speed such as $V_2 = 1.2V_{\text{stall}}$ may be adopted. This assumption is particularly useful when sizing the EM requirements, as the V_2 point is where the maximum in EM power requirements is typically observed across the takeoff process. The contribution of an EM to the static thrust of an aircraft can also be determined through a thermodynamic analysis of the propulsion system that relates the shaft power to the temperature jump and mass flow across a propulsor. However, this requires more detailed propulsion system modelling, and thus, for simplicity, one can alternatively use an actuator disk model to obtain a first-order estimate of static thrust based on induced power. With the addition of the propulsive efficiency, this calculation is performed by

$$T = \eta_{\text{p}} P^{2/3} \left(2\rho A\right)^{1/3}, \tag{15}$$

where ρ is the density at the propulsor face and A is the actuator disk area. Typically, η_{p} under static conditions is much less than those characteristic of forward-flight conditions, with representative values closer to 0.6.

Figure 7 illustrates the conversion of a thrust-based constraint into an equivalent power-based representation for the sizing of a turbofan, an EM, and a battery. In the case of parallel hybrid turbofan architectures, for example, the thrust can effectively have contributions from three separate sources: the core of a turbofan $T_{\text{core, GT}}$, the turbine-powered bypass flow through the fan $T_{\text{BP, GT}}$, and EM-powered bypass flow through the fan $T_{\text{BP, em}}$.

$$T/W = \left(T_{\text{core, GT}} + T_{\text{BP, GT}}\right)/W + T_{\text{BP, em}}/W. \tag{16}$$

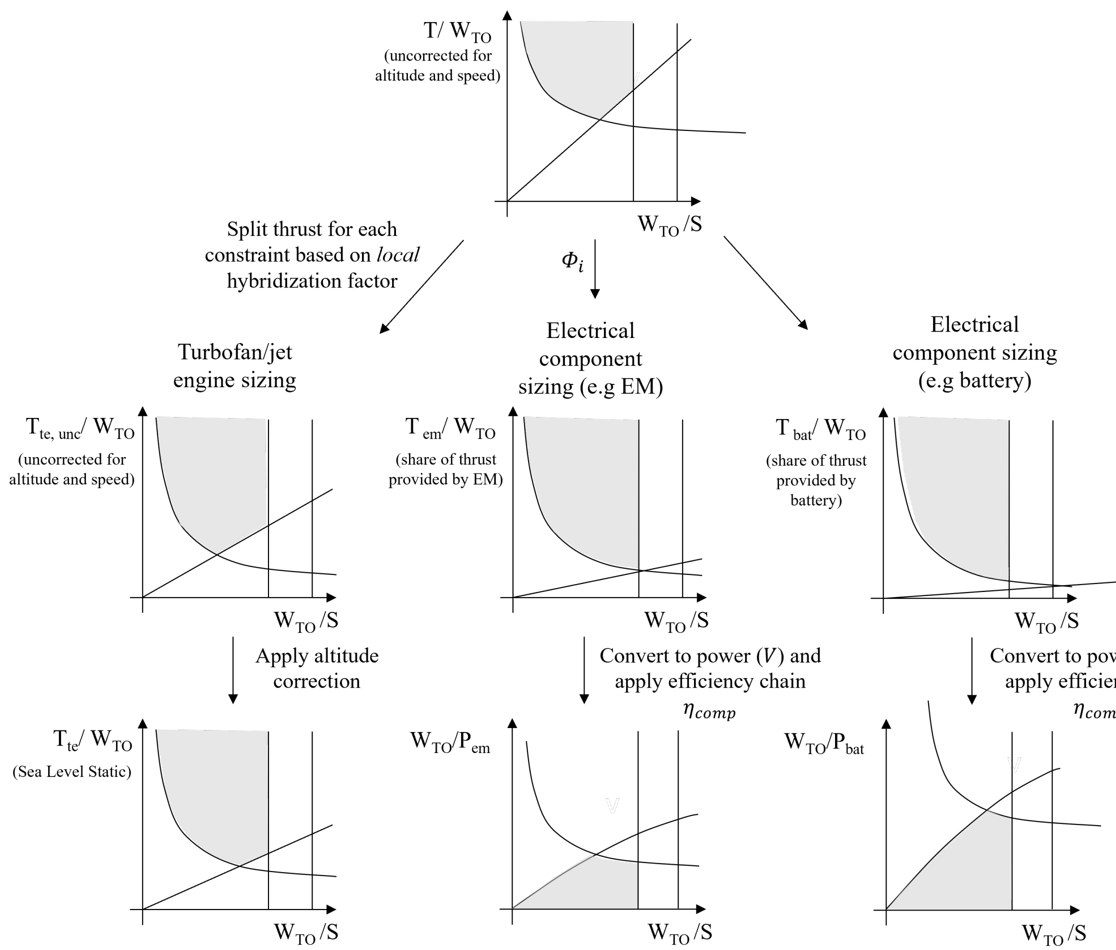

Fig. 7 Transformation of a thrust-based SMP into a power-based representation. Note that here the gas-turbine core and bypass contributions are lumped into a single "thermal engine contribution, $\left(T_{\text{core, GT}} + T_{\text{BP, GT}}\right) = T_{\text{te}}$.

Starting from a T/W_{TO} versus W_{TO}/S SMP, the total thrust requirement is decomposed into effective contributions associated with thermal and electric power sources. The individual thrust contribution of the EM can be related to propulsive power (Eq. 13) and used to calculate the corresponding EM shaft power for sizing across a corresponding W/P from the SMP. This procedure yields multiple *partial* thrust-based SMPs associated with each propulsive component. In a parallel hybrid turbofan architecture, since the EM augments power across the low-pressure spool, the propulsive efficiency can be determined from the fan pressure ratio. It is noted that the supplied power ratio, Φ_i, is not necessarily equal to the proportional power split imposed between the gas turbine and EM. Rather, Φ_i represents the proportional split of supplied power from the energy systems, which may vary across different constraints in the corresponding SMP diagrams.

For thrust-sized components such as turbofan or turbojet engines, appropriate corrections can be applied to ensure that thermal-power contributions are referenced to consistent operating conditions, typically SLS, as discussed in Section V.B.4. The resulting thrust-to-weight design point can then be directly used for engine sizing.

For power-based components such as EMs and batteries, the partial thrust contributions ($T_{\mathrm{em}}/W_{\mathrm{TO}}$ and $T_{\mathrm{bat}}/W_{\mathrm{TO}}$) can instead be converted into power loading form (W_{TO}/P_{em} and $W_{\mathrm{TO}}/P_{\mathrm{bat}}$) using representative flight speeds and propulsive efficiency assumptions, as shown in Eqs. (14) and (15). Steps 6 to 10 of the methodology described in Section V.B.2 can then be applied directly to complete the component sizing process.

4. Effect of altitude on engine-rated power/thrust

Some simplified models are commonly used to estimate the effect of altitude on the maximum available engine power or thrust and should be applied for those SMP constraints that are not in SLS conditions, such as maximum cruising speed or ceiling altitude. The first model applies to turboshaft engines. In this formulation, the power $P_{te,z}$ at altitude z is expressed as

$$P_{\mathrm{te,z}} = P_{\mathrm{te,r}} \left(\frac{\rho}{\rho_{\mathrm{c}}}\right)^{\xi} \tag{17}$$

where ρ and ρ_{c} denote the air density at the operating altitude and at the engine critical altitude, respectively. The exponent ξ is an engine-dependent parameter typically ranging between 0.7 and 0.9 [35, 36]. In the present case, a value of $\xi = 0.8$ is assumed. The critical altitude z_{c} is defined as the maximum altitude at which the engine can deliver the full rated power P_{r}.

A similar formulation is used for piston engines, commonly referred to as the Gagg and Ferrar model [6]. For turbocharged engines,

$$P_{\mathrm{te},z} = \begin{cases} P_{\mathrm{te,r}}, & \text{for } z \leq z_c \\ P_{\mathrm{te,r}} \left(a\sqrt{\frac{\rho}{\rho_c}} + b\right), & \text{for } z \geq z_c \end{cases} \tag{18}$$

where $a = 1.132$ and $b = -0.132$. For normally aspirated engines, the critical altitude z_c corresponds to sea level.

In contrast, EMs do not experience a combustion-related power lapse with altitude. Since their operation is not directly dependent on air density, the available shaft power can be approximated as constant with altitude, subject to thermal and electrical limits. A simple model can therefore be written as

$$P_{\mathrm{em},z} = P_{\mathrm{em,r}} \tag{19}$$

where $P_{\mathrm{em,r}}$ is the rated electric motor power. Nevertheless, altitude effects may arise indirectly through reduced convective cooling capability, which remains density-dependent. In hybrid-electric architectures, the total available propulsion power at altitude depends on the relative contribution of the thermal engine (which exhibits power lapse) and the electric machine (which can partially compensate for it).

As with airbreathing power-rated systems, thrust-rated engine systems, like turbofans or turbojets, also experience a lapse in rated thrust with increased altitude. Capturing this reduction in thrust capability at higher flight levels is particularly important to SMP constraints, as the TOC requirements commonly serve as the critical sizing constraint for many thrust-rated thermal engines used on high-speed aircraft. This thrust lapse can be simply expressed based on the sea-level thrust and the ratio of local pressure to sea-level pressure [4],

$$T_z = T_{\mathrm{r}} \left(\frac{p_z}{p_{\mathrm{SL}}}\right) \tag{20}$$

where T_{r} represents the maximum static take-off thrust at sea-level, p_{SL} is the sea-level pressure, and p_z is the pressure at a given altitude.

Assuming the ICAO standard atmosphere (ISA) conditions, this scaling indicates that a turbofan engine produces less than 30% of its static sea-level thrust at typical tropopause altitudes. While the thrust required for steady level flight also decreases with altitude, the excess power available to this system will gradually decrease until a minimum in rate of climb is reached at the service ceiling.

Tips & tricks

- The use of power-rated battery systems and electric machines in combination with thrust-rated turbofan systems offers a wealth of opportunities to efficiently size power systems, given that these electric power system components do not experience the severity in power lapse inherent to airbreathing engines. For this reason, concepts of "peak shaving" are often envisioned to meet top-of-climb turbofan sizing requirements with an engine system that is inherently smaller, lighter, and more efficient across a cruise throttle setting.
- While electrical components may not present a significant power lapse with altitude, this does not mean they can operate safely up to any altitude: as the air density decreases, the breakdown voltage reduces (see Paschen's law), and additional insulation or separation is required to prevent failures, increasing their mass. When looking for data of e.g. electric motors or cables, ensure they are rated up to the desired voltage at the desired altitude.

5. Effect of hybridization on thermal engine performance

The fuel-burn benefit of a hybrid-electric aircraft is mediated not only by electric-path efficiency and battery mass, but also by how hybridization changes the operating point of the gas turbine. Any low-fidelity sizing method that assumes fixed TSFC or fixed BSFC irrespective of electrical boost, shaft-power offtake, throttle setting, and altitude can therefore misrank concepts or operating schedules [37–42]. At the same time, full thermodynamic cycle simulation is not always necessary in the earliest conceptual loops. A practical approach is to use hybridization-aware regressions or low-order engine maps for most design-space exploration, and reserve higher-fidelity engine models for cases in which hybridization materially perturbs operability, cycle matching, or thermal limits. Such lower-order models should ultimately be reflected in the efficiency of the thermal engine used in the equations of Table 7:

$$\eta_{\mathrm{te}} = \frac{P_{\mathrm{eng}}}{\dot{m}_{\mathrm{f}} \cdot e_{\mathrm{f}}} \tag{21}$$

where e_{f} is the heat of combustion of the fuel (see Appendix D subsection A for values).

Power-rated gas turbines: For power-rated turboprop or turboshaft engines, a useful first-order model is

$$\dot{m}_{\mathrm{f}} \approx c_{\mathrm{BSFC}} P_{\mathrm{te}}, \tag{22}$$

where $\dot{m}_{\mathrm{f}}$ is the fuel mass-flow rate, c_{BSFC} is the effective brake-specific fuel consumption, and P_{te} is the gas-turbine shaft power. This approximation follows from the off-design assumption that component efficiencies are approximately constant with performance requirements and throttle settings, which yields an approximately linear relation between fuel flow and output power [39]. In a parallel-hybrid shaftline,

$$P_{\mathrm{te}} = P_{\mathrm{s}} - P_{\mathrm{em}}, \tag{23}$$

where $P_{\mathrm{shaft,req}}$ is the required shaft power at the propulsor input and P_{em} is the electric-machine shaft-power contribution to the same shaft, taken as positive in motoring mode and negative in generating mode. Accordingly, electric boost reduces the power carried by the gas turbine, whereas recharge or generator operation increases it. This approach is, in essence, analogous to specifying a power split in the constraint diagrams. If an engine deck or cycle-code response surface is available, c_{BSFC} may be replaced by a BSFC map in power and flight condition while retaining the same load-balance logic, in which case additionally the efficiency parameter is updated (note that BSFC is inversely proportional to the efficiency of the thermal engine).

Thrust-rated gas turbines: For thrust-rated gas turbines, a hybridization-aware extension of the ICAO-based regression used in e.g. the Future Aircraft Sizing Tool (FAST; see Table 20) can be written in terms of an equivalent thrust, T_{eqv}, that represents the load actually seen by the gas turbine [39, 40]:

$$\dot{m}_{\mathrm{f,modified}}(T_{\mathrm{eqv}}, h) = a \left[C_{ff3} \left(\frac{T_{\mathrm{eqv}}}{T_{\mathrm{eqv,max}}} \right)^3 + C_{ff2} \left(\frac{T_{\mathrm{eqv}}}{T_{\mathrm{eqv,max}}} \right)^2 + C_{ff1} \left(\frac{T_{\mathrm{eqv}}}{T_{\mathrm{eqv,max}}} \right) \right] + C_{ff,ch} T_{\mathrm{eqv}} h, \tag{24}$$

where $\dot{m}_{\text{f,modified}}$ is the fuel mass-flow rate, T_{eqv} is the equivalent thrust, $T_{\text{eqv,max}}$ is the maximum static equivalent thrust of the electrified configuration, h is altitude, C_{ff1}, C_{ff2}, and C_{ff3} are polynomial fuel-flow coefficients fit to ICAO fuel-flow data, $C_{ff,ch}$ is the altitude-correction coefficient obtained from a cruise TSFC anchor point, and a is a scaling factor used to adapt the reference-engine regression to the electrified configuration [39, 40].

For a battery-boosted parallel hybrid architecture,

$$T_{\text{eqv}} = T_{\text{output}} - \frac{P_{\text{EM}}}{V_{\text{air}}}, \tag{25}$$

where T_{output} is the total propulsive thrust, P_{EM} is the electric propulsive power contribution, and V_{air} is airspeed. In this case, $T_{\text{eqv}} < T_{\text{output}}$ because part of the propulsive work is supplied electrically [40]. This approach in essence assumes that the effective contribution of electric motor to total thrust is proportional to its contribution in terms of power, similarly to Eq. 16.

When higher fidelity is needed: These simplified models are appropriate for aircraft-level sizing, mission screening, and architecture trade studies. Higher-fidelity gas-turbine modelling becomes necessary when hybridization materially changes compressor operating line, corrected flow, surge margin, spool matching, variable-geometry scheduling, turbine temperature limits, or transient response. Zhao et al. showed, for example, that positive hybridization in a parallel hybridized gas turbine can move the compressor toward surge, which is not captured by a fixed-BSFC or equivalent-thrust regression alone [41].

A practical fidelity ladder is therefore recommended. For early conceptual trade studies, use a calibrated BSFC or TSFC regression with altitude correction and architecture-aware P_{GT} or T_{eqv}. For late conceptual and preliminary design, replace this with response surfaces or tabulated maps derived from cycle-code analyses across throttle, altitude, Mach number, and electrical power exchange. For operability, control, and certification-sensitive assessments, use the full-cycle model or the engine deck directly. This progression preserves computational efficiency where it matters most while ensuring that the co-design of gas turbine, electric system, and operating strategy remains physically credible.

C. Control & Stability: Tail Sizing

During conceptual aircraft design, basic control & stability assessments of the aircraft are performed to estimate the size of the stabilizing (horizontal and vertical tail) and control surfaces (ailerons, elevator, and rudder) of the aircraft. For initial sizing, only the horizontal and vertical tail areas are estimated, since they will be required to estimate tail mass and tail drag.

1. Low Fidelity

An initial estimate of horizontal and vertical tail surface areas can be determined using tail volume coefficients. This approach is treated in detail by Raymer in [2, p. 158] and in Roskam [1, Part II]. The horizontal (S_{h}) and vertical (S_{v}) tail surface areas are estimated as follows:

$$S_{\text{h}} = \frac{c_{\text{h}}\,\bar{c}_W\,S_W}{L_{\text{h}}} \tag{26}$$

$$S_{\text{v}} = \frac{c_{\text{v}}\,b_W\,S_W}{L_{\text{v}}} \tag{27}$$

$$\tag{28}$$

where c_{h} and c_{v} are the horizontal and vertical tail volume coefficients, which are based on empirical data. Table 10 provides typical values of the volume coefficients. The parameters b, S, $\bar{c}$ are the wing span, area, and mean aerodynamic chord, respectively, which can be obtained once the wing loading and an initial guess of the aircraft weight are known. L_{h} and L_{v} are the tail moment arms, that is, the distance between the quarter-chord location of the mean aerodynamic chord of the wing and the horizontal or vertical tail, respectively. According to Raymer [2, p. 167], the tail arm can be approximated as ~60%, 50-55%, or 45-50% of the fuselage length for aircraft with fuselage nose-mounted engines, wing-mounted engines, and aft-mounted engines, respectively.

Table 10 Typical values for horizontal and vertical tail coefficients. Values extracted from Raymer [2], Table 6.4.

Aircraft category	c_h	c_v
General aviation, single engine	0.70	0.04
General aviation, twin engine	0.80	0.07
Agricultural	0.50	0.04
Twin turboprop	0.90	0.08
Jet transport	1.00	0.09
Military transport	1.00	0.08

2. Mid Fidelity

The next step in fidelity typically involves actively calculating the aircraft's center of gravity (CG) and using X-plots to determine the horizontal and vertical tail areas required to satisfy a set of control and stability requirements. These equations require a set of aerodynamic coefficients, which can be assumed or obtained from mid-fidelity aerodynamic analyses of the initial aircraft geometry. Since the tail size determines the aircraft's CG, the CG determines the wing position, and the wing position determines the tail arm, an iterative approach is required to solve for the wing position and tail size. For more information, see Ref. [1], Part II, Section 11.

3. High Fidelity

High-fidelity control and stability analyses use six-degree-of-freedom flight dynamics simulations of the aircraft to verify if specific performance requirements can be met. Such analyses are used to verify the required control-surface sizes and the forces and moments on the control surfaces, which can, in turn, be used to size actuators and other elements of the flight control system. These flight dynamics models require accurate aerodynamic data, including both static and dynamic coefficients. Such data can be obtained from CFD simulations, wind-tunnel tests, and (scaled) flight tests.

4. Tips & Tricks

- The volume coefficient method with a fixed tail moment arm can lead to inaccurate results for aircraft with a lot of batteries, for two reasons. First, the battery strongly affects the position of the CG, and thus the position of the wing [43], particularly if placed in the fuselage. Second, this usually goes hand-in-hand with a large energy mass compared to the payload mass, which in turn can lead to a large wing relative to a small fuselage [44]. This can lead to unrealistic vertical tail area values since the volume coefficient is defined using wing span, while in practice the fuselage length also plays an important role—thus leading to less reliable values for aircraft with unconventional proportions between wing and fuselage. We therefore recommend moving to a "medium fidelity" approach, including CG estimation as soon as possible for fully-electric or "heavy" series-hybrid aircraft.
- Aircraft with leading-edge distributed propulsion can have significantly lower yawing moments in an OEI scenario, but it depends on the number and placement of the propellers. To assess the potential benefits with respect to tail sizing, we recommend adopting a "medium fidelity" approach to quantify the yawing moments as soon as possible for aircraft with distributed propulsion.
- Distributed electric propulsion can be used for yaw control through differential thrust, which, especially in the case of engine failure, can be very useful to reduce the yawing moment required from the vertical tail. Earlier research has shown that this could reduce the vertical tail size by e.g. 30% [45]. However, this assumes that future certification will allow differential thrust in emergency scenarios. In civil applications, this would require extensive testing and the development of new means of compliance; therefore, the designer should assess whether this is something they can count on for their application.

D. Energy Estimation

For conventional aircraft, energy estimation has traditionally been conducted via fuel mass estimation. Since fuel serves as the sole onboard energy source, determining aircraft energy requirements reduces to sizing the required fuel mass. In all-electric and hybrid-electric aircraft, this is no longer sufficient, as energy is stored across multiple media with varying specific energies. Depending on the powerplant architecture and the stage of the design process, energy can be estimated at different levels of fidelity.

The mission profile that the aircraft must fly, defined from take-off brake release to a full stop after landing, serves as the primary input for the sizing process. However, as illustrated in Figure 8, the nominal mission profile only accounts for a portion of the total energy requirement. To satisfy safety and operational regulations, the total onboard energy must also include several or all of the following contributions:

- **Diversion:** Energy required to fly from the destination to a specified alternate airport. Note that while regulations mandate this reserve, the minimum distance to the alternate is not strictly prescribed and depends on the specific operational route. A typical value assumed for a ~180-seater narrow-body jet airplane is 200 NM.
- **Loiter:** An endurance-based reserve, typically calculated as 30 minutes of flight at 1,500 ft over the alternate airport for FAR-25/CS-25 turbine-powered aircraft or 45 min at 1,500 ft for FAR-23/CS-23 airplanes.
- **Contingency Reserve:** Typically 5% of the nominal mission fuel/energy to account for operational uncertainties.
- **Non-propulsive Off-takes:** Power for cabin pressurization, avionics, environmental control systems, ice protection systems and, in the case of some electrified aircraft, thermal management systems.
- **Residual Energy:** For fuel this represents unusable/trapped fuel (approx. 1%). For batteries, this corresponds to a minimum state of charge margin (usually 10-20%) which is not exceeded to prevent cell degradation, maintain minimum power delivery, and avoid overheating due to high internal resistance.

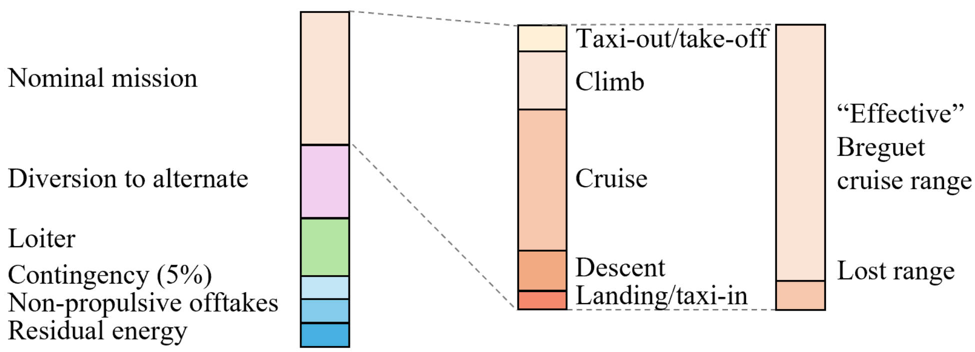

Fig. 8 Buildup of total energy required on-board for a typical commercial transport application. This breakdown is applicable to fuel energy, battery energy, or both. Bars not to scale.

1. Low-fidelity: Fuel/Energy fractions and Breguet range equation

During the conceptual design stage, it is often acceptable to estimate the total mission fuel or energy based on the cruise requirement, with approximate corrections for the non-cruise phases of flight. This can be done with the Breguet range equation. This equation provides a useful analytical relationship between the desired mission range R_{mis}, the specific fuel consumption C, aerodynamic efficiency L/D, and the aircraft weight ratio at the beginning and the end of the segment $W_{\text{init}}/W_{\text{fin}}$:

$$R_{\text{mis}} = \frac{V \cdot \frac{L}{D}}{C} \ln\left(\frac{W_{\text{init}}}{W_{\text{fin}}}\right) \tag{29}$$

The lift-to-drag ratio can be obtained from the methods in Sec. V.A and the SFC from e.g. Raymer [2, p. 38], while the ratio of initial weight (MTOW) to final weight is what needs to be solved for, since that gives the fuel mass required.

For hybrid-electric aircraft with a constant hybridization factor, Φ, the Breguet range equation can be modified as described by Ref. [34]. The derivation follows the classical Breguet range formulation and assumes steady, level flight at constant speed and lift-to-drag ratio. The modified equation incorporates the transmission efficiencies of the different power branches, grouped as η_1, η_2, and η_3 as shown in Figure 9 and listed in Table 11. These efficiencies depend on the powertrain type, as defined by the schematics in Figures 3a and 3b. Also, the constant power-split ratio Φ, and the specific energies of the fuel and battery (e_{f} and e_{bat}), yielding

$$R_{\text{mis}} = \eta_3 \frac{e_{\text{f}}}{g} \left(\frac{L}{D}\right) \left(\eta_1 + \eta_2 \frac{\Phi}{1-\Phi}\right) \ln\left(\frac{W_{\text{init}}}{W_{\text{fin}}}\right). \tag{30}$$

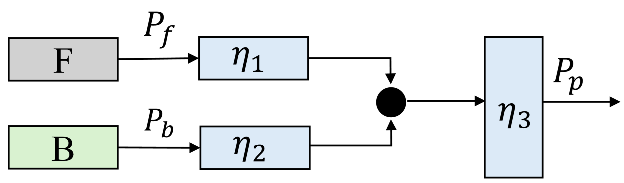

Fig. 9 Simplified powertrain architecture

Table 11 Powertrain branches simplified efficiencies.

Simplified representation	Parallel architecture	Series architecture
$\eta_1 =$	η_{te}	$\eta_{\mathrm{gt}}\eta_{\mathrm{eg}}$
$\eta_2 =$	η_{em}	1
$\eta_3 =$	η_{p}	$\eta_{\mathrm{em}}\eta_{\mathrm{p}}$

By inverting Eq (30) we can get the fuel fraction for cruise as

$$\frac{W_{\mathrm{fin}}}{W_{\mathrm{init}}} = \exp\left[\frac{-R_{\mathrm{mis}}}{\eta_3 \frac{e_{\mathrm{f}}}{g}\left(\frac{L}{D}\right)\left(\eta_1 + \eta_2 \frac{\Phi}{1-\Phi}\right)}\right] \tag{31}$$

or, alternatively, by breaking down the weights in their sub-components, we can relate the range to the total energy content on board instead:

$$R_{\mathrm{mis}} = \eta_3 \frac{e_{\mathrm{f}}}{g}\left(\frac{L}{D}\right)\left(\eta_1 + \eta_2 \frac{\Phi}{1-\Phi}\right)\ln\left[\frac{W_{\mathrm{OE}} + W_{\mathrm{PL}} + \frac{g}{e_{\mathrm{bat}}}E_{0,\mathrm{bat}} + \frac{g}{e_{\mathrm{f}}}E_{\mathrm{f}}(t_{\mathrm{start}})}{W_{\mathrm{OE}} + W_{\mathrm{PL}} + \frac{g}{e_{\mathrm{bat}}}E_{0,\mathrm{bat}} + \frac{g}{e_{\mathrm{f}}}E_{\mathrm{f}}(t_{\mathrm{end}})}\right]. \tag{32}$$

In this expression W_{OE} and W_{PL} are the operating empty weight and payload weight, while $E_{0,\mathrm{bat}}$ is the total battery energy at the start of the mission, $E_f(t_{\mathrm{start}})$ and $E_{\mathrm{f}}(t_{\mathrm{end}})$ are the fuel energies at the beginning and end of the considered segment.

When Φ tends to zero or one, the expression collapses to the classical fuel-based and purely electric range equations, respectively, with the latter being

$$R_{\mathrm{mis}} = \eta_2\eta_3\left(\frac{L}{D}\right)\frac{e_{\mathrm{bat}}}{g}\frac{\frac{g}{e_{\mathrm{bat}}}E_{0,\mathrm{bat}}}{W_{\mathrm{OE}} + W_{\mathrm{PL}} + \frac{g}{e_{\mathrm{bat}}}E_{0,\mathrm{bat}}}. \tag{33}$$

Following the methodology in [4], an additional equivalent range, referred to as the *lost range* R_{lost}, can be added to the mission range R. This represents a fictitious distance that accounts for the additional energy required for takeoff, climb, and acceleration to cruise conditions. The energy consumed during descent, approach, and landing is conservatively assumed to be equal to that required for cruising over an equivalent distance.

$$R_{\mathrm{lost}} = (1.1 + 0.5\,\eta_{\mathcal{M}})\left(\frac{L}{D}\right)(h_{\mathrm{e}})_{\mathrm{cruise}} \tag{34}$$

where

$$(h_e)_{\mathrm{cruise}} = h_{\mathrm{cruise}} + \frac{V_{\mathrm{cruise}}^2}{2g} \tag{35}$$

is the cruise energy height. The parameter $\eta_{\mathcal{M}}$ accounts for engine sensitivity to Mach number and is typically taken as 0 for propeller-driven aircraft and 0.2–0.5 for turbofan-powered aircraft [4, 46].

By including the lost range in Eq. (30), and assuming $W_{\mathrm{init}} = W_{\mathrm{TO}}$ and $W_{\mathrm{final}} = W_{\mathrm{TO}} - W_{\mathrm{f}}$, the fuel weight fraction can be expressed as

$$\frac{W_{\mathrm{f}}}{W_{\mathrm{TO}}} = 1 - \exp\left[\frac{-(R_{\mathrm{mis}} + R_{\mathrm{lost}})}{\eta_3 \frac{e_{\mathrm{f}}}{g}\left(\frac{L}{D}\right)\left(\eta_1 + \eta_2 \frac{\Phi}{1-\Phi}\right)}\right]. \tag{36}$$

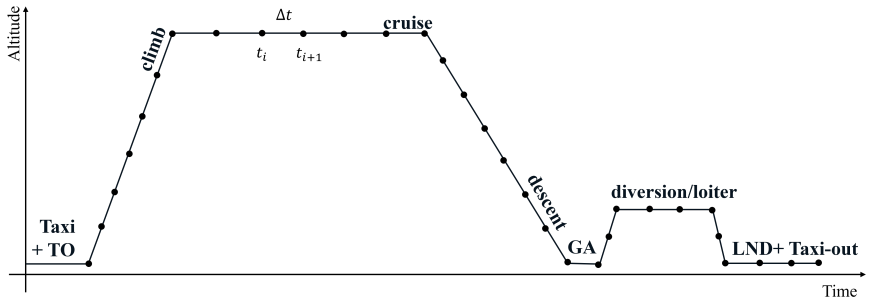

Fig. 10 Illustration of a discretized flight trajectory for time-marching mission analysis.

The corresponding fuel mass is then $M_\mathrm{f} = W_\mathrm{f}/g$, from which the fuel energy can be obtained as

$$E_\mathrm{f} = M_\mathrm{f}\, e_\mathrm{f}, \tag{37}$$

where e_f is the fuel-specific energy. The required battery energy is then

$$E_\mathrm{bat} = E_\mathrm{f} \frac{\Phi}{1 - \Phi}. \tag{38}$$

It is important to note that this formulation assumes a constant supplied power ratio Φ throughout the mission. If the hybridization level varies across mission segments, a higher-fidelity approach is recommended. This can be achieved either through time-stepping methods, as described in Section V.D.2, or by partitioning the mission into multiple segments and applying the Breguet formulation piecewise with segment-specific values of Φ.

For loiter segments, a simplified endurance expression can be obtained from Eq. (30) by dividing by the cruise speed. In that case, the aircraft would typically fly at a lower speed, closer to the max-endurance speed, to minimize energy consumption (see classical handbooks for the derivation).

2. Mid/High-fidelity: Time-Stepping

For mid- to high-fidelity energy estimation, the mission is simulated using a time-stepping approach. In this framework, the flight profile is divided into a series of segments or legs, and the aircraft state is updated over small time increments. This process generally involves:

1) Dividing the mission into successive flight phases and discretizing each phase into small time intervals Δt as illustrated in Fig. 10.
2) Computing the instantaneous aircraft trim and the associated aerodynamic and propulsive requirements at each time step.
3) Estimating fuel burn and electrical energy use by integrating the relevant power flows over the mission.

This type of simulation explicitly accounts for variations in aircraft weight, altitude, airspeed, and flight-path angle throughout the mission. It also allows for flexible power-management strategies, making it particularly suitable for the design or optimization of hybrid-electric aircraft, where the distribution of power between thermal and electrical branches may vary from one segment to another.

A typical implementation represents the mission as a sequence of flight segments, each terminated when a prescribed condition is satisfied. For instance, taxi, takeoff, landing, and loiter segments are commonly defined based on elapsed time, whereas cruise and diversion segments are defined by distance travelled, and climb and descent segments by altitude change. For steady-state phases such as cruise or loiter, larger time steps may be used to improve computational efficiency without compromising accuracy.

During ground operations (engine start, warm-up, taxi-out, and taxi-in), power is typically assumed at idle conditions for approximately 10- 20 minutes, depending on aircraft class and airport characteristics. Taxi duration can be significant, particularly for commercial aircraft operating at congested airports, and in some cases may exceed airborne segment durations. The corresponding energy consumption can be estimated using the installed propulsion system power, with idle power approximated as 2–8% of rated takeoff power (see Section V.B).

For takeoff, full rated power (100%) is typically assumed over a duration of approximately 60–90 seconds. The landing phase has a comparable duration; however, energy consumption is generally much lower and can be approximated using idle power levels consistent with taxi operations.

Airborne segments (climb, cruise, descent, and loiter) are defined by prescribed airspeeds and, where applicable, climb or descent rates, or, alternatively, a predefined throttle setting, allowing propulsive power to be calculated throughout the mission. In the absence of specified top-level aircraft requirements (TLARs), representative performance conditions may be adopted. Specifically, the best-range speed is typically assumed for cruise and diversion segments, while the best-endurance speed is used for loiter [2, 4, 32]. Climb performance can be defined using a best-rate-of-climb speed derived from standard performance methods; in practice, commercial transport aircraft often operate at approximately 250 kn below 10,000 ft. Descent speeds are generally comparable to cruise speeds [2]. When TLARs are unavailable, representative airspeeds and vertical profiles may also be derived from operational data sources such as FlightRadar24[¶], FlightAware[‖], or the EUROCONTROL Performance Database[**].

To implement/code this in a simulation tool, at each time step, the aircraft is assumed to be in trimmed, symmetric, quasi-steady flight, with thrust aligned with the flight path and small angles of attack. Under these assumptions, the lift coefficient can be computed from vertical equilibrium as

$$C_L = \frac{W \cos \gamma_c}{\frac{1}{2}\rho V^2 S} \tag{39}$$

where W is the instantaneous aircraft weight and γ_c is the climb angle, which is negative during descent. Once C_L is known, the drag coefficient C_D can be determined from the adopted aerodynamic model as described in Section V.A. The required power to sustain the flight condition is then

$$P_{\text{req}} = \frac{1}{2}\rho V^3 S C_D + W V \sin \gamma_c. \tag{40}$$

Assuming trimmed flight, the propulsive power equals the required power, i.e.

$$P_{\text{p}} = P_{\text{req}}. \tag{41}$$

In addition to propulsive power, a contribution from non-propulsive (auxiliary) systems should be included. These include avionics, environmental control systems, flight controls, and other onboard electrical loads. In conceptual design, this auxiliary power is often approximated as a fixed fraction of propulsive power, typically on the order of 3–10%. Approximate regression-based models derived from existing aircraft data can also be used to estimate auxiliary power as a function of key aircraft parameters (e.g., number of passengers or MTOM), as discussed in [47]. However, such models are primarily based on conventional aircraft and may not fully capture the characteristics of hybrid-electric configurations. Conservatively, the auxiliary power may be approximated as

$$P_{\text{aux}} \approx 0.05\, P_{\text{p}}, \tag{42}$$

so that the total required power becomes $P_{\text{p}} + P_{\text{aux}}$.

As explained in Section V.B, for hybrid-electric aircraft, the propulsive power is distributed between the thermal and electric propulsion branches according to the selected architecture and power-management strategy. Consistent with the efficiency definitions introduced in Table 11, the fuel power can be expressed as

$$P_{\text{f}} = \frac{P_{\text{p}}}{\eta_3} \left[\eta_1 + \frac{\Phi}{1-\Phi}\eta_2 \right]^{-1} \tag{43}$$

and the battery power as

$$P_{\text{bat}} = \frac{P_{\text{p}}}{\eta_3} \left[\frac{\Phi}{1-\Phi}\eta_1 + \eta_2 \right]^{-1}. \tag{44}$$

[¶]https://www.flightradar24.com/

[‖]https://www.flightaware.com/

[**]https://learningzone.eurocontrol.int/ilp/customs/ATCPFDB/default.aspx?

The supplied power ratio Φ and the efficiencies η_1, η_2, and η_3 may vary throughout the mission and can therefore be treated as design or optimization variables for component sizing and energy management, for example, to minimize mass, fuel or energy consumption, or thermal load, subject to power and state-of-charge constraints.

The total battery energy required over the mission is computed as

$$E_{\text{bat}} = \frac{1}{SoC_{\text{max}} - SoC_{\text{min}}} \sum_{i=1}^{N} P_{\text{bat}}(t_i)\,\Delta t \tag{45}$$

where $(SoC_{\text{max}} - SoC_{\text{min}})$ represents the usable battery SOC window. In practice, SoC_{max} may be limited below unity to account for battery degradation and end-of-life considerations (discussed further in Section VI.F.2), while SoC_{min} ensures that a minimum reserve is maintained to avoid deep discharge and preserve battery health.

Fuel consumption is evaluated in an analogous manner. Given the instantaneous fuel power, the corresponding fuel mass flow rate can be estimated as

$$\dot{m}_{\text{f}}(t_i) = \frac{P_{\text{f}}(t_i)}{e_{\text{f}}} \tag{46}$$

The total fuel consumed over the mission is then

$$m_{\text{f}} = \frac{1}{1 - f_{l,\text{min}}} \sum_{i=1}^{N} \dot{m}_{\text{f}}(t_i)\,\Delta t, \tag{47}$$

where $f_{l,\text{min}}$ represents the minimum allowable fuel level/reserve fraction to account for contingency requirements, only to be used if the contingency energy is not accounted for separately, as in the breakdown of Table 12. Note that, in each time step, the aircraft's weight must be updated to account for fuel burn:

$$W(t_i) = W(t_{i-1}) - \dot{m}_{\text{f}}(t_i)\, g\, \Delta t. \tag{48}$$

The full mission definition should include segments that are not part of the nominal trajectory, such as diversion to an alternate airport and loiter. In practice, diversion can be modelled as a concatenated flight segment appended to the nominal mission and simulated within the same time-stepping framework.

To conclude, Table 12 summarizes the proposed approaches for low- and mid/high-fidelity mission energy estimation discussed in this section. It should be noted that such mission-level simulations represent an initial step in the simulation process. As the aircraft definition matures, higher-fidelity analyses incorporating full flight dynamics and the complete equations of motion are typically required. These are essential for stability assessment, control system design, and more accurate energy and performance predictions, and are generally performed in subsequent design phases.

Table 12 Summary of energy estimation approaches by mission phase for low- and mid/high-fidelity simulations.

	Mission phase	Low fidelity	Mid/high fidelity
Nominal mission	**Taxi-in** **Takeoff** **Climb** **Cruise** **Descent** **Landing** **Taxi-out**	Breguet range equation + lost range ($R_{\text{mis}} + R_{\text{lost}}$)	Time stepping
	Diversion to alternate (~200NM)	Breguet range equation + lost range ($R_{\text{div}} + R_{\text{lost}}$)	Time stepping
	Loiter (30/45 min)	Breguet endurance equation	Time stepping
	Contingency (5%)	~5% nominal mission fuel/energy	
	Non-propulsive offtakes	~5% propulsive power	
	Residual energy	For fuel: 1% fuel trapped. For batteries: 10%–20% SoC margin	

VI. Mass Estimation

Once the power loading (or thrust-to-weight ratio), wing loading, an initial guess of the MTOM, and the energy required to fly the mission are known, we have to calculate the mass of the aircraft and use that to update the original MTOM assumption (see Fig. 1). Mass estimation is a discipline in itself, and finding reliable mass data or models can be challenging. In this section, we provide values and equations for mass buildup, as shown in the example in Appendix A. However, please note that these are not necessarily the only, or even the best methods – that depends on the exact configuration and aircraft category being designed. It is up to the designer to select and compare the methods that are most appropriate for the aircraft they are designing.

A. Overview and types of mass breakdowns

There are many ways to divide the mass of the aircraft into sub-elements. This paper describes two approaches, a "Class I" breakdown and a "Class II" breakdown. Note that here we talk about different "classes" of mass breakdown rather than levels of fidelity, since both are based on analytical equations and can therefore be considered low-fidelity approaches. For more accuracy, physics-based models (sometimes referred to as "Class 2.5" or higher) or actual data are required. The difference between a Class I and a Class II breakdown is shown in Fig. 11. In the Class-I breakdown of a hybrid/electric aircraft, the maximum take-off mass m_{MTO} of the aircraft comprises four terms:

$$m_{\mathrm{MTO}} = m_{\mathrm{PL}} + m_{\mathrm{f}} + m_{\mathrm{bat}} + m_{\mathrm{OE}}, \tag{49}$$

where the terms on the right-hand side represent the payload mass, fuel mass, battery mass, and operating empty mass of the aircraft, respectively. Throughout this paper, we talk about maximum take-off mass (MTOM) as the "total" mass of the aircraft for simplicity; however, note that this is not the same as the "take-off mass" (depends on fuel mass for a particular mission) or the "ramp mass" (includes fuel to taxi to runway). Analogously, this paper only addresses the operating empty mass (OEM), but this should not be confused with the manufacturing empty mass, delivery empty mass, or basic empty mass, which exclude the operational items (see e.g. Torenbeek [3], Figure 8.2). Also note how the batteries are not considered part of the OEM, even though they are a fixed component on the aircraft. This distinction is beneficial because they are energy carriers like fuel, and because most OEM mass correlations do not account for propulsion batteries.

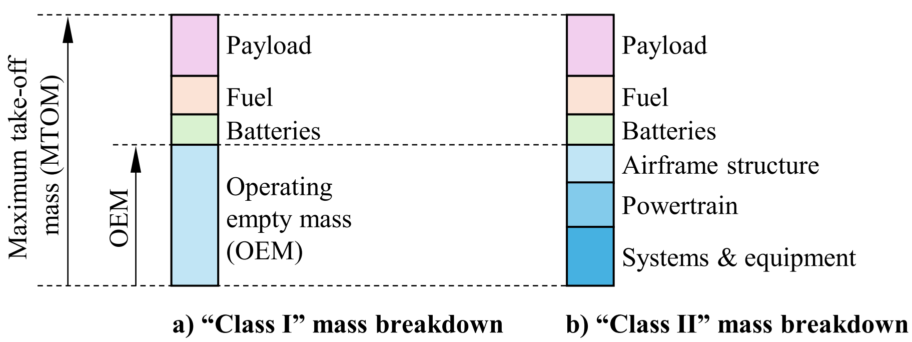

Fig. 11 Simplified aircraft mass breakdown used in this paper.

In the Class-II breakdown, the aircraft OEM is further subdivided into groups. In this paper, we distinguish three groups: airframe structure, powertrain, and systems & equipment:

$$m_{\mathrm{OE}} = m_{\mathrm{airframe}} + m_{\mathrm{powertrain}} + m_{\mathrm{systems}}. \tag{50}$$

While the literature contains some ambiguity, the powertrain is defined in this paper as the complete system responsible for providing propulsive power. This includes the energy source(s) (fuel and/or battery), energy conversion devices (thermal engines, cables, electric motors, gearboxes, etc.), thrust-producing devices (propellers, fans, etc.), and associated systems (fuel tanks, fuel lines, pumps, vents, cooling systems, controls, etc). However, the mass of the energy sources is estimated separately, as in the Class-I approach. In this simplified breakdown, the operating items, including operator-specific furnishing and pilots, are considered part of the systems & equipment, though often they are considered a separate category.

In Eq. 49, the payload mass is specified as a top-level requirement and the remaining terms need to be computed. Since many (semi-)empirical component mass equations depend, directly or indirectly, on the MTOM of the aircraft, in most cases the designer needs to assume an initial value for MTOM and iterate until converging on MTOM. An exception to this is when formulae are available for the empty mass *fraction* and the energy mass *fractions* of the aircraft—as opposed to their actual value—in which case Eq. 49 can be rearranged into:

$$m_{\mathrm{MTO}} = \frac{m_{\mathrm{PL}}}{1 - \frac{m_{\mathrm{OE}}}{m_{\mathrm{MTO}}} - \frac{m_{\mathrm{f}}}{m_{\mathrm{MTO}}} - \frac{m_{\mathrm{bat}}}{m_{\mathrm{MTO}}}}. \tag{51}$$

The designer can choose a Class-I or Class-II approach based on the available information and the level of detail needed. Often, a Class-I estimate is used as an initial guess for a Class-II calculation. In the following sections, we first provide correlations for the OEM in a Class-I breakdown. Then, we provide correlations for the various sub-components of OEM in the case of a Class-II breakdown.

Tips and Tricks

- The terms "mass" and "weight" are often used interchangeably when talking about aircraft and their components. We recommend sticking to "mass", expressed in kg or lb, to avoid confusion. "Weight" is expressed in N or lbf and is used when evaluating the forces acting on the aircraft ($W = m \cdot g$).
- Be careful when combining mass equations from different books and other sources—they often have different definitions of what is included, and they can be based on data from different types of aircraft, leading to an inconsistent buildup.

B. Fuel mass

The fuel mass m_{f} can be obtained by dividing the fuel energy required for the mission, as obtained from Section V.D, by the specific energy of fuel: typically 43.5 MJ/kg for aviation gasoline and 42.8 MJ/kg for jet fuel. See Appendix D subsection A for more information.

C. Battery mass

See the paragraph on batteries in Sec. VI.F.2.

D. Operating empty mass (Class I)

For a Class-I estimate, we need a correlation that relates the OEM or the OEM fraction ($m_{\mathrm{OE}}/m_{\mathrm{MTO}}$) to the MTOM and/or payload mass. Raymer [2, p.33] provides the following equation:

$$\frac{m_{\mathrm{OE}}}{m_{\mathrm{MTO}}} = A \cdot m_{\mathrm{MTO}}^{C}, \tag{52}$$

where m_{MTO} is given in lbs and the constants A and C depend on the category of the aircraft. Several values are given in Table 13. These constants are obtained statistically; they should not be used outside of the range of m_{MTO} for which they are valid, as given by Figure 3.1 of Ref. [2]. An alternative expression for m_{OE} can be found in Roskam [1], Part I.

Equation 52 can be applied to aircraft with a low to modest degree of hybridization (i.e. with a limited amount of batteries). However, in the case of fully electric aircraft or hybrids with a significant battery mass, the high battery mass fraction can lead to significantly lower empty mass fractions as a result of the mass scaling of several components. For more information on these scaling effects, see Ref. [31] or Ref. [4], Sec. 2.3. In that case, Eq. 52 will over-estimate the empty mass fraction, and the equation proposed by Torenbeek in 2013 [4] can be more suitable:

$$m_{\mathrm{OE}} = C_{\mathrm{mpl}} m_{\mathrm{PL}} + C_{\mathrm{MTO}} m_{\mathrm{MTO}} + m_{\mathrm{fix}}. \tag{53}$$

Here, the masses are given in kg, and the first term on the right-hand side represents the body group mass (primarily payload-driven), the second represents the components which are MTOM-driven, and the third represents components

Aircraft Type	A (mass in lbs)	A (mass in kg)	C
General aviation (metal; single engine)	1.250	1.164	−0.090
General aviation (metal; twin piston engines)	1.289	1.210	−0.080
General aviation (composite)	0.878	0.844	−0.050
Turboprop transport	0.975	0.937	−0.050
Jet transport	1.272	1.202	−0.072
Business jet	0.777	0.761	−0.027
Military cargo / bomber	0.737	0.712	−0.043
Ultralight	0.700	0.673	−0.050
Agricultural aircraft	1.205	1.122	−0.090

Table 13 Values of the A and C constants for selected aircraft types. Extracted from Raymer [2], Table 3.1.

that are aircraft size-independent. Table 14 provides values for the constants C_{mpl}, C_{MTO}, and m_{fix} for narrowbody and widebody jet transports. The constants of the first column have been found to be reasonably accurate for large regional turboprops with a high degree of hybridization if batteries are installed in the wing [44], but for other aircraft types, additional data correlations are necessary to obtain these coefficients.

Number of decks	one	one	two
Number of aisles	one	two	four
C_{mpl} [-]	1.25	1.50	1.75
C_{MTO} [-]	0.20	0.21	0.22
m_{fix} [kg]	500	600	700

Table 14 Coefficients for Eq. 53 for narrowbody and widebody jet transports, adapted from Torenbeek (2013) [4], Table 2.4.

E. Airframe Structure (Class II)

Airframe mass estimation is typically performed in more detail from Class II onward. Class II component mass estimation methods are typically based on statistical relations of existing aircraft, arranged by propulsion type and/or configuration or aircraft category. and related to geometrical (such as span, length or installed power) or performance characteristics (such as speed or altitude). Classical aircraft design handbook methods are found in books by Roskam [1], Raymer[2], Torenbeek [3], Nicolai [5], etc. These equations typically formulate mass fractions of different airframe components and systems in terms of MTOM, which can sum up to a (different) OEM estimate. Hence, they also introduce a required iteration on the previous Class I estimate.

Among the different handbook methods, different levels of detail can be found in these mass estimation relations. For example, relations exist that are configuration-agnostic and simply relate airframe total mass to MTOM; when more information about the aircraft is available, other relations can be used to estimate wing, tail, fuselage, landing gear, on-board systems, and propulsion systems separately, or even by subsystem or subcomponent. Systems and powertain mass estimation will be covered in subsequent sections, and here some helpful relations from Torenbeek[3] are provided for the main structural components. For more detailed methods and explanations, the reader is referred to aircraft design handbooks as mentioned above. Table 15 provides recommended references for the airframe mass estimation of various categories of aircraft (as defined in Table 1).

Wing mass

$$\frac{W_{\text{w}}}{W_{\text{G}}} = k_{\text{w}} b^{0.75} \left(1 + \sqrt{\frac{b_{\text{ref}}}{b_{\text{s}}}}\right) n_{\text{ult}}^{0.55} \left(\frac{b_{\text{s}}/t_{\text{r}}}{W_{\text{G}}/S}\right)^{0.30} \qquad (54,\ [3, \text{eq. } 8\text{-}12])$$

Aircraft category	Cert. basis	Recommended reference(s)
Commercial jet	Part/CS-25	Torenbeek[3], Raymer[2]
Regional turboprop	Part/CS-25	Torenbeek[3], Raymer[2]
Business jet	Part/CS-23 or 25	Torenbeek[3], Raymer[2]
Commuter aircraft	Part/CS-23	Torenbeek[3], Raymer[2]
General aviation	Part/CS-23	Gudmundsson[6], Nicolai & Carichner[5], Roskam[1]
Small general aviation	Part/CS-23	Gudmundsson[6], Nicolai & Carichner[5], Roskam[1]
Military transport	Military	Nicolai & Carichner[5], Roskam[1], Raymer[2]

Table 15 Recommended reference for airframe mass estimation for different categories of aircraft.

Here, $b_{\text{ref}} = 1.905m$ is the reference span, with structural span $b_{\text{s}} = b/\cos(\Lambda_{0.5c})$ m, S is the wing planform area in m^2, root thickness t_r in meters and n_{ult} the ultimate load factor. For large transport category ($W_{\text{G}} > 12500$ lb), $k_w = 6.67e^{-3}$ and W_{G} is the maximum zero fuel mass in kilograms. For light transport ($W_{\text{G}} < 12500$ lb), $k_w = 4.90e^{-3}$ and W_{G} is MTOM in kg. The resulting wing mass W_{w} in kg. You may reduce W_{w} by 5% or 10% for 2 or 4 wing-mounted engines, respectively. Reduce by 5% if the main undercarriage is not attached to the wing.

Tail mass

For light, low-speed aircraft (up to dive speed $V_D = 250$ kts EAS), maneuvering loads are critical, and empennage mass can be found according to:

$$W_{\text{tail}} = k_{\text{wt}} \left(n_{\text{ult}} S_{\text{tail}}^2 \right)^{0.75} \quad (55,\ [3, \text{eq. } 8\text{-}13])$$

Here, $k_{\text{wt}} = 0.64$, S_{tail} is the total tail area in m^2.

For transport aircraft, the tail plane masses (horizontal and vertical), a relation can be derived from the data provided by Torenbeek [3, fig. 8-5]. Applying a polynomial fit, we find:

$$x = \frac{(V_{\text{D}}/1000) \cdot S_{\text{tail surface}}^{0.2}}{\sqrt{\cos \Lambda_{0.5c}}} \quad (56)$$

The mass of each respective surface in kg can then be found according to a polynomial fit to [3, fig. 8-5], with x defined in Equation 56:

$$W_{\text{tail surface}} = k_{\text{surface}} \cdot S_{\text{tail surface}} \left(0.408x^4 - 3.4945x^3 + 7.8427x^2 - 2.5529x + 1.2754 \right) \quad (57)$$

Here, V_{D} is the dive speed in knots *equivalent* air speed (EAS), $S_{\text{tail surface}}$ is the respective area (horizontal or vertical), and $\Lambda_{0.5c}$ is the half-chord sweep angle. k_{surface} is 1 for a horizontal fixed stabilizer, 1.1 for a variable incidence stabilizer, 1 for a vertical tail when the horizontal tail is fuselage-mounted and defined according to 58, [3, p. 282] for a fin-mounted horizontal stabilizer.

$$k_{\text{v}} = 1 + 0.15 \frac{S_{\text{h}} h_{\text{h}}}{S_{\text{v}} b_{\text{v}}} \quad (58,\ [3, \text{p. } 282])$$

Here, S_{h} is the horizontal tail area, h_{h} the height of the horizontal tail above the fin root, S_{v} the vertical tail area, and b_{v} is the span of the vertical tail (measured tip to local fuselage center line).

Fuselage mass

The initial geometry of the fuselage is defined by its length and diameter. For commuter or regional transport aircraft, the length and diameter are driven by the number of passengers and the layout of the cabin. As a first estimate a statistical correlation provided by Raymer [2, p. 163] can be used and is as follows:

$$l_{\text{fus}} = a\, W_{\text{G}}^{C} \quad (59)$$

where

l_{fus} = Fuselage length in feet
a = Empirical coefficient (use 0.504 for twin-turboprop aircraft)
W_{G} = Gross weight in lbs
c = Empirical coefficient (use 0.476 for twin-turboprop aircraft)

The fuselage mass can alternatively be found according to:

$$W_{\text{fus}} = k_{\text{wf}}\sqrt{V_{\text{D}}\frac{l_t}{b_{\text{fus}} + h_{\text{fus}}}}S_{\text{G}}^{1.2} \quad (60,\ [3, \text{eq. } 16])$$

Here, $V_{\text{D}}D$ is the dive speed in equivalent airspeed (EAS) in m/s, $k_{\text{wf}} = 0.23$, S_{G} is the gross shell area of the fuselage in m^2, b_{fus} the fuselage width in m, h_{fus} the height of the fuselage in m, and l_{t} is the tail arm between the 25% chord location of the root chord of the main wing and the horizontal tail, measured in top-view on the fuselage centerline (consult fig. D-2 from [3]), to find W_{fus} in kg. For cabin pressurization, 8% must be added, and an additional 4% for fuselage-mounted engines. If the main landing gear is attached to the fuselage, an extra 7% should be added. For freighter aircraft, an extra 10% should be added. In case there is no attachment structure or landing gear bay, 4% may be subtracted.

Landing gear mass
The landing gear mass (of main gear and nose gear) can be found according to:

$$W_{\text{uc}} = k_{\text{uc}}\left(A + B \cdot W_{\text{TO}}^{3/4} + C \cdot W_{\text{TO}} + D \cdot W_{\text{TO}}^{2/3}\right) \quad (61,\ [3, \text{eq. } 17])$$

Here, k_{uc} is 1 for low-wing aircraft and 1.08 for high-wing aircraft. For retractable nose gear: $A = 9.1, B = 0.082, C = 0, D = 2.97e^{-6}$ and for retractable main gear: $A = 18.1, B = 0.131, C = 0.019, D = 2.23e^{-5}$. The resulting mass is in kilograms.

Nacelle and pylon mass
Nacelle mass, including pylon and extended nacelle structure, as well as noise suppression materials, struts, firewalls, and baffles, must be added on top of the mass of the engine installation (see VI.F). For regional propeller aircraft, the mass in kilograms is related to the equivalent take-off shaft horsepower. 0.018 kg per horsepower must be added if the landing gear is retractable into the nacelle, and another 0.05 kg for over-wing exhausts.

$$W_{\text{n}} = 0.0635 \cdot \text{ESHP}_{\text{TO}} \quad (62,\ [3, \text{p. } 24])$$

For aircraft with pod-mounted turbojet or turbofan aircraft ($k_{\text{TO}} = 0.055$) and high-bypass-ratio turbofan aircraft ($k_{\text{TO}} = 0.065$), the mass in kilograms is related to the take-off thrust. The mass may be reduced by 10% in case no thrust reverser is present.

$$W_{\text{n}} = k_{\text{n}} \cdot T_{\text{TO}} \quad (63,\ [3, \text{eq. } 25])$$

Tips and Tricks:

- The integration of novel energy carriers or propulsion systems may impact certain airframe component masses directly, not only through their presence but also through their location. For example, a fuselage-integrated hydrogen tank implies extra fuselage length or width, in addition to adding an airframe component (the tank). Similarly, including batteries requires additional volume, which must be considered in aircraft sizing (as for the hydrogen tank, see [48, 49]). It can also be necessary to include extra mass penalties to account for structural reinforcements or crash structures. However, these penalties are generally unknown until a higher fidelity weight estimation is performed. Therefore, it is advisable to perform sensitivity studies on the effects of those components that are "novel" (i.e. those that are not found in the statistical dataset underlying the Class II mass estimation method that is used) by making conservative and optimistic assumptions if no information is available, or by using physics-based methods to assess their impact in more detail if needed. This can be done in the sizing calculations themselves or using the tools listed in Sec. VIII.

- Be very cautious about combining various handbook methods. Some authors use slightly different component breakdowns or include specific factors for specific aircraft categories or configurations. A common source of errors is also the unit that is used or the units of the various parameters in the relations.

F. Powertrain (Class II)

1. Fuel-Burning Powertrain Components
Following the treatment of Chapter 6 of Gudmundsson [6] and Chapter 15 of Raymer [2], the mass of a fuel-burning aircraft propulsion system consists of the following components:

- Installed-engine mass, which is further subdivided as follows:
  - Engine mass: the mass of the uninstalled engine.
  - Air inlet & exhaust, including thrust reversers if used.
  - Propeller mass (if a propeller is used).
  - Gearbox mass (if a gearbox is used).
  - Installation mass: the mass of the engine controls, starters, propeller controls (if used), and oil system.
- Fuel system mass: the mass of fuel tanks and associated systems (fuel lines, pumps, vents, controls, etc.).

Uninstalled engine
Uninstalled-engine mass m_{engine} is best obtained from data for existing engines, such as from Refs. [50, 51]. In the absence of such data, m_{engine} can be estimated via

$$m_{\text{engine}} = \begin{cases} K_{\text{engine}} P_{\text{rated}} + m_0 & \text{for piston, turboprop, or turboshaft engines} \\ K_{\text{engine}} T_{\text{rated}} + m_0 & \text{for turbofan engines} \end{cases} \tag{64}$$

where m_{engine} is the mass of a single uninstalled engine, P_{rated} and T_{rated} are the rated engine power[††] and thrust respectively, and K_{engine} and m_0 are constants. Values for the latter two parameters are provided in Table 16.

Table 16 Engine mass constants for use with Equation 64.

	$\mathbf{K_{engine}}$	$\mathbf{m_0}$
Piston	0.814 kg/kW; 1.338 lb/hp	23.2 kg; 51.0 lb
Turboprop	0.225 kg/kW; 0.369 lb/hp	-4.4 kg; -9.8 lb
Turboshaft	0.077 kg/kW; 0.126 lb/hp	101.1 kg; 222.9 lb
Turbofan	17.55 kg/kN; 0.172 lb/lbf	256.6 kg; 565.8 lb

The constants in Table 16 were obtained by applying a linear regression to an author-compiled database of popular aircraft and helicopter engines (mostly from Ref. [51]). This approach is similar to that in Chapter 6 of Gudmundsson [6], although the focus in this work is on engines that are still in production.

Installed engine
The next step is to obtain the mass of the installed engine(s) $m_{\text{installed}}$, not including the propeller or gearbox (if either are used). $m_{\text{installed}}$ can be estimated via

$$m_{\text{te}} = m_{\text{installed}} = \begin{cases} 1.223\ m_{\text{engine}} N_{\text{engines}} & \text{for piston engines} \\ 1.205\ m_{\text{engine}} N_{\text{engines}} & \text{for turboprop engines} \\ 1.128\ m_{\text{engine}} N_{\text{engines}} & \text{for turbofan engines} \end{cases} \tag{65}$$

where m_{engine} is the mass of an uninstalled engine (from data or Equation 64) and N_{engines} is the number of engines. The leading constants in Equation 65 were obtained by applying a linear regression to aircraft mass data from Appendix A

[††] Rated power in Equation 64 refers to the brake power (before transmission) for piston engines, but to the shaft power (after transmission) for turboprops. Brake and shaft power are identical for piston engines without gearboxes, but shaft power is typically slightly lower if a gearbox is used.

of Roskam [50]. This approach is similar to that from Table 15.2 of Raymer [2], but propeller mass is broken out separately here in case the engine is used as a turbogenerator (in which case no propeller is used). Equation 65 does not include a model for turboshaft engines; the turboprop model may be applied to turboshafts with caution.

Propeller mass $m_{\text{propellers}}$ (if used) can be estimated for piston engines via

$$m_{\text{propellers}} = K_{\text{prop}}\ m_{\text{engine}} N_{\text{engines}} \tag{66}$$

and for turboprop engines via

$$m_{\text{propellers}} = K_{\text{prop}} P_{\text{rated}}^{0.678} N_{\text{engines}} \tag{67}$$

where K_{prop} is a constant, equal to 0.221 for piston engines and 1.003 kg/kW$^{0.678}$ (1.812 lb/hp$^{0.678}$) for turboprops. The K_{prop} value for piston engines (Equation 66) was obtained by applying a linear regression to piston-engine propeller mass data from Appendix A of Roskam [50]. The K_{prop} value for turboprop engines (Equation 67) was obtained using propeller mass data from Table 6.2 of Filippone [52]. A linear regression worked poorly at higher engine-rated power, so Equation 67 was instead generated using a monomial fit [53].

Gearboxes

In addition to first-principles torque-density sizing [54], the mass of a reduction gearbox (if used) can be estimated using empirical correlations derived from existing aerospace planetary gearbox designs. Tallerico *et al.* [55] present a performance-based mass scaling relationship that relates gearbox mass to the transmitted power and the input/output shaft rotational speeds. The original form of the correlation is expressed as:

$$m_{\text{gb}} \propto \text{HP}^{0.76} \left(\frac{\text{RPM}_{\text{in}}^{0.13}}{\text{RPM}_{\text{out}}^{0.89}} \right), \tag{68}$$

where m_{gb} is gearbox mass, HP is transmitted shaft power in horsepower, RPM_{in} is the input shaft speed, and RPM_{out} is the output (propeller) shaft speed. To express this in terms of torque and gear ratio, we note that the output torque is given by:

$$P = T_{\text{out}} \omega_{\text{out}}, \tag{69}$$

and the gear ratio is defined as:

$$r = \frac{\omega_{\text{in}}}{\omega_{\text{out}}}. \tag{70}$$

Substituting these relations into (68) and simplifying yields:

$$m_{\text{gb}} \propto T_{\text{out}}^{0.76} r^{0.13}. \tag{71}$$

Equation (71) highlights the dominant influence of output torque on gearbox mass, reflecting the structural requirements imposed by tooth contact stress and shaft bending. The weak dependence on gear ratio ($r^{0.13}$) indicates that increasing the reduction ratio does not significantly increase mass unless additional stages are required. This relationship is particularly useful in early-stage propulsion architecture studies, where motor speed, propeller speed, and required shaft torque are known, but detailed gear geometry has not yet been defined. If propeller speed is unknown, using the propeller diameter and setting the tip Mach number around Mach=0.8-0.83 can be used to estimate rpm out, and rpm in would then be determined by the gearbox gear ratio.

Fuel system

The final component of fuel-burning propulsion-system mass is that of the fuel system. Rodriguez and Liscouët-Hanke [56] provide an empirical model for fuel-system mass $m_{\text{fuel system}}$ of general-aviation and narrowbody transport aircraft weighing less than 175,000 lbs. It is reformulated here as

$$m_{\text{fuel system}} = K_{\text{fs}} m_{\text{f}}^{0.480} \times 10^{0.297 N_{\text{engines}} + 0.028 N_{\text{tanks}}} \tag{72}$$

where m_{f} is the fuel mass, N_{engines} is the number of thermal engines, and N_{tanks} is the number of fuel tanks. K_{fs} is a constant, equal to 0.454 kg$^{0.52}$ (0.686 lbs$^{0.52}$).

Tips & tricks

- Turboshaft engines, especially those with a takeoff power above 1000 kW, can be much lighter than turboprop engines with the same rated power. For example, Equation 64 predicts that the uninstalled mass of a 2000 kW turboprop engine is about 446 kg, but the uninstalled mass of a turboshaft with the same power is about 255 kg (43% lower). However, turboprop engines are generally more fuel-efficient than turboshafts: about 10-15% more efficient is typical based on specific fuel consumption at max thrust. Therefore, turboshaft engines may be more useful for reserve energy systems (ex. [31, 44]), where efficiency matters little because the engine is only used in emergencies. By contrast, turboprops may be more useful for aircraft where the engine is the primary power source on every flight, since fuel efficiency is paramount in such an application. A trade study may help select the optimal engine type.
- The maximum continuous power of turboprop and turboshaft engines is typically about 80% of their maximum rated power. If either engine type is to be sized by continuous power (as may be the case for a turbogenerator), its rated power in Equation 64 can therefore be estimated as $P_{\text{rated}} = 1.25P_{\text{continuous}}$.
- Turboprop-engine propellers can be much heavier than piston-engine propellers. For example, the PT6A-67B turboprop (which powers the Pilatus PC-12) has a mass of 240.4 kg and a rated power of 895 kW [51]. Equation 67 for turboprops shows that a propeller for this engine should weigh about 100.6 kg (41.9% of uninstalled-engine mass). However, if a piston engine were used instead, Equation 66 shows that a propeller should weigh 22.1% of uninstalled-engine mass, just over half the value for a turboprop. This difference is explained in part by the mass of the governor[‡‡]. A propeller equipped with a governor is called a constant-speed propeller, which is needed by turboprop propellers but not by the fixed-pitch propellers often used with piston engines.
- Most of the models in this section are empirical and are derived from data from conventional aircraft. Therefore, they may be inaccurate for use with hybrid-electric aircraft. Physics-based sizing methods that are applicable to hybrid-electric aircraft are discussed in Section VI.G.3.

2. Electric Powertrain Components

Batteries

Demand for fuel-free propulsion systems has accelerated the development of electrochemical energy storage technology. Increased use of battery technologies in aviation, including Nickel-Cadmium (Ni-Cd), Sealed Lead-Acid, and Lithium-Ion (Li-Ion) chemistries, has occurred in recent decades [57–59]. While battery-electric aircraft offer improved powertrain efficiency and scalability, their widespread adoption is hindered by the low specific energy of current battery technologies [60]. Current efforts aim to improve energy density, power density, cycle life, and safety. Significantly, programs such as ARPA-E's PROPEL-1K seek to advance battery technology to reduce aviation-related emissions. Safe operation and endurance depend on the cell's ability to foresee energy, load, and temperature. We need standard language to avoid confusion in this section before addressing techniques for analyzing these features. A *cell* refers to the smallest independent energy source, which can be in cylindrical, pouch, or prismatic format. A *module* is a regular electrically connected set of cells. Finally, a *pack* can be thought of as a collection of modules on the vehicle that collectively power an electric powertrain. All non-cell components of a pack contribute to its mass overhead, denoted k_{pack}. Current collection, pack configuration, heat protection and management, battery management, and others will be covered. Advanced packs have a 15-20% overhead [61].

When determining the battery mass, the sizing condition can be either the energy required from the battery to perform the mission – as is usually the case – or the maximum power required from the battery. If it is unknown beforehand which of the two cases is limiting, we must evaluate both and select the most limiting one (i.e. the heaviest). Battery volume is not addressed here since it does not directly affect the sizing calculations of the aircraft as presented in this paper; however, it is important to verify that the battery volume fits in the aircraft. For more information, see Appendix D subsection D and Heit and Liscouët-Hanke [62].

Sizing for Energy: The mass of the battery pack is determined by the amount of battery energy required for the mission E_{bat} and the usable energy density at pack-level, e_{bat}:

$$m_{\text{bat}} = \frac{E_{\text{bat}}}{e_{\text{bat}}}, \tag{73}$$

[‡‡]A governor is a device that automatically varies the propeller blade pitch to maintain a set engine RPM [3]

where e_{bat} is expressed in J/kg instead of the typical Wh/kg, if E_{bat} is expressed in Joules.

The usable battery energy density at pack-level depends on the cell energy density and a series of "knockdown" factors, as described in Ref. [61]. If e_{cell} is the energy density of a new cell as measured in an infinitely slow discharge (i.e. without internal losses), then we can relate the two through

$$e_{\text{bat}} = e_{\text{cell}} \cdot k, \tag{74}$$

$$k = k_{\text{pack}} k_{\text{DOD}} k_{\text{SOH}} k_R. \tag{75}$$

In Eq. 75, k_{pack} accounts for the mass overhead of the pack components relative to the cells alone, k_{DOD} accounts for the maximum depth of discharge that the battery can reach for safety and charging-time reasons, k_{SoH} accounts for degradation in capacity[§§] (State of Health) as the battery ages, and k_R accounts for losses due to internal resistance when discharging at a finite rate (i.e. the cell discharge efficiency). Table 17 provides ranges of typical values that can be assumed for these factors, based on literature and the author's experience. Table 18 provides typical cell energy densities that can be assumed, depending on the technology type, if not known beforehand.

Table 17 Typical ranges of values for each of the knockdown factors that relate (new) cell energy density to (usable) pack energy density.

Parameter	Typical values	Notes
k_{pack}	0.7 – 0.85	Typically ≤0.8 for commercial aircraft due to stringent safety requirements.
k_{DOD}	0.8 – 0.9	Depends on cell chemistry and on how long charging is allowed to take.
k_{SOH}	0.8 – 0.9	This is a choice: how much capacity loss is allowed before the battery is swapped.
k_R	0.9 – 0.95	Depends on cell chemistry and is lower for higher discharge rates.

Table 18 Simplified overview of typical state-of-the-art cell energy density assumptions for different technologies.

Technology	e_{cell}
Mainstream Li-ion cells with good power density, cycle life (> 1000 cycles), and low costs	~200 Wh/kg
High-performance Li-ion cells with good power density and cycle life (>1000 cycles)	~300 Wh/kg
High-energy advanced Li-ion cells with moderate power density and cycle life (~300 cycles)	~400 Wh/kg
Lab-level high-energy density cells (Li-metal or solid state) with low cycle life (< 100 cycles)	~500 Wh/kg
Next-generation Li-metal or solid state cells (>100 cycles)	>500 Wh/kg
Non-rechargeable (primary) cells with low power density, such as Al-air	>1000 Wh/kg

Finally, if more information is known about the battery, such as the energy content per cell E_{cell} and the number of cells required in series (n_{s}) and parallel (n_{p}) to match a particular pack voltage level and total energy content, then more refined mass estimates can be made using (with the cell energy density in J/kg):

$$m_{\text{bat}} = k \frac{E_{\text{cell}}}{e_{\text{cell}}} n_{\text{p}} n_{\text{s}}. \tag{76}$$

Sizing for Power: In this case, the mass of the battery pack is determined by the maximum battery power required for the aircraft (as obtained from the SMP diagrams in Sec. V.B) and the battery specific power (in W/kg), sometimes referred to as the battery power density. Again, we need to make a distinction between the power density at a pack level, p_{bat}, and at a cell level, p_{cell}. For simplicity, we assume here that the maximum power a cell can deliver is independent of the duration of the power pulse, the cell's state of charge, and the cell's state of health. We also assume that the reduction in maximum discharge power due to internal losses is negligible; in practice, the higher the discharge rate, the higher the losses. Under these conditions,

$$m_{\text{bat}} = \frac{P_{\text{bat}}}{p_{\text{bat}}}, \tag{77}$$

[§§]For simplicity, we assume a reduction in battery capacity directly translates into an equal reduction in battery energy.

$$p_{\text{bat}} = p_{\text{cell}} \cdot k_{\text{pack}}, \tag{78}$$

where typical values of the pack mass knockdown factor are given in Table 17.

For the cell power density p_{cell}, one can make a table similar to Table 18 but focusing on the W/kg characteristics of the cells, instead of the Wh/kg. However, it is more common to express the discharge capabilities of a cell in terms of the discharge rate or "C-rate", C, measured in h^{-1}. Table 19 shows typical values of maximum discharge rates for different types of cells. By combining a value from this table with a value from Table 18, we can obtain the assumed cell power density through

$$p_{\text{cell}} = e_{\text{cell}} \cdot C. \tag{79}$$

Note that in practice, the maximum discharge rate is not a clearly defined value but a grey area which, if exceeded, drastically reduces cell life or increases internal resistance and thus the heat production and risk of thermal runaway significantly. Also note that cells that are designed for high energy density typically present a low power density, i.e. if we assume a high energy density in Table 18, then it is more realistic to assume a lower maximum C-rate in Table 19. Referencing a Ragone plot[63] will help ensure a realizable pair of energy and power density is used for a given battery cell chemistry.

Table 19 Simplified overview of typical state-of-the-art cell maximum discharge rates.

Technology	C
Ultra-high-energy-density cells, cells for consumer electronics, or non-rechargeable cells like Al-air	<0.5 h^{-1}
High energy density cells with moderate power capabilities	1 – 2 h^{-1}
High power cells with lower energy density	2 – 5 h^{-1}

Supercapacitors

Supercapacitors can act as complementary energy storage devices to both batteries and fuel cells. While supercapacitors offer very high specific power (in the order of several kW kg^{-1}), their specific energy remains relatively low (typically only a few Wh kg^{-1}) compared to batteries and hydrogen fuel cells. This characteristic makes them particularly well-suited for handling short-duration, high-power transients, such as those during takeoff, landing, or load fluctuations. At the same time, the batteries or fuel cells provide the sustained energy supply required for longer-duration flights. The useful energy stored in a supercapacitor pack is given by [64]:

$$E_{\text{SC}} = \frac{3}{8} \frac{N_{\text{PSC}}}{N_{\text{SSC}}} C_{\text{cell}} V_{\text{SC}}^2 \tag{80}$$

where C_{cell} is the nominal capacitance of one cell (F), V_{SC} is the maximum voltage of one cell (V), N_{SSC} and N_{PSC} are the numbers of series and parallel cells, respectively.

The total mass of the supercapacitor pack can be obtained from its useful energy and specific energy density ρ_{SC} (Wh/kg) as

$$m_{\text{SC}} = \frac{E_{\text{SC}}}{\rho_{\text{SC}}}. \tag{81}$$

If electrical efficiency η_{SC} of the system is included, then

$$m_{\text{SC}} = \frac{E_{\text{req}}}{\eta_{\text{SC}}\, \rho_{\text{SC}}}, \tag{82}$$

where E_{req} is the required useful energy to be delivered to the DC bus.

Motors/Generators

An electrical machine is an energy conversion device that transforms electrical energy into mechanical power (motor mode) or vice versa (generator mode) through electromagnetic interactions. High torque density can be achieved by operating at higher rotational speeds (>20,000 rpm) and designing for higher current densities (> 25 A/mm^2), both of which enable greater power output within strict mass and volume limits. However, these improvements demand careful management of thermal stresses, material limits, and rotor dynamics. Effective integration with fuel cells and batteries further relies on a co-designed propulsion system, where electrical, thermal, and control subsystems are developed in close partnership. Such collaborative design ensures optimal power sharing, manages thermal interactions, and enhances overall system efficiency and reliability.

The simplest way to estimate the mass of an electric machine is by assuming a power density, typically expressed in kW/kg. Aircraft-level design parameters that strongly influence the power density of the machine include the motor diameter, rotational speed, and the type of cooling. Values for power density can range from ~5 kW/kg for a direct-drive machine (i.e. at the typical RPM of a propeller) to over 15 kW/kg for state-of-the-art high-speed machines (see e.g. Ref. [65]), in some cases even exceeding 50 kW/kg in terms of peak power[¶¶]. When selecting a power density based on literature, it is important to verify that the value is expressed with respect to maximum continuous power, that the machine can provide the right RPM (else additional mass of a gearbox is needed), and whether the mass includes the inverter and/or elements of the cooling system.

A second approach, which can be more accurate—since current, and thus torque, is the main driver of the mass of active parts of the machine—is to estimate the mass based on the torque density. From the relation between power, torque, and the motor speed ω in rad/s, we get:

$$m_{\text{motor}} = \frac{P_{\text{em}}}{T_{\text{TorqueDensity}}\,\omega} \tag{83}$$

where m_{motor} is the motor mass, $T_{\text{TorqueDensity}}$ is the motor torque density without its cooling, $\omega = \frac{2\pi\,\text{RPM}}{60}$ with rotational speed in revolutions per minute and P_{em} is the motor shaft power. For a detailed high-fidelity modelling of a motor, refer to [66] and [67]. Reference [68], pages 75-77, presents various existing electrical machine data that could be used as a starting point for calculating motor mass.

Inverter

An inverter is a power electronic converter that transforms direct current (DC) from sources such as batteries or fuel cells into controlled alternating current (AC) to drive electrical machines. Achieving high power density and high efficiency in aerospace inverters relies on advanced wide-bandgap (WBG) semiconductors; notably silicon carbide (SiC) and gallium nitride (GaN), which allow higher switching frequencies, lower losses, and operation at elevated temperatures, reducing cooling mass and volume. The design strategy depends strongly on the voltage–current trade-off: at high voltage and low current (e.g., 2–5 kV systems), conduction losses are reduced and cabling becomes lighter, but insulation, EMI, and partial discharge withstand capability become critical; conversely, low-voltage, high-current designs (e.g., 48–800 V fuel-cell systems) require heavy parallelization, thick busbars, and advanced cooling to manage extreme conduction losses. High efficiency inverters can reach efficiencies above 99% and power densities of 12 kW/kg using SiC MOSFETs [69], with recent developments targeting values over 20 kW/kg. In contrast, cryogenic inverters, designed for superconducting machines, operate at or near cryogenic temperatures (20–80 K) and can handle kiloampere-level currents with minimal resistive loss. These systems integrate with the cryostat and may use superconducting links to minimize $R \times I^2$ heating, while non-cryogenic inverters remain thermally isolated and cooled at ambient conditions. Overall, the co-design of inverter, motor, and thermal architecture, whether cryogenic or conventional, is essential to achieve the extreme efficiency, reliability, and integration required for next-generation electrified aircraft propulsion.

Inverter mass m_{inverter} can be estimated as

$$m_{\text{inverter}} = \frac{P_{\text{inverter}}}{PD_{\text{inverter}}} \tag{84}$$

where PD_{inverter} is the power density of the inverter and P_{inverter} is the maximum rated power of the inverter. For a simple inverter model, refer to [66]. For a detailed understanding of power electronics and converter design, refer to [70] and [71].

[¶¶] See for example `https://yasa.com/news/yasa-smashes-own-unofficial-power-density-world-record-pushing-state-of-the-art-electric-motor-to-staggering-new-59kw-kg-benchmark/` (accessed 12 May 2026).

Cables

Cables for high-voltage, low-current architectures minimize cable cross-section and resistive losses, reducing cabling mass and improving transmission efficiency. However, they introduce challenges in insulation and partial discharge control, particularly under reduced-pressure flight environments where dielectric strength degrades [72]. In contrast, low-voltage, high-current systems simplify insulation design and mitigate arcing risks but suffer from significant conduction losses, increased thermal load, and heavier conductors. These resistive losses scale quadratically with current, motivating interest in superconducting cables, which can carry kiloampere-level currents with negligible resistive loss when cooled below their critical temperature. Superconducting distribution could therefore enable low-voltage, high-current propulsion architectures, provided the cryogenic infrastructure is efficient and lightweight [73]. The choice between DC and AC transmission further influences system behaviour: DC systems reduce reactive losses and simplify rectification, while AC offers easier isolation and compatibility with electrical machines. To mitigate cabling penalties and thermal losses, we favour highly co-located, integrated architectures that combine inverters, motors, and energy sources into compact propulsion units, minimizing current transmission distances and enhancing the overall power density, efficiency, and reliability of the aircraft's electrified powertrain.

Cable mass m_{cable} can be estimated as

$$m_{\text{cable}} = L\,(\rho_c A_c + \rho_i A_i) \tag{85}$$

where L is the cable length, ρ_c is the density of conductor, ρ_i is the density of insulation, and the cross-sectional areas of conductor and insulation are A_c and A_i. For detailed modelling of cables, refer to [74]. Azizi and Ghassemi [75] provide the necessary information to determine the minimum conductor cross-sectional area required for a given current level. Once that area is known, cable mass can be calculated using basic geometric and material relationships. However, simple cable mass estimation ultimately depends on the available installation space, routing constraints, and material selection (e.g., copper versus aluminum conductors, insulation type and thickness). After selecting a feasible conductor geometry and insulation thickness meeting voltage and partial discharge requirements, the cable mass can be calculated.

For example, for a preliminary sizing of 800 V aircraft power distribution systems, rule-of-thumb mass-per-length values can be adopted based on published data. For a single power cable run (one insulated and shielded conductor typical of aircraft transmission), readers may assume approximately 0.5 to 0.8 kg/m for cables in the 300 to 400 A class. For higher current levels in the 450 to 650 A range, mass typically increases to approximately 0.9 to 1.5 kg/m, corresponding to conductor cross-sections on the order of 100 mm^2. For very high-current runs requiring large cross-sections or parallel conductors, installed cable mass may reasonably fall in the range of 1.5 to 3 kg/m, particularly once insulation, shielding, and installation hardware are included. These values provide first-order assumptions for conceptual powertrain mass estimation, with refinement performed through detailed ampacity and insulation coordination analysis.

Other electric powertrain components

Other components, such as circuit protection devices (e.g. fuses, circuit breakers, power controllers), voltage regulating devices (e.g. DC-DC transformers), charging ports, and brackets, add additional mass to the system. Whether such components are required or how many are required is highly dependent on the electrical system architecture, which is generally not yet known in the early conceptual design phase. No equations for these elements are provided in this paper, and therefore, it is good to add some margin to the estimations made using the equations of the sections above. Alternatively, the designer can find sources where the whole power distribution system is sized, and compute an equivalent "kW/kg" power density of all systems combined. Of these additional components, particularly DC-DC converters can add a significant mass penalty. On the flip side, they allow the motors and other elements to operate at a constant voltage, which would in turn reduce their mass.

Tips & tricks

- The mass contribution of "other powertrain components" can be significant; in fact, it can be larger than the mass of the cables, depending on the architecture and physical layout of the powertrain. In case of doubt, it is highly recommended to be conservative and include margins. The same can be said for Thermal management systems mass (following section).
- Most correlations in this section ignore the impact of system voltage, which has a large impact on the mass of electrical components. After performing the conceptual design using the equations provided here, the system

voltage is one of the main design choices to investigate in more detail. The availability of off-the-shelf components can play a large role in that decision, with components below 800 VDC typically being readily available or under development, while higher voltages (e.g. 3 kV) are still in very early development stages.

3. Thermal Management

The thermal management system (TMS) can be modelled in different ways, typically requiring an estimate/sizing per component of the powertrain since the TMS mass is highly dependent on the architecture, duration of heat rejection required and operating envelope of the powertrain in question. If those details are not available yet, Ref. [25] provides ranges of values of TMS mass per kW of heat load rejected on the powertrain as a whole for different aircraft categories. For other aircraft-level TMS assessments, see e.g. Refs. [76, 77]. In any case, the mass estimation should be done per component (motor, battery, etc.) if sufficient information is available.

Battery Cooling/Heat Removal Systems The Battery Thermal Management System (BTMS) mass can be estimated using a physics-based approach, following [78]. The system is sized based on the peak battery heat generation during the mission. The heat that must be rejected by the BTMS is approximated as

$$\dot{Q}_{\text{gen}} = P_{\text{bat}}(1 - \eta_{\text{bat}}), \tag{86}$$

where P_{bat} is the peak battery power and η_{bat} is the battery discharge efficiency.

The BTMS is sized to remove this heat load, and its mass is approximated as the sum of the main components

$$m_{\text{BTMS}} \approx m_{\text{HAS}} + m_{\text{HEX}} + m_{\text{aux}}, \tag{87}$$

where, m_{HAS} = heat acquisition system (cooling plates/channels), M_{HEX} = heat exchanger and m_{aux} = pumps, coolant, reservoir, and plumbing.

The component masses are determined from the required heat transfer performance and resulting geometry, as described in [78]. For a top-level design, the BTMS mass can be related directly to the required heat rejection

$$m_{\text{BTMS}} \propto 0.6\dot{Q}_{\text{gen}}, \tag{88}$$

indicating that the system mass scales with peak thermal load. For detailed values, refer to Tables 9 and 10 in Ref. [79].

Motor Cooling/Heat Removal Systems

Cooling techniques for conventional electrical machines (non-superconducting, non-cryogenic) include a range of air, liquid, and phase-change systems designed to manage rising thermal loads. Air cooling remains prevalent in low- to medium-power applications due to its simplicity and low maintenance. Air cooling depends strongly on how the motor is integrated within the overall system and on how effectively the cooling airflow is directed over the motor. This must be addressed at the system design level; otherwise, it may lead to additional weight penalties [80]. In contrast, liquid cooling, using water-glycol or dielectric fluids, is preferred for compact, high-power-density systems, enabling direct heat removal from stator windings or housing. Advanced approaches such as oil-spray, micro-channel, and two-phase evaporative cooling further enhance performance [81]. Cooling strategies must adapt to design considerations (geometry, insulation materials, and environmental conditions), evolve with motor age as thermal paths and insulation degrade, and intensify with increasing current density, which elevates resistive losses and necessitates more effective active cooling to preserve diverse operating conditions at higher efficiencies.

The mass of the motor cooling system can be estimated using

$$m_{\text{motorCooling}} = \frac{P_{\text{Motorloss}}}{PD_{\text{motorCooling}}} = \frac{P_{\text{inverter}}(1 - \eta_{\text{motor}})}{PD_{\text{motorCooling}}} \tag{89}$$

where $PD_{\text{motorCooling}}$ is the power density of the motor cooling system (thermal management system), and the unit is considered to be kW/kg. P_{inverter} is the inverter power (equal to the motor shaft power divided by the motor efficiency) and η_{motor} is the motor efficiency***. We can also consider the following equation for a more detailed analysis:

***Note that throughout this paper we use the parameter $\eta_{\text{em}} = \eta_{\text{motor}} \cdot \eta_{\text{inverter}}$ to refer to the overall efficiency of the electric motor including inverter, since these are often installed together.

$$m_{\text{motorCooling}} = \frac{Q * t_{\text{coolantCirculation}}}{c_p \Delta T} \tag{90}$$

Where $Q = P_{\text{loss}} = P_{\text{inverter}}(1 - \eta_{\text{motor}})$ and $t_{\text{coolantCirculation}}$ is the total time that the coolant stays in the system or the residence time. By rearranging, we have:

$$m_{\text{motorCooling}} = \frac{P_{\text{inverter}}(1 - \eta_{\text{motor}}) * t_{\text{coolantCirculation}}}{c_p \Delta T} \tag{91}$$

Where:

- $Q = P_{\text{loss}}$: Heat to be dissipated
- c_p: Specific heat capacity of the cooling medium (e.g., for water, $c_p \approx 4184\,\text{J/kg} \cdot \text{K}$)
- ΔT: Allowable temperature rise of the cooling medium (in K)

Students can use the specific heat rejection values reported by [82] and [83] as a top-level sizing parameter for the preliminary estimation of the motor cooling mass. In this study, aircraft thermal management systems are reported to achieve approximately $PD_{\text{motorCooling}}$ of 1 to 2 kW/kg, with a more conservative effective range of 0.83 to 1.67 kW/kg when additional pump and plumbing mass is included.

Selecting the lower bound ($\approx$ 0.8 kW/kg) provides a conservative estimate suitable for early-stage design, while higher values ($\approx$ 1.5 to 2 kW/kg) can represent advanced or aggressively optimized systems. This approach enables rapid system-level trade studies without requiring detailed thermal modelling during preliminary design.

Inverter Cooling/Heat Removal Systems

In conventional (non-superconducting) systems, inverter cooling focuses on efficiently dissipating the heat generated by power semiconductor switching and conduction losses (from devices like IGBTs or SiC/GaN MOSFETs). The most common method is liquid cooling, where cold plates or micro-channel heat sinks transfer heat from the semiconductor modules to a coolant such as water–glycol. The cooling design depends on power level, switching frequency, packaging density, and environmental conditions. As current density and switching speed increase in modern inverters, advanced thermal interface materials, heat spreaders, and integrated liquid-cooled substrates are increasingly adopted to ensure reliable operation, compactness, and extended component lifetime.

$$m_{\text{inverterCooling}} = \frac{P_{\text{Inverterloss}}}{PD_{\text{inverterCooling}}} = \frac{P_{\text{bat}}(1 - \eta_{\text{inverter}})}{PD_{\text{inverterCooling}}} \tag{92}$$

where $PD_{\text{inverterCooling}}$ is the power density of the inverter cooling system (thermal management system), and the unit is considered to be kW/kg. This equation assumes that only power from the battery flows to the inverter; in for example a serial configuration where both the battery and the turbogenerator simultaneously power the electric propulsion units, the total electrical power would have to be used instead. As an alternative method, the mass can be estimated following:

$$m_{\text{inverterCooling}} = \frac{P_{\text{bat}}(1 - \eta_{\text{inverter}}) * t_{\text{coolantCirculation}}}{c_p \Delta T} \tag{93}$$

Where:

- $Q = P_{\text{loss}}$: Heat to be dissipated
- c_p: Specific heat capacity of the cooling medium (e.g., for water, $c_p \approx 4184\,\text{J/kg} \cdot \text{K}$)
- ΔT: Allowable temperature rise of the cooling medium (in K)

The concepts of Technology-based thermal management systems can be assessed using scaling expressions that correlate the rejected heat load with TMS mass, parasitic power, and aerodynamic drag for different applications. For electrically driven systems, individual electric-component TMS architectures typically manage heat loads below 200 kW. From the results reported in [82], the corresponding specific heat rejection can be post-processed and is found to range from approximately $1.25\,\text{kW}\,\text{kg}^{-1}$ to $5\,\text{kW}\,\text{kg}^{-1}$. These values provide a practical, top-level metric for early-stage cooling sizing: given a component heat load Q, a first-order estimate of the required cooling-system mass can be obtained via $m_{\text{cooling}} \approx Q/(\text{specific heat rejection})$, with the lower end of the range representing more conservative assumptions and the upper end reflecting more aggressive, advanced TMS concepts.

G. Systems & equipment (Class II)

Estimating the weight of aircraft systems is important, as it can account for up to 30% of the aircraft's empty weight for a conventional aircraft. In addition, the power required by these systems impacts aircraft fuel burn and propulsive power demand; also, ram air cooling and fairings impact aircraft drag. Fig. 12 provides an overview of a conventional system architecture with the main systems groups typically considered for weight estimation.

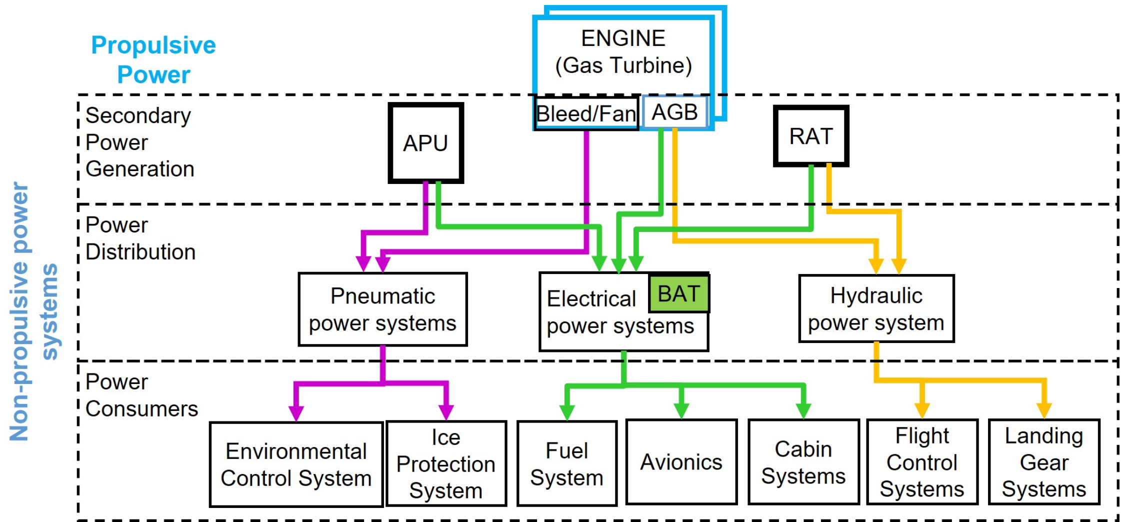

Fig. 12 Overview of a conventional system architecture with main power flow and functional groups, BAT: Battery; AGB: Accessory Gear Box; RAT: Ram Air Turbine; APU: Auxiliary Power Unit

For electric and hybrid electric aircraft, power requirements can inform the sizing of batteries and other energy sources. Furthermore, thermal management systems are becoming increasingly important to address the high heat loads generated by batteries, electrical generators, and other equipment operating at high electrical power levels.

Sizing systems at the conceptual level can be performed using traditional statistical or handbook methods, using physics-based methods, or a mix of both, as required. However, empirical methods should be used only after reviewing the *system architecture*, as the technology of some systems depends heavily on their propulsion architecture. For most hybrid-electric or electric-propulsion aircraft, it is required to implement a partial, so-called "more-electric" system architecture; e.g., pneumatic power from the engine bleed air is no longer available if no gas turbine is used in the propulsive power system.

General guidelines for the typical technologies for various aircraft sizes are provided in Appendix F, Tables 39, 40, and 41. Using these tables, it is recommended to proceed as follows:

1) Analyze **propulsive power type** and redundancy available for the propulsion system (e.g., if the architecture has one or two gas turbines, we can still use bleed air; if we have only batteries, we might need to consider adding APUs or using a bleed-less architecture)
2) Define the **system technology/power type of the consumer systems** (ECS, Ice Protections, Flight Controls, etc) using the guidelines in Tab. 39. Estimate weight and power demand.
3) Define the total **power demand for the power distribution systems** (based on the previous step), for each power type (electrical, hydraulic, pneumatic), according to Tab. 40. Estimate the mass and power required from each power generation source
4) Defined the **needs for secondary power generation** according to Tab. 41.(gas turbine power off-takes, battery-electrical demand, emergency power, etc) and size the system accordingly. Estimate the mass and foresee the corresponding power budget for the propulsion architecture (for ground, normal flight, and emergency operation). The integration of this power over the mission determines the "non-propulsive" energy required for the energy breakdown (Sec. V.D).

1. Mass estimation

In general, the NASA Flight Optimization System (FLOPS) Weight Estimation [84] Method for estimating the weight of aircraft systems is a good starting point; as a semi-empirical method, it utilizes data from existing (older) aircraft to develop mass estimation relations, while ensuring that the derived relations capture the key physical drivers that influence system weight. NASA Flops includes distinguishing between aircraft types (i.e., transport and general aviation), which provides some flexibility in setting mass estimation for a particular system architecture. For more physics-based methods, i.e., for smaller aircraft, and more-electric actuation, [85, p. 9] provides examples and additional references.

2. Subsystem Power Demand Estimation

It is important to account for the electrical power demand of the aircraft systems when sizing the propulsion system. In particular, if the aircraft requires a conditioning and ice-protection system, and if no gas-turbine is available to provide bleed air for these functions. A good approach is to benchmark the electric power generator size for a given aircraft size and system architecture. For ground power demand, the total electrical power provided by the APU must be accounted for; for in-flight power demand, the installed electrical power of the engine-mounted generators must be accounted for. If the conditioning system is bleed-less, the power demand has to be multiplied by a factor of 2-3. In addition [85, p. 25] provides equations for estimating the power demand required by the several subsystems.

3. Tips & Tricks

While deep-diving into the complexity of the system architecture is not possible during concept definition, it is important to ensure that the selected system architecture meets safety, performance, and weight requirements, so as not to discover it later as a "showstopper". As such, system architecture baselines from past aircraft programs can be used, or, where available, formalized and validated heuristics can be used in specifying an initial system architecture. As a general rule, it is recommended to keep the system architecture as simple as possible to minimize additional electrical power demands in a hybrid or electrically powered aircraft (e.g., in small aircraft, keep flight controls mechanically powered if possible). Ref. [85] provides an example evaluation of several system architectures for various degrees of hybridization of a commuter aircraft (Do228). It also provides insights into which parameters to use for a more physics-based approach to various systems of interest and the relevant standard documents that can be used for this purpose. Below are some key items to consider:

- Starting from an existing **system architecture baseline** might be an easier start on the system architecture definition. The reader can select a baseline for an aircraft with similar size and performance characteristics. However, complete system architectures and schematics are rarely available and must be built from descriptions/schematics of individual systems. A good collection of system descriptions is available on SmartCockpit[†††].
- To enhance the baseline approach mentioned above, the following resources provide system architecture heuristics for flight control systems ([86, p. 62],[87], [88, p. 181]) and aircraft fuel systems (also considering hybrid-electric architectures) ([89, p. 23]).
- For a more thorough approach, the reader can follow a **functional approach to the system architecture definition**. Ref. [90] provides insight into how to proceed with the functional approach and provides a list of design drivers for individual systems. In addition, [91] also provides equations for selected subsystems.
- Do not forget to **reserve space for systems** in the aircraft! Typically, 30-40% of the aircraft volume is used to install systems [92]. The following references treat this topic with examples: [92], [93].
- Do not forget the **parasitic drag** that can be caused by systems. If systems need cooling and/or ram air flow, this will create a drag penalty. See Sec. V.A.4 or foresee some margin in your design.
- **Safety** is paramount and might affect weight. The selected system architecture needs to meet safety requirements to be considered feasible. The safety heuristics introduced above help ensure that the architecture has sufficient redundancy. However, a detailed safety assessment is required to demonstrate compliance with safety and certification requirements. At the conceptual design stage, it is possible to perform some elements of safety assessment to ensure that the aircraft configuration under consideration is compatible with the system architecture. Some analyses such as evaluating if sufficient internal volume is available to accommodate the systems [92], ensuring systems are not placed in hazardous zones within the aircraft [94] and evaluating the impact of specific safety risks [93] can be carried out in early design stages.
- Do not forget to add the mass of **operational items** such as flight crew or cabin crew.

[†††] `https://www.smartcockpit.com/my-aircraft/`

VII. System-Level Trade Studies and Operational Strategy

The preceding sections describe the main analyses required to obtain a first conceptual sizing of an electrified aircraft. In practice, these steps are not applied only once to a fixed design. They are repeated across alternative aircraft configurations, propulsion architectures, component ratings, technology assumptions, and mission operating strategies to determine whether a candidate concept is feasible and competitive. For electrified aircraft, this system-level trade-space exploration is especially important because the aircraft configuration, installed power, energy-storage mass, thermal-management requirements, and mission power schedule are strongly coupled.

Consequently, choices such as the degree of hybridization, battery capacity, gas-turbine rating, electric-machine rating, generator sizing, propulsor arrangement, and use of electric power in different mission segments should not be treated independently. A change in one of these variables can shift the active sizing constraint, alter the required wing or power loading, change fuel and battery energy requirements, or introduce additional penalties in thermal management, electrical distribution, and systems integration. Trade studies are therefore used not only to compare final aircraft concepts, but also to test whether assumed technologies, requirements, and operating modes are mutually compatible within the sizing process described in this paper.

Formal multidisciplinary design analysis and optimization (MDAO) methods can support these studies by organizing coupled analyses, automating convergence loops, exploring design spaces, or optimizing selected objectives such as MTOM, fuel burn, energy consumption, emissions, operating cost, or battery life [95–97]. However, a full MDAO formulation is not required for the introductory conceptual-design workflow presented here. The more immediate objective is to make the relevant couplings explicit and to encourage designers to vary architecture, sizing, and operation together rather than optimizing individual subsystems in isolation. As the design matures, the same framework can be expanded toward design-of-experiments studies, surrogate-based trade studies, trajectory optimization, or full multidisciplinary optimization. For hybrid-electric aircraft, especially the optimization of the power split throughout the mission can have a non-negligible impact and has been the focus of numerous studies (see e.g. Refs. [98–100]).

This section, therefore, focuses on one of the most important cross-disciplinary decisions in hybrid-electric aircraft design: the operational strategy. The way electric power is allocated across taxi, takeoff, climb, cruise, diversion, loiter, recharge, and reserve conditions can determine whether hybridization reduces system-level mass and fuel burn or simply adds battery mass and conversion losses. The following subsection discusses how operational strategy can be treated as a design variable and provides guidance for interpreting common modes such as peak-power shaving, climb boosting, electric taxi, cruise hybridization, and in-flight recharge. The discussion focuses on aircraft that use both batteries and energy, in particular when used for longer ranges. However, additional strategies can be considered for aircraft designed for shorter ranges (e.g. use fuel only for reserves or for occasional range extension while using batteries as sole source of energy for most missions [101, 102]) or for military aircraft.

A. Operational Strategy as a System-Level Design Variable

Hybridization is most effective when it is treated as a system-level design variable rather than as an add-on to an otherwise fixed aircraft. In conceptual design, the sizes (i.e., the installed ratings) of the gas turbine, electric machine, generator, battery, and propulsor jointly determine takeoff gross weight, climb capability, cruise fuel burn, and even the active sizing condition of the propulsion system [42, 103, 104]. As a result, the propulsion architecture, component ratings, and energy/power management strategy should be co-designed and, when possible, co-optimized from the earliest aircraft sizing loops.

A useful practical distinction is between *energy substitution* and *power substitution*. Because liquid hydrocarbon fuels continue to provide much higher specific energy than batteries, hybridization is rarely most valuable when electricity is used to replace fuel over long mission durations. Instead, the highest leverage often comes from using electricity to reshape the *power* profile seen by the gas turbine and the aircraft, for example by assisting takeoff, selectively boosting climb, enabling electric taxi, or supporting propulsor arrangements that improve installation or aerodynamic performance [7, 38, 42, 104–106]. The design question is therefore *not* "how much of the mission should be electrified" in the abstract, but rather "*where does electric power change the sizing, matching, or operation of the total system most favorably?*"

The answer depends strongly on the architecture. In a parallel hybrid, the electric machine can directly offset or supplement shaft power and therefore supports gas-turbine downsizing and phase-dependent boost strategies. In a series or turboelectric architecture, the gas turbine is decoupled from at least part of the propulsive load, which creates additional freedom in propulsor placement and engine operating point selection, but also introduces extra conversion losses and new sizing degrees of freedom [39, 107, 108].

For architectures with multiple junctions, redundant branches, power off-takes, or bidirectional flows, a single "hybridization factor" is often too restrictive to represent the full set of admissible operating modes. In such cases, it is generally more informative to work with phasewise source and branch power splits, as formalized by Mokotoff and Cinar [109]. These additional power-split variables are not merely bookkeeping parameters; they introduce operational degrees of freedom that can materially affect the resulting optimum aircraft design. Moreover, this operational freedom can be leveraged by hybrid-electric aircraft flying off-design [106]. When a full power-split optimization is not included in the aircraft sizing loop, the following operational strategies offer practical guidance for how hybrid-electric aircraft may be designed and operated, depending on the propulsion architecture selected:

- **Peak power shaving** is one of the most useful parallel-hybrid design strategies among the candidate operational strategies. In this mode, the gas turbine engine can be downsized toward the top-of-climb requirement, while the electric machine supplies the incremental power needed during takeoff and part of climb [38, 42, 110]. This can reduce engine mass and, more importantly, move the gas turbine toward a more favourable operating region over a larger fraction of the mission. For transport aircraft, this often suggests a design in which cruise power is provided predominantly, and in many cases entirely, by the gas turbine, while battery energy is reserved for short-duration, high-leverage segments. The objective is not to maximize electric energy use per se, but to improve the system-level matching between installed power, mission power demand, and gas-turbine efficiency.
- **Climb boosting** requires more nuanced guidance. Electric boost early in climb may be required when a downsized gas turbine would otherwise violate takeoff or initial-climb constraints, including one-engine-inoperative or minimum climb-gradient requirements. By contrast, boosting the later portions of climb can be advantageous because gas-turbine thrust or shaft power lapses with altitude whereas electric-machine capability is far less sensitive to altitude [42, 104]. Consequently, some aircraft benefit from allocating battery power immediately after liftoff, whereas others benefit more from reserving part of the battery for the upper climb and top of climb. The preferred schedule is therefore aircraft- and mission-dependent. Extending boost for too large a fraction of the climb is also not free: increasing boost power or duration increases required battery energy, which increases battery mass, which in turn increases the power required to meet the same climb performance targets [42].
- **Electric taxi (or e-taxi)** is another operational mode that can be beneficial even when cruise hybridization is not. E-taxi can be accomplished by using one or both installed electric machines to drive the propellers during taxi, or by introducing an additional wheel-motor system. This can reduce fuel burn and local emissions at the airport, while also exploiting the fact that electric machines remain efficient at low torque and speed, whereas turbine engines are comparatively inefficient at low throttle settings [42, 104]. Importantly, e-taxi is not a "free" add-on: the taxi thrust requirement imposes a lower bound on electric-motor sizing, so its benefit must be evaluated inside the same aircraft sizing loop as the other mission modes.
- **Cruise hybridization and in-flight recharge** require particular caution. Even modest cruise hybridization can demand substantial battery energy because cruise duration is long. The resulting battery mass increases takeoff, climb, and landing weight and can erase the intended benefit. In-flight recharge can help when ground charging infrastructure or turnaround time is limiting, but it usually increases block fuel because the gas turbine must supply both propulsive power and charging power. Whether recharge is acceptable is therefore again a system-level trade, not a propulsion-only choice [42, 104].

  Advanced optimization studies can go further by optimizing aircraft sizing variables, the mission profile (trajectory), and mission-point power management simultaneously, rather than prescribing a constant segmentwise hybridization schedule [111]. The designer should also be cautious about the duration of hybridization. Extending battery use over longer segments usually increases required battery energy, which increases battery mass, which in turn increases takeoff gross weight and the power required to satisfy the same field and climb requirements. This positive feedback can erase the apparent benefit of "more electrification" if the electric energy is applied over too much of the mission [39, 42].

VIII. Recommended Tools for Electrified Aircraft Design

Many freely available open source tools and data are available, and are continuously being developed, to analyze electrified aircraft design that implement/extend analyses represented in this paper. Commercial-off-the-shelf (COTS) and Government-off-the-shelf (GOTS) software may outperform this open-source software, but producing a full list of COTS and GOTS software for aircraft sizing relevant to electrified aircraft is beyond the scope of this paper. Therefore, Table 20 summarizes various tools, frameworks, datasets or data exchange formats that are available and useful for (electrified) aircraft design and optimization.

Table 20 Example tools, frameworks and datasets for analysis, design and optimization of electrified aircraft. Tools marked with an asterisk include features developed specifically for electrified aircraft.

Name	Description	Reference
Aircraft Design Frameworks		
NDARC (NASA Design and Analysis of Rotorcraft)*	Aircraft sizing and analysis of existing designs, developed for vertical take-off and landing, but can also be used for fixed-wing aircraft. Contains component performance models. Validation using high-fidelity methods (CREATE-AV [112] for X-57 hybrid electric aircraft). Models, data and validation for X-57 [113] and Airbus Vahana are available [114].	[115]
Aviary*	Multidisciplinary Aircraft Design Framework leverages OpenMDAO and Dymos to address limitations of legacy codes and unconventional designs by providing methods to support higher fidelity analysis.	[116]
FAST*	Open-source, MATLAB-based aircraft sizing environment for rapid conceptual and preliminary design. Combines historical-aircraft regressions with multi-fidelity physics-based models to size and analyze conventional and electrified aircraft, including a wide range of propulsion architectures and operating strategies.	[117]
SUAVE	Open-source, Python-based aircraft conceptual design, focused on analysis and optimization, providing methods for conceptual design	[118]
RCAIDE*	*[Successor to SUAVE]* Open-source, Python-based preliminary design and flight simulation code for both conventional and advanced powertrain aircraft. Leverages advances in scientific computing and multi-fidelity methods to perform MDAO and mission simulation.	[119, 120]
HEAST*	Hybrid Electric Aircraft Sizing Tool, particularly focused on conceptual design of novel powertrain architectures. Enables assessment of individual powertrain component design points.	[121]
MDAO Frameworks		
OpenMDAO	Open-source tool for multidisciplinary design, analysis, and optimization (MDAO). Can be applied to any domain and extended with standalone packages e.g. for surrogate modelling [122].	[123]
DAKOTA	Framework for robust optimization, including a large suite of optimization algorithms (gradient-based, gradient-free and Bayesian). Also suited for uncertainty quantification, sensitivity studies and robust optimization.	[124]
Geometry Modelling and Simulation		
BLENDER	Open-source parametric CAD software	[125]
Engineering Sketch Pad	Toolkit for geometry definition, fully differentiated to provide design parameter sensitivities	[126]
FREECAD	Open-source parametric CAD software	[127]
GASP	Python-based geometry processor and simulation	[128]
OpenVSP	Open Vehicle Sketch Pad, aimed at parametric aircraft geometry generation. Includes aircraft primitives, including hybrid electric and is easily coupled to an integrated aerodynamics solver.	[129]
Aerodynamic, Stability and Flight Dynamics Analysis		
VSPaero	Potential flow solver integrated in OpenVSP [129], can also capture propeller-airframe interactions	[130]
XFOIL	Viscous (or inviscid) analysis of an existing airfoils, airfoil (re)design	[131]
XFLR5	Built on top of XFOIL, providing GUI	[132]

SU2	Open-source software tool for numerical solution of partial differential equations (PDE) and performing PDE-constrained optimization. The primary applications is CFD.	[133]
OpenFOAM	Open-source CFD software	[134]
Aircraft Digital DATCOM	Digital DATCOM is a computer program that implements the methods contained in the USAF Stability and Control DATCOM to calculate the static stability, control and dynamic derivative characteristics of fixed-wing aircraft.	[135]
AVL	Athena Vortex Lattice (AVL) is a program for the aerodynamic and flight-dynamic analysis of rigid aircraft of arbitrary configuration. It employs an extended vortex lattice model for the lifting surfaces, together with a slender-body model for fuselages and nacelles.	[136]
Structural Analysis		
OpenAeroStruct	Aerostructural optimization using OpenMDAO couples a vortex-lattice method (VLM) and a 6 degrees of freedom (per node) 3-dimensional spatial beam model to simulate aerodynamic and structural analyses using lifting surfaces.	[137]
NeoCASS	Free suite of MATLAB modules that combines state-of-the-art computational, analytical and semi-empirical methods to tackle all the aspects of the aero-structural analysis of a design layout at the conceptual design stage.	[138]
Engine and Propeller Analysis		
PyCycle	Thermodynamic cycle modelling library, designed primarily to model jet engine performance. It is built on top of the OpenMDAO framework, and the design is heavily inspired by NASA's NPSS software.	[139]
GSPy	Python-based tool for modelling and simulating propulsion and power system performance. Developed by the creators of GSP.	[140]
T-MATS*	Toolbox for the modelling and Analysis of Thermodynamic Systems, including turbofans and in particular an electrified geared turbofan	[141, 142]
CROTOR	Design and analysis of propeller performance, adds blade lofting	[143]
XROTOR	Design and analysis of propeller performance, based on blade element momentum theory	[144]
Flight Profile Analysis		
FLOPS	Flight profile analysis toolbox is a multidisciplinary system of computer programs for conceptual and preliminary design and evaluation of advanced aircraft concepts. It consists of six primary modules: 1) weights, 2) aerodynamics, 3) propulsion data scaling and interpolation, 4) mission performance, 5) takeoff and landing, and 6) program control.	[145]
DYMOS	Optimal control theory toolbox, leveraging OpenMDAO. Can be used for trajectory optimization.	[146]
Emissions and Life-cycle Assessment		
CASCADE	Boeing Cascade Climate Impact Model is a data modelling and scenario analysis tool that quantifies the potential of decarbonization strategies to cut emissions, including aircraft, operations, energy and offsets.	[147]
OpenAirclim	OpenAirClim is a model for simplified evaluation of the approximate chemistry-climate impact of air traffic emissions. The model represents the major responses of the atmosphere to emissions in terms of composition and climate change. Developed by DLR.	[148]

Aviation Emissions Inventory Code (AEIC)	Combines a variety of data sources to characterize gas emissions from aviation	[149]
Cost modelling		
Comparative Analysis on Aircraft Direct Operating Cost Models*	Summary paper comparing the wide variability in cost prediction across many aircraft conceptual design tools documented in literature.	[150]
Data sets		
UIUC	Airfoil database	[151]
Public Domain Aerospace Software	A repository of many other open-source tools	[152]
Airfoil Tools database	Database of airfoils and airfoil analysis tools.	[153]
U.S. Department of Transportation	Collects data on transportation (historical)	[154]
Bureau of Transportation Statistics	Collection of statistical data on transportation, of particular interest is the dataset on aircraft routes and usage.	[95]
OpenFlights	Data collection of flight data.	[155]
Airport data	Overview of worldwide airport (runway) data.	[156]
Eurostat	European Union statistical office. Collects statistical data across Europe, including transportation and aviation data.	[157]
Data exchange formats		
CPACS	Common Parametric Aircraft Configuration Schema: data definition for the air transportation system. Enables exchange of information between tools. Describes the characteristics of aircraft, rotorcraft, engines, climate impact, fleets and mission in a structured, hierarchical manner. Can also be used to store and process information. Follows a central model approach, reducing the number of interfaces to a minimum. Developed by DLR.	[158]
CMDOWS	Common MDO Workflow Schema: open-source, neutral, data definition and exchange format for MDAO problems (including disciplines, optimizers, tools, their process connections and exchanged data in an MDAO architecture). Neutral XML-based data representation. Can be used to translate any MDO system formulation into an executable workflow and has been extended to also support dynamic MDAO workflows [159], enabling the active switching of product architectures and associated analysis software during optimization. Developed by TU Delft.	[160]

IX. Conclusion

This paper presents a sizing process for the conceptual design of aircraft with electrified propulsion systems. It represents a best effort by the authors to combine traditional handbook design methods with the new aspects of hybrid/electric propulsion reported in academic papers, such as the impact on powertrain sizing and mass estimation. Typical values for key parameters of electrified powertrains are provided, as well as a collection of open-source tools that can be used. Where possible, tips and tricks based on academic or industry experience are presented. The paper is intended for students and engineers starting in the field of electrified aircraft design. A design exercise that follows the presented methods step by step is given in Appendix A as an example. We recommend that the "new designer of electrified aircraft" uses the material presented in this paper to familiarize themselves with the sizing process, and then expand it to accommodate more accurate performance modelling and—especially—better mass estimation methods for their particular application. This will help the designer to explore the design space and develop the next generation of electrified aircraft.

A. Appendix A: Design Example

In this Appendix, we go through a design exercise step by step to put the theory of this paper into practice. The design is based on Ref. [102]: the same TLARs are used, and the design choices or assumptions are reverse-engineered or directly taken from Ref. [102]. For simplicity, we only size the aircraft for the short-range mission on batteries, and do not evaluate the full payload-range envelope. The main steps of the design process are shown in Fig. 1. In this case, we perform a Class I mass estimation, which is used as an initial guess for the Class II mass estimation, to illustrate how both sets of equations can be used. We do not address the detailed geometrical sizing of other components, such as the tail (which requires a CG analysis) or fuselage, and therefore, a simplified drag polar is used, and no outer convergence loop on aerodynamics is required.

The numbers provided in this Appendix were calculated using a Python-based Jupyter Notebook[‡‡‡], which is available open access at: `https://github.com/EAT-AD-TC/ElectricAircraftDesignExample_AIAA2026`.

Problem statement

The engineer is asked to design a 19-passenger aircraft, designated as "E19", that utilizes a hybrid-electric propulsion system to enable zero-emission, fully electric flight with state-of-the-art (2019) technology on shorter routes, while maintaining operational flexibility with a combustion-based gas turbine range extender for IFR reserves and extended-range capabilities. The top-level aircraft requirements are provided in Table 21.

Table 21 E19 Top-Level Aircraft Requirements (TLARs).

Requirement	Value	Rationale/Remark
Certification	Part 23 (commuter)	Standard for aircraft with 19 seats or fewer.
Payload capacity	1,805 kg (3980 lbs)	Based on 19 passengers at 95 kg each (incl. luggage).
Electric range (max PL)	190 km (103 nmi)	Covers ~50% of the current commuter market.
Takeoff field length	1,440 m (4,725 ft)	Matches the performance of the BAe Jetstream 31.
Takeoff/landing altitude	0 m (0 ft)	Assume sea level for simplicity.
Approach speed	56 m/s (109 kts)	Optimized to reduce wing and engine sizing constraints.
IFR reserves	185 km (100 nmi) + 45 min	Serviced via kerosene range extender to preserve battery.
Cruise altitude	3048 m (10,000 ft)	Design choice.
Service ceiling	7,620 m (25,000 ft)	Standard for pressurized regional operation, obtain a similar result for verification purposes.

Step 1: Requirements Analysis

The first step is to look at the top-level aircraft requirements and see whether they are realistic and clearly defined. In this example, we assume the requirements are formulated correctly by the client. The first TLAR, which states that the aircraft shall be certified under FAR Part 23 (similar to EASA CS23), imposes a long list of additional (safety) requirements. Here, for simplicity, we focus on two sets of requirements specified in Part 23. The first are the minimum climb rate and climb gradient requirements, and the second is a maximum take-off mass of 8,618 kg (19,000 lbs), respectively, as specified in Table 22.

Furthermore, Table 21 specifies a minimum range in fully-electric mode at max payload, and IFR reserves to be covered using the fuel-based gas turbine[§§§]. However, the problem statement also specifies that the gas turbine can be used for extended (nominal) range capabilities. Since no additional requirements are given, we assume the harmonic mission (i.e. maximum range at maximum payload) is performed only on batteries, and that payload can be traded against additional fuel mass to increase range. The ferry range (i.e. maximum range at zero payload) is therefore not a TLAR, but an outcome of the design.

[‡‡‡] See `https://jupyter.org/try` to run Jupyter Notebooks in a web browser environment.

[§§§] Using a fuel-based gas turbine to cover reserves is actually already a configuration choice and would in practice not be specified as a requirement by the customer.

Table 22 Derived E19 Top-Level Aircraft Requirements. For Part 23.67 we assume take-off flaps are most favourable.

Requirement	Value	Rationale/Remark
MTOM limit	8,618 kg (19,000 lbs)	Set at the maximum CS-23 limit to allow for high battery mass.
Climb rate	1.52 m/s (300 fpm)	Part 23.65, flaps TO, gear retracted, sea level, AEO.
Climb gradient	4%	Part 23.65, flaps TO, gear retracted, sea level, AEO.
Climb gradient	1.2%	Part 23.67, flaps TO, gear retracted, 5,000 ft, OEI.
Climb gradient	0.6%	Part 23.67, flaps TO, gear retracted, sea level, OEI.
Climb gradient	3.33%	Part 23.77, flaps landing, gear extended, sea level, AEO.
Ferry range	N/A	Ensure sufficient fuel tank volume to trade payload for fuel.

Step 2: Configuration selection
Now that we know what the aircraft needs to do, we first select a set of reference aircraft designed for similar missions, so we can make assumptions for our design based on them. Then, we need to make a decision for each major configuration choice of our aircraft (e.g. high vs. low wing, number of engines, etc.). For simplicity, we only evaluate one aircraft configuration in this exercise. The selected aircraft configuration is a low-wing, conventional-tail aircraft with wing-mounted engines and landing gear. The selected configuration is based on the E-19 aircraft described in [102]. A three-view diagram of the E-19 aircraft taken from [102] is shown in Fig. 13.

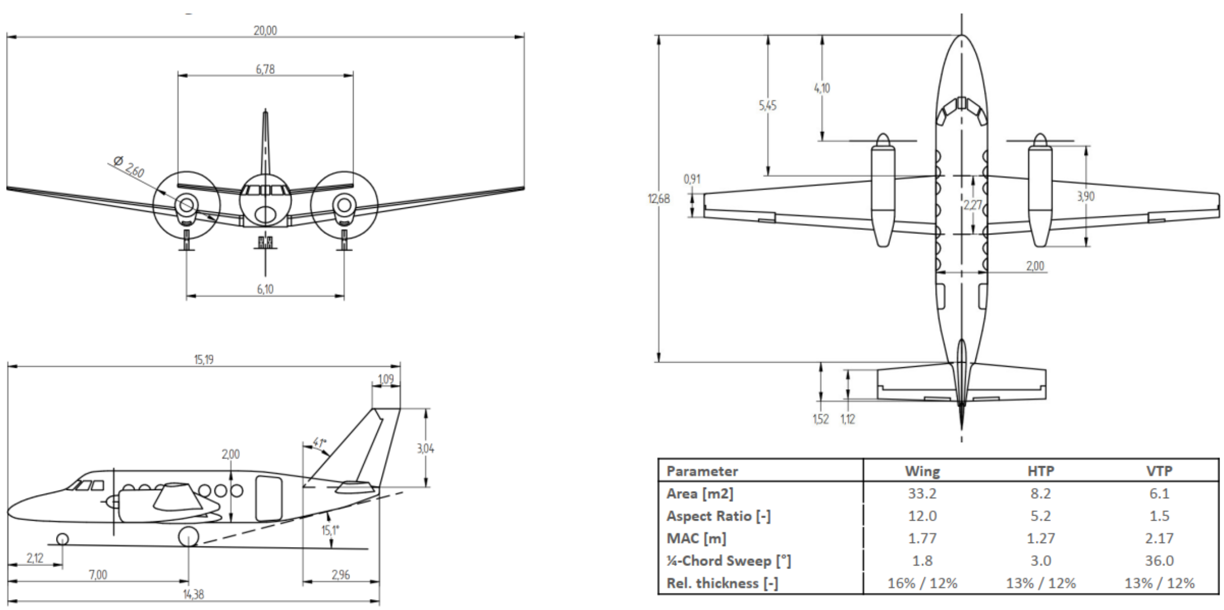

Parameter	Wing	HTP	VTP
Area [m2]	33.2	8.2	6.1
Aspect Ratio [-]	12.0	5.2	1.5
MAC [m]	1.77	1.27	2.17
¼-Chord Sweep [°]	1.8	3.0	36.0
Rel. thickness [-]	16% / 12%	13% / 12%	13% / 12%

Fig. 13 Reference aircraft 3-view diagram from [102]

The design parameters selected for the wing are given in Table 23. The same 3-abreast fuselage geometry as the reference aircraft, based on a Jetstream 31, is assumed. A parallel hybrid powertrain architecture is chosen to enable both fully-electric and fully-fuel-based flight in particular conditions. The components of the electrified powertrain, including batteries, are assumed to be installed inside the nacelles. Additional parameters are given throughout this Appendix when necessary (e.g. for mass estimation).

Table 23 Selected wing configuration parameters.

Parameter	Symbol	Value	Units
Aspect Ratio	A	12	–
Taper Ratio	λ	0.39	–
Half-chord Sweep	$\Lambda_{c/2}$	0	deg
Wing Configuration	–	Low wing	–
Thickness-to-Chord (root)	$(t/c)_{\text{root}}$	0.12	–

Fig. 14 shows the aircraft systems architecture that we select for the E-19 aircraft. For this small aircraft, the flight controls are assumed to be mechanically powered (pilot input), except for the flaps. Here, we assume hydraulically powered flaps (electrical is also an option, but typically heavier), as well as a small hydraulic system for landing gear operation (extension, retraction, steering, and braking). As the BAe JS31, we assume a 1.5 hydraulic system (one regular system plus a reduced emergency system). Typically, this type of hydraulic system also uses lower pressure (2000 psi instead of 3000 psi). As for pneumatics, we assume a pressurized cabin and hence a bleed-driven ECS (taking advantage of the Gas Turbine's presence). Ice protection is chosen as a pneumatic de-icing boot system, minimizing in-flight power demand. Note that we assume that this aircraft does not have an APU, which leads to operational limitations on the ground (i.e. to run the ECS on ground, at least one engine must be running. The masses of these systems will be estimated using the equations given in Table 24.

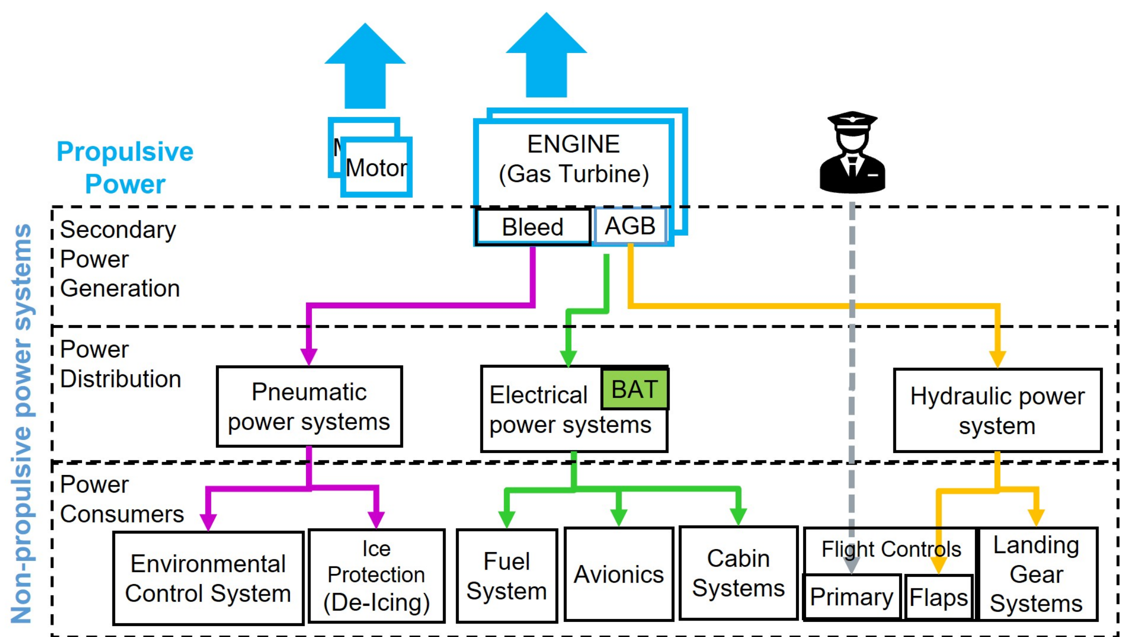

Fig. 14 Baseline systems architecture selected for the E19 design.

Table 24 Resources for system weight estimation for the E19 example

Subsystem	Reference	Suggested adaptations
Hydraulics	FLOPS, Eq. (105) from [145]	Divide by 2 to account for reduced redundancy (1.5 instead of 3 systems).
Landing Gear Systems	Typically included in landing gear structural mass	Not required.
Flight Controls	FLOPS general aviation equation, Eq. (99) from [145]	No adaptation required.
Electrical System	FLOPS, Eq. (106) from [145]	Divide by 2, since the estimated value is too high for a small aircraft.
Avionics	FLOPS, Eq. (108) from [145]	Divide by 2, since the estimated value is too high for a small aircraft.
Cabin Systems	Included in furnishing and equipment mass and estimated using Eq. (110) of [145] or Eq. (16) of [85]	Not required.
Fuel Systems	Eq. (72) from [56]	No adaptation required.
Ice Protection Systems	FLOPS, Eq. (115) from [145]	No adaptation required.
Env. Control System	FLOPS, Eq. (113) from [145]	Typically includes pneumatic power systems.

Step 3: Create aerodynamic polar

For the drag polar, a clean C_{D0} value of 0.020 is selected based on Table 5 for a large turbopropeller aircraft. Similarly, an Oswald efficiency factor of 0.80 is selected for the clean configuration. The C_{D0} and e values will be corrected for different configurations, such as take-off and landing, based on the flap and landing gear positions using delta values from Table 3.6 of Ref. [1]. Finally, the C_L values are taken from the "small twin engine props" section of Table 6. The higher limit of the values provided is selected, and C_D is calculated by applying Eq. 1, i.e, the drag polar equation. No aero-propulsive interaction correction factors are applied in this exercise. A summary of both assumed and computed aerodynamic parameters is shown in Table 25:

Table 25 Summary of aerodynamic parameters.

Parameter	Value	Units	Notes
C_{D0}	0.020	-	Assumed based on Table 5
e	0.80	-	Assumed based on Table 5
$C_{L,\text{max,clean}}$	1.80	-	Assumed based on Table 6
$C_{L,\text{max,TO}}$	2.00	-	Assumed based on Table 6
$C_{L,\text{max,landing}}$	2.50	-	Assumed based on Table 6
$C_{L,\text{cruise}}$	0.77	-	Output: Cruise speed and altitude were adapted to fly near optimum C_L
$C_{D,\text{cruise}}$	0.039	-	Output: Computed with retracted landing flaps and landing-gear configuration

Step 4: Powertrain and wing sizing

Create propulsive power loading diagram ("Aircraft level SMP")

From the TLAR analysis, we identify the following performance requirements: take-off distance, approach speed, cruise altitude, and service ceiling from Table 21, and five climb requirements from Table 22. A constraint analysis is performed using the inputs shown in Table 26. For each constraint, we evaluate the equations provided in Appendix C for each value of wing loading between 0 and 5000 N/m^2. One exception is the approach speed constraint, which is calculated as an upper bound on wing loading. For this, we relate the approach speed to the stall speed of the aircraft (i.e. the speed at which the aircraft flies at $C_{L\max}$) through $V_s = V_{app}/1.3$, since historically Part 23/CS-23 regulations require the approach speed to be at least 1.3 times the stall speed (see e.g. CS23 Amendment 4, 23.73). All constraints are assumed to be performed at maximum throttle, and the W/S and W/P values obtained are normalized to maximum take-off mass. The resulting constraint diagram is shown using the sizing matrix plot in Figure 15.

Table 26 Constraint Analysis Input Parameters

Parameter	Value	Units	Description
Stall speed V_{stall}	43.1	m/s	Approach speed divided by a factor 1.3.
Landing distance	1200	m	Required landing field length.
Takeoff field length	1440	m	Required takeoff field length.
Aircraft type	Twin turboprop	–	Selected aircraft configuration category.
Cruise speed V_{cruise}	82.3	m/s	Aircraft speed during cruise flight condition.
Climb gradient	0.06	–	Required ratio of vertical climb distance to horizontal distance.
Rate of climb	1.52	m/s	Vertical climb velocity requirement.
Sea level density ρ	1.225	kg/m^3	Air density at sea-level standard atmosphere.
Ceiling density $\rho_{ceiling}$	0.549	kg/m^3	Air density at service ceiling altitude.
Cruise density ρ_{cruise}	0.905	kg/m^3	Air density at cruise altitude.
Climb density ρ_{climb}	1.100	kg/m^3	Assumed air density during climb condition.
Propeller efficiency η_p	0.8	–	Assumed for all flight conditions.

Select design point

Figure 15 shows the feasible region bounded by curves corresponding to the constraints listed in Table 22. The OEI constraint at 5000 ft is plotted to outline the power required by the remaining engine and also the combined or installed power required to meet the constraint. The selection of the design point within this space depends on several factors, including the designer's experience. Typically, one selects a point within the feasible region close to the allowable wing loading limit that results in a low power requirement, for example, the top-right corner of the feasible design space. However, this may not always be the case. It is advisable to select several design points, evaluate them and perform trade-offs on MTOM between them. Raymer [2, p. 718] provides additional information on performing these kinds of trade studies. Here, the marked design point in Fig. 15 is selected to match that of the E-19 aircraft derived from the information provided in [102]. Note that the required power computed in Ref. [102] is significantly higher than the limiting value here (i.e. the power loading is *lower* than the limiting value identified here) since they conservatively assume the aircraft must be able to do the whole take-off run with one engine failed. The selected design point is described in Table 27.

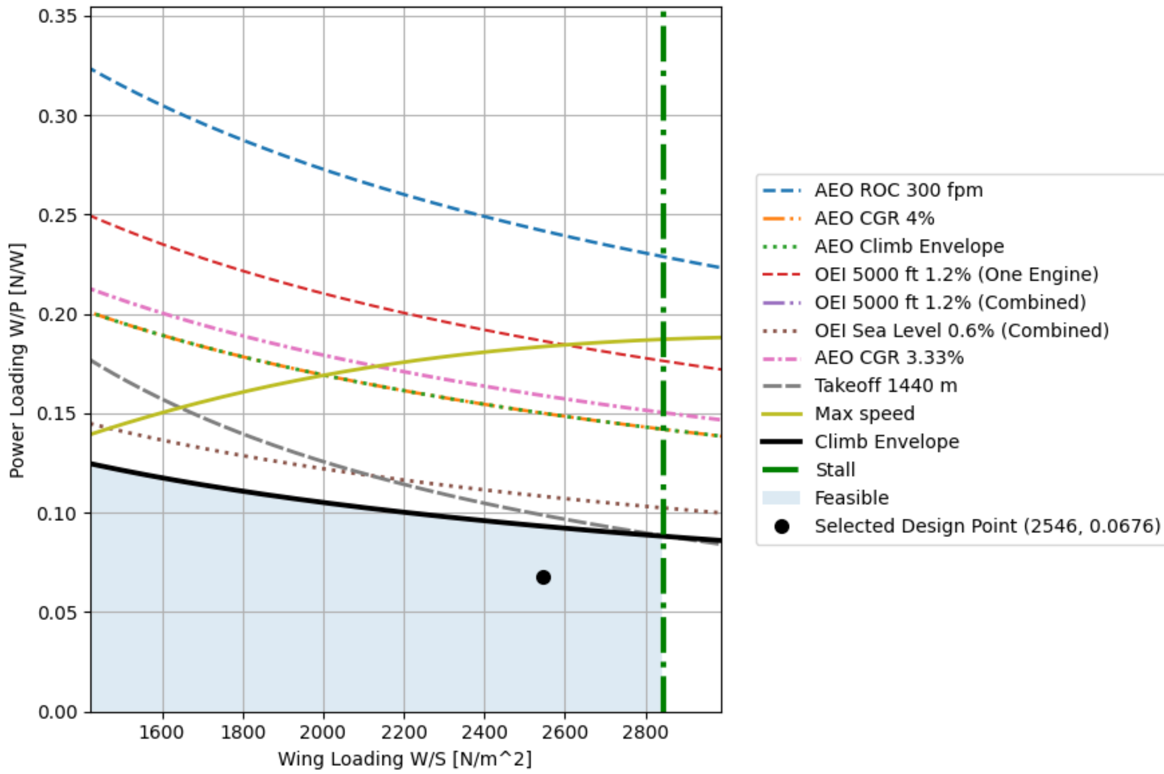

Fig. 15 Sizing Matrix Plot of the E19 aircraft.

Table 27 Constraint Analysis and Selected Design Point

Parameter	Value	Units	Description
Feasible point found	Yes	–	–
Selected wing loading W_{TO}/S	2546	N/m^2	Wing loading selected from the feasible region to match that of the E-19 aircraft.
Selected power loading W_{TO}/P	0.0676	N/W	Power loading selected from the feasible region to match that of the E-19 aircraft.
Derived wing area S_{wing}	33.2	m^2	Wing area computed from selected W/S and MTOM (only available later).
Derived total power	1251	kW	Total installed propulsive power at the selected design point (only available later).

Convert propulsive power to powertrain component power
Next, the propulsive W/P ratio can be used to determine the power requirement for the combined powertrain. Then the equations from Table 7 are applied for a parallel architecture to determine the individual power requirements for each powertrain component. These equations incorporate powertrain component efficiencies to determine the final component power requirement.

In this exercise, the aircraft is sized to cover the 190 km range using electric motors alone, and therefore the power split for the electric motor W/P equation from Table 7 is set to 1. The powertrain is expected to provide a range-extender function powered solely by the gas turbine. For simplicity, we assume that the aircraft flies the range extension at the same cruise speed and altitude as the nominal mission. In that case, the gas turbine (i.e. a turboshaft) can be sized using the cruise W/P at the selected design W/S, correcting for the power lapse. The power requirements for the electric motor and the battery are obtained by applying the equations from Table 7 for $\Phi = 1$ to the chosen design power loading. The assumed component efficiencies used for powertrain sizing are shown in Table 28.

Table 28 **Powertrain sizing parameters.**

Parameter	Value	Units	Description
Thermal engine efficiency η_{te}	0.24	–	Efficiency of the turbine engine.
Motor efficiency η_{em}	0.95	–	Efficiency of the electric motor incl. inverter.
Gearbox efficiency η_{gb}	0.99	–	Mechanical efficiency of the gearbox transmission.
Propeller efficiency η_{p}	0.80	–	Efficiency of converting shaft power into propulsive power.
Hybridization factor Φ (nominal)	1.0	–	Fully-electric nominal mission.
E-motor specific power PD_{motor}	4.94	kW/kg	Assumed motor power density used in mass estimation.
Inverter specific power PD_{inverter}	12	kW/kg	Assumed inverter power density used in mass estimation.

Step 5: Energy estimation (Class I)

Initial guess for MTOM and m_{OE}
The initial MTOM guess is set to 8600 kg, as it is close to mass limit of CS23 given in Table 21. The empty mass (m_{OE}) is then computed using Eq. 53.

Estimate cruise energy
The energy required for the electric cruise phase is computed using Eq. 33 at the cruise L/D of 19.3.

Estimate total energy
On top of the nominal mission cruise energy, we need to add the energy required for non-intensive phases as well as diversion and loiter. In this example, the set of energy allowances taken from [102] and shown in Table 29 have been applied to capture typical energy requirements of non-intensive flight phases, instead of using a lost-range equivalent.

Table 29 Time and energy consumption by flight phase, from Ref. [102].

Segment	Time [min]	Energy [kWh]
Taxi out	3.0	0.8
Take-off	1.1	24.7
Approach & Landing	2.0	6.1
Taxi in	3.0	0.8
Total	9.1	32.4

It is important to ensure that the energy allowances in Table 29 are converted to Joules to size the battery.

Step 6: Class I mass estimation

Battery and fuel mass
The battery mass is calculated using Eq. 73, for which the battery-specific energy is set to an effective value of 160 Wh/kg (from [102]); therefore, no additional knockdown factors related to battery pack capacity are required here. However, in practice, it is recommended to apply appropriate knockdown factors to obtain a more realistic estimate of battery mass. For Eq. 73, the battery specific energy must be converted to J/kg. We assume here that the battery pack can discharge a sufficiently high rate such that the power requirements is not sizing for battery mass. For diversion (185 km) and loiter (45 mins), which are performed using the range extender, Eq. 29 is used to estimate the fuel mass directly assuming a brake-specific fuel consumption of 0.34 kg/kWh is for the turboshaft. This can be related to the energy content of the fuel through its heating value. For these mission segments, the aircraft is assumed to fly at the same lift coefficient, and thus the same L/D, as in cruise.

Convergence loop
Convergence is achieved as follows: First, the initial guess MTOM is used to determine an initial m_{OE}, as indicated in the first line of Table 30. Second, the m_{OE} and payload values are used in the electric Breguet equation with the energy split set to 1 to determine the total energy, as indicated in the previous paragraphs. The total energy is then used to estimate battery mass, and finally, the fuel mass for the range extender is calculated. The m_{OE}, payload mass, fuel mass and battery mass are summed up to obtain an MTOM, which is then fed back into Eq. 53 to determine a new m_{OE}. This process continues until the difference between successive MTOM estimates reduces to below an acceptable value. The results of Class I sizing are shown in Table 31.

Table 30 Class I MTOM convergence history.

Iter	MTOM guess [kg]	OE [kg]	$E_{0,\mathrm{total}}$ [J]	Battery [kg]	MTOM new [kg]	Error [kg]
1	8600	4476	1.024×10^9	2576	9056	456
2	9056	4567	1.039×10^9	2606	9188	132
3	9188	4594	1.043×10^9	2615	9226	38
4	9226	4601	1.045×10^9	2618	9237	11
5	9237	4604	1.045×10^9	2618	9240	3
6	9240	4604	1.045×10^9	2619	9241	1

Table 31 Summary of the converged Class-I design.

Parameter	Value	Units	Notes
MTOM	9240	kg	Final converged Class I maximum takeoff mass.
OE	4604	kg	Final converged operating empty mass.
Battery mass	2619	kg	Final converged battery mass.
Mission $E_{0,\mathrm{total}}$	1.045×10^9	J	Final onboard mission energy.
Mission $E_{0,\mathrm{total}}$	1045	MJ	Final onboard mission energy.
Fuel mass	213	kg	Total fuel mass.
Iterations	6	–	Number of convergence iterations performed.
Final error	0.93	kg	Final MTOM convergence residual.

As seen in Table 31, the converged MTOM is significantly higher than the Part 23 mass limit. The Class I m_{OE} equation appears to over-predict the empty mass, which then leads to a snowball effect on the MTOM. Nonetheless, it is good practice to perform a sanity check at this stage to determine whether the converged MTOM is realistic, an artifact of the mass model used or due to errors in the inputs to the mass estimation equation. If the value is deemed sound, some early trades on MTOM can be executed at this stage. In this exercise, we will proceed to carry out a Class II mass estimate and further evaluate the resulting MTOM.

Step 7: Energy estimation (Class II)
We follow the same steps as in Step 5, but in this case, we use MTOM and OE obtained from the Class I mass breakdown as an initial guess. Additional energy allowances need to be made for power-consuming systems. These power estimates can be determined using the equations listed in Table A1 of [85, p. 25] and converted to Joules based on the total mission time. In practice, at this stage, the designer should consider using time-stepping methods to improve the fidelity of the energy estimate.

Step 8: Class II mass estimation

Battery and fuel mass
Same as in Step 6.

Operating empty mass
Here, the operating empty mass is taken as the sum of airframe, powertrain, and systems masses (including pilots). The airframe mass is estimated using the suite of equations provided in section VI.E for each component of the airframe structure. The parameters in Table 32 are used as inputs to these equations:

Table 32 Class II airframe structure sizing inputs.

Parameter	Value	Units	Description
Number of passengers n_{pax}	19	–	Total passenger capacity.
Number of crew n_{crew}	2	–	Number of flight crew members.
Speed of sound a	340.3	m/s	Assumed speed of sound at reference conditions.
Maximum Mach number	0.24	Maximum aircraft Mach number.	
Engine diameter	0.53	m	Engine diameter based on Honeywell TPE331 data.
Propeller efficiency η_p	0.80	–	Propulsive efficiency of the propeller.
Total efficiency η_{total}	0.19	–	Combined gas turbine, gearbox, and propeller efficiency.
Power specific fuel cons.	0.34	kg/kWh	Fuel consumption per unit shaft power.
Energy allowances	233.28×10^6	J	Additional mission energy for taxi, takeoff, descent, landing, and warmup.
Selected wing loading W/S	2546	N/m^2	Selected wing loading used for sizing.
Aspect ratio A	12	–	Wing aspect ratio.
Taper ratio λ	0.39	–	Ratio of tip chord to root chord.
Root t/c ratio $(t/c)_{\text{root}}$	0.12	–	Wing root thickness-to-chord ratio.
Half-chord sweep angle $\Lambda_{c/2}$	0	deg	Wing half-chord sweep angle.
Ultimate load factor n_{ult}	5.7	–	Ultimate structural load factor.
Aircraft category	Light	–	Aircraft classification used in sizing equations.
Wing-mounted engines	2	–	Number of engines mounted on the wing.
Main gear attached to wing	True	–	Indicates whether landing gear is wing-mounted.
Reference span b_{ref}	1.905	m	Assumed reference span parameter.
Tail weight factor k_{wt}	0.64	–	Empirical tail weight correction factor.
Hor. tail volume coeff. c_{h}	0.90	–	Horizontal tail sizing coefficient.
Ver. tail volume coeff. c_{v}	0.08	–	Vertical tail sizing coefficient.
Fuselage coefficient a_{fus}	0.169	–	Empirical fuselage coefficient from Raymer.
Fuselage coefficient c_{fus}	0.51	–	Empirical fuselage coefficient from Raymer.
Horizontal tail arm fraction	0.52	–	Fraction of fuselage length used for horizontal tail arm.
Vertical tail arm fraction	0.52	–	Fraction of fuselage length used for vertical tail arm.
Fuselage length l_{fus}	18.37	m	Total fuselage length.
Dive speed V_{D}	144.0	m/s	Assumed aircraft dive speed.
Tail arm length l_{t}	9.55	m	Distance between wing and horizontal tail aerodynamic centers.
Fuselage width b_{fus}	2.2	m	Maximum fuselage width.
Fuselage height h_{fus}	2.4	m	Maximum fuselage height.
Gross shell area S_{G}	95.0	m^2	Total fuselage shell area.
Wing-fus. correction factor k_{wf}	0.23	–	Empirical wing-fuselage correction factor.
Pressurized fuselage	True	–	Indicates whether cabin pressurization is included.
Fuselage-mounted engines	False	–	Indicates whether engines are fuselage-mounted.
Main gear attached to fuselage	False	–	Indicates whether landing gear is fuselage-mounted.
Freighter configuration	False	–	Indicates whether aircraft is configured as a freighter.
No gear bay	False	–	Structural configuration assumption.
Wing configuration	Low	–	Low-wing aircraft configuration.
Retractable landing gear	True	–	Indicates retractable landing gear configuration.
Equivalent shaft horsepower	1600	hp	Shaft horsepower used for nacelle sizing.

Parameter	Value	Units	Description
Gear retracts into nacelle	True	–	Indicates whether landing gear retracts into nacelle.
Over-wing exhaust	False	–	Indicates over-wing exhaust configuration.
Nacelle type	Prop	–	Propeller nacelle configuration.
Loiter time	2700	s	Required loiter duration.
Loiter speed	65.84	m/s	Aircraft loiter flight speed.
Total aileron area	2×1.345	m^2	Total estimated aileron area based on DO-228 data.
Total rudder area	1.5	m^2	Estimated rudder area.
Total elevator area	0.30×8.33	m^2	Elevator area estimated as 30% of horizontal tail area.

All powertrain masses are estimated using the equations provided in Section VI.F. The battery cooling and thermal management system mass is estimated first by determining the battery heat load using Eq. 86, followed by Eq. 88. Equation 92 is used to determine the inverter cooling mass, and Eq. 89 is used to calculate the motor cooling mass. For motor and (thermal) engine component masses, we divide the MTOW by the corresponding design power loading (W/P) to obtain the installed power, which is in turn used for the mass estimation. Finally, the systems masses estimated using the equations referenced in Table 24 are tabulated below in Tables 33 and 34. The mass of two pilots has been added as operating items not captured by the FLOPS equations, assuming 90 kg per pilot plus hand luggage.

Table 33 Systems Mass Summary

System	Mass (kg)
Hydraulic	44
FCS	91
ECS	75
Electrical	252
IPS	41
Avionics	124
Instrumentation	57
Total Systems Mass	**684**

Table 34 Additional Systems and Miscellaneous Mass Estimation

Parameter	Value	Units	Description
Galley and Furnishings mass	572	kg	Estimated cabin furnishings and equipment mass.
Operator items mass	180	kg	Estimated operator and operational items mass.

Convergence loop

Convergence is achieved in a similar manner to step 6. The m_{OE} estimated by summing airframe structure, powertrain, and systems masses is added to the battery mass, fuel mass and payload mass to obtain an MTOM. This MTOM is then passed into the battery and powertrain component sizing equations, and the process is repeated until the difference between successive MTOM values is below an acceptable limit. The converged results are shown in Table 35.

Table 35 Class II converged results.

Parameter	Value	Units	Notes
MTOM	8763	kg	Final converged maximum takeoff mass.
Airframe Mass	2486	kg	Final converged airframe mass.
Battery mass	1964	kg	Final converged battery mass.
Mission $E_{0,\text{total}}$	0.700×10^9	J	Final onboard mission energy.
Fuel mass	202	kg	Total mission fuel mass.
Iterations	8	–	Number of convergence iterations performed.
Final error	0.61	kg	Final MTOM convergence residual.
Turboshaft mass	80	kg	Final propulsion-system turboshaft mass.
Propeller mass	65	kg	Final propeller mass estimate.
Fuel system mass	26	kg	Final fuel-system mass estimate.
BTMS* Mass	101	kg	Final BTMS mass estimate.
Inverter Mass	139	kg	Final inverter mass estimate.
Motor Cooling Mass	105	kg	Final motor cooling mass estimate.
Inverter Cooling Mass	13	kg	Final inverter cooling mass estimate.
Motor mass	325	kg	Final electric motor mass estimate.
Motor controller mass	14	kg	Final motor controller mass estimate.
Motor power per motor	803	kW	Final electric motor power rating per motor.
Turboprop power	167	kW	Final turboprop power rating.
Wing mass	889	kg	Structural wing mass estimate.
Tail mass	94	kg	Structural tail mass estimate.
Fuselage mass	985	kg	Structural fuselage mass estimate.
Landing gear mass	387	kg	Landing gear mass estimate.
Nacelle mass	130	kg	Nacelle structural mass estimate.
Fuselage length l_{fus}	17.3	m	Estimated fuselage length.
Horizontal tail arm L_{h}	9.0	m	Distance from wing aerodynamic center to HT.
Vertical tail arm L_{v}	9.0	m	Distance from wing aerodynamic center to VT.
Horizontal tail area S_{h}	5.66	m^2	Horizontal tail reference area.
Vertical tail area S_{v}	6.04	m^2	Vertical tail reference area.
Wing area S	33.77	m^2	Final wing reference area.
Wing span b	20.12	m	Final wing span.
Root chord c_{root}	2.41	m	Wing root chord length.
Tip chord c_{tip}	0.94	m	Wing tip chord length.
Root thickness t_{root}	0.29	m	Wing root thickness.
Mean aerodynamic chord $\bar{c}_{\text{w}}$	1.68	m	Estimated mean aerodynamic chord.
Total tail area S_{tail}	11.70	m^2	Combined horizontal and vertical tail area.

* BTMS = Battery thermal management system

Step 9: Visualize geometry & present results
Table 35 summarizes the results of this sizing activity. The converged MTOM is 1.6% higher than the reference and the MTOM limit for part 23 certification. This is mainly due to a higher m_{OE} compared to the baseline and an additional allowance for operational items. The increased m_{OE} and the allowance for systems' power draw also increase the battery mass, leading to a higher MTOM. In any case, these deviations are relatively small and are considered well within the uncertainty band of the conceptual sizing methods presented in this paper. It is important for the designer to determine a

confidence interval for reporting the results and to evaluate the design with higher-fidelity methods in subsequent design stages to reduce uncertainty.

In this exercise, no sketch of the sized aircraft is made for brevity, since it would look similar to the reference aircraft (which we are replicating) shown in Fig. 13. Visualizing the result or creating an initial CAD model would be a logical next step to start investigating the volumes allocated to the various subsystems of the aircraft. Other logical next steps would include performing sensitivity analyses or trade studies to investigate whether other design choices lead to more optimal solutions.

B. Appendix B: Low-fidelity estimation of maximum lift-to-drag ratio

Early in the sizing process, the Breguet range equation (Sec. V.D.1) may be used to determine the energy required to fly a certain distance. This equation requires an initial estimate of the lift-to-drag ratio. The maximum lift-to-drag ratio in subsonic flight can be estimated with the following equation from Chapter 3 of Ref. [2]:

$$\left(\frac{L}{D}\right)_{\max} = K_{\mathrm{LD}} \cdot \sqrt{\frac{A}{(S_{\mathrm{wet}}/S_{\mathrm{ref}})}}, \tag{94}$$

where A is the wing aspect ratio, $S_{\mathrm{wet}}/S_{\mathrm{ref}}$ is the ratio of wetted area to wing reference area, and K_{LD} is a constant which varies with the aircraft configuration. While the aspect ratio is a design variable that must be selected by the designer, the wetted-area-to-reference-area ratio is dependent on the aircraft geometry and typically ranges from 4 to 8, depending on the size of the wing relative to the other components of the aircraft (fuselage, tail, nacelles, etc.). Additional information is given in Raymer [2], Fig. 3.6. Finally, Table 36 shows typical values of K_{LD} and wetted area ratio. Note that in practice the aircraft often flies at a lower lift-to-drag ratio than the maximum; see e.g. Torenbeek [3], Fig. 5-11.

Aircraft Type	K_{LD}
Civil Jets	15.5
Military Jets	14
Prop Aircraft with Retractable Landing Gear	11
Prop Aircraft with Non-Retractable Landing Gear	9
High Aspect Ratio Aircraft	13
Sailplanes	15

Table 36 Values of K_{LD} for different aircraft types, from Raymer [2], pages 42-43.

C. Appendix C: Examples of Main Performance Constraints in the SMP

This Appendix provides equations to calculate the performance constraints of the SMP for cruise, take-off, stall speed, and rate of climb. Figure 16 shows how these constraints appear in the diagram, and what their sensitivity to main performance assumptions look like.

Stall Speed

A fundamental constraint is the minimum allowable stall speed, V_{s}. This constraint is obtained from the lift equilibrium at stall:

$$\frac{W}{S} = \frac{1}{2}\rho V_s^2 C_{L,\mathrm{max,L}}. \tag{95}$$

where ρ is the air density and $C_{L,\mathrm{max,L}}$ is the maximum lift coefficient in landing configuration[¶¶¶]. This expression defines a vertical constraint in the SMP (see Appendix C), usually independent of propulsion (except in the case of DEP, please see Section V.A.3). As a result, the required wing loading is decoupled from power or thrust sizing. The primary assumption is the value of $C_{L,\mathrm{max,L}}$, which can be estimated based on aircraft type (see Table 6).

[¶¶¶]For passenger aircraft, the stall speed constraint is usually the most critical in landing conditions. Often an *approach speed* requirement is provided instead; in that case, relate the approach speed to the stall speed with $V_{\mathrm{app}} = k \cdot V_{\mathrm{s}}$, where k is a safety margin imposed by the regulations.

Takeoff

The takeoff constraint relates aircraft performance to runway length, often using the takeoff parameter (TOP) in the conceptual design phase. For propeller-driven aircraft, it is defined as:

$$TOP_{\text{prop}} = \frac{(W_{\text{TO}}/S)(W_{\text{TO}}/P_s)}{C_{L_{\text{max,TO}}}} \tag{96}$$

The lift coefficient at liftoff is approximated as:

$$C_{L_{\text{TO}}} = \frac{C_{L,\text{max,TO}}}{1.21}. \tag{97}$$

Please note that the power loading used in Eq. (96) already refers to shaft power, and not the usual propulsive power. The shaft power loading needs to be converted to propulsive power loading to be represented on the SMP. The TOP parameter is empirically related to takeoff distance (ground roll s_{TOG} or total distance s_{TO} in feet) using correlations from [1] or [2]. For example, from [1] we have that for FAR Part 23 aircraft:

$$s_{\text{TOG}} = 4.9\,\text{TOP}_{23} + 0.009\,\text{TOP}_{23}^2 \tag{98}$$

and

$$s_{\text{TO}} = 8.134\,\text{TOP}_{23} + 0.0149\,\text{TOP}_{23}^2 \tag{99}$$

For turbojet or turbofan aircraft, thrust loading (T/W) replaces power loading, and a different definition of TOP must be used. Please refer to Table 9. Also note that Eq. (96) uses the TOP parameter in imperial units (lb^2 ft^{-2} hp^{-1})

Therefore, when converting the computed propulsive power loading in SI units, the appropriate unit conversion factors need to be applied.

Maximum Cruising Speed

The maximum cruising speed constraint is derived from steady level flight equations at a given altitude. For propeller-driven aircraft, it can be expressed as:

$$\frac{W}{P_{\text{p}}} = \frac{1}{\frac{1}{2}\rho V_{\max}^3 C_{D_0}\left(\frac{1}{W/S}\right) + \frac{2K}{\rho V_{\max}}\left(\frac{W}{S}\right)} \tag{100}$$

where $V_{\max}$ is the maximum level-flight speed, C_{D_0} is the parasite drag coefficient, and $K = 1/(\pi e AR)$ is the induced drag factor.

It is important to note that both W/P_{p} and W/S correspond to cruise conditions rather than takeoff. In particular, engine power is reduced relative to sea-level conditions, and aircraft weight is typically lower (often approximated as $0.5 - 0.8 W_{\text{TO}}$ for conventional aircraft). Conversion to equivalent SLS power should be applied as discussed in Section V.B.4 in case the constraint is applied to a thermal component.

Rate of Climb and Ceiling (or Top of Climb)

Rate of climb performance constraints are imposed through a minimum required rate of climb (ROC) at a specified altitude. The maximum rate of climb can be written as:

$$ROC_{\max} = \frac{1}{\frac{W}{P_{\text{p}}}} - \frac{1}{\sqrt{2\rho}}\left(\frac{W}{S}\right)^{1/2}\frac{1}{\frac{C_L^{3/2}}{C_D}}. \tag{101}$$

This expression shows that, for a propeller-driven aircraft, the maximum climb performance is achieved at the condition that maximizes the aerodynamic efficiency term $C_L^{3/2}/C_D$, which occurs at

$$C_{L_{\max\text{ROC}}} = \left(3C_{D_0}\pi A e\right)^{1/2}, \tag{102}$$

with the corresponding drag coefficient

$$C_{D_{\max\text{ROC}}} = 4C_{D_0}. \tag{103}$$

By isolating W/P_{p} on the left-hand side of the equation in Eq. 101, the designer can use this equation to calculate the power loading needed to achieve a given rate of climb at the given wing loading. This can be used for a variety of typical TLARs:

- Absolute ceiling: altitude at which ROC = 0.
- Service ceiling/Top of Climb (TOC): altitude at which a minimum climb rate is maintained (typically 100 ft/min for propeller aircraft or 500 ft/min for jets).
- Climb rate requirements imposed by the safety regulations.
- For requirements that need to be met with one engine inoperative (OEI), the resulting W/P value can be divided by the factor $N/(N-1)$ to "over-size" the powertrain for the case of component failure, where N is the number of engines[17].

In the context of the SMP formulation, the service ceiling (or TOC) constraint plays an important role because it often becomes the most demanding sizing condition for a thermal-based transport aircraft propulsion system. This behaviour is directly linked to the altitude-dependent reduction in available thermal engine power/thrust performance discussed in Section V.B.4.

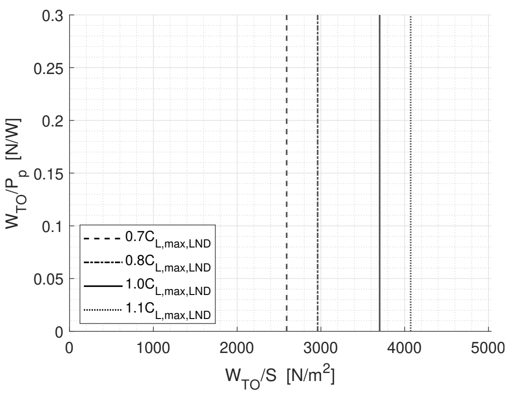

(a) Stall speed constraint.

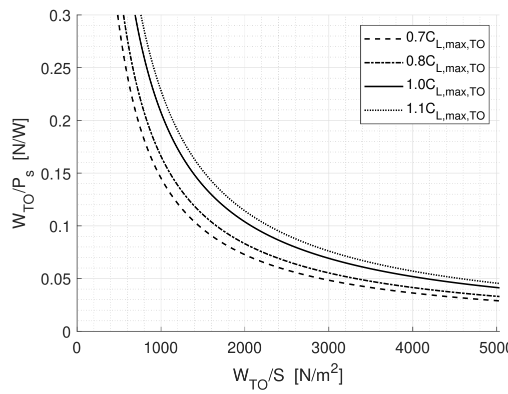

(b) Takeoff constraint.

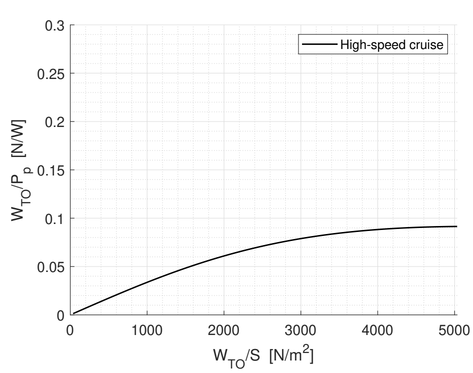

(c) Maximum cruising speed constraint.

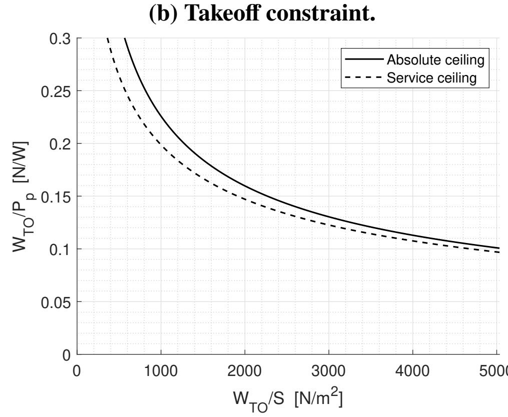

(d) Rate of climb/ceiling constraint.

Fig. 16 Constraints on SMP. Each subfigure illustrates a specific constraint: (a) Stall speed, (b) Takeoff, (c) Maximum cruising speed, and (d) Rate of climb/ceiling.

[17]Assuming the number of propulsors equals the number of electric motors and/or thermal engines. If not, this correction must be done on a per-component basis taking into account the number of instances of that particular component.

D. Appendix D: Additional Properties of Energy Carriers

A. Aviation Fuel Properties

Piston engines typically run on aviation gasoline (avgas), of which the most common grade is 100LL (short for 100 octane, low lead). Gas turbine engines typically run on jet fuel (also called kerosene, aviation turbine fuel, or ATF) [2]. The most common types of jet fuel are Jet-A (used mostly in the US) and Jet-A1 (used in the rest of the world). Jet-B is less common; it is sometimes used in colder climates due to its lower freezing point. Synthetic aviation fuel (SAF) is discussed in subsection B of this appendix. All aviation fuel must meet the relevant ASTM certification standards [161–163]. Fuel properties obtained from these standards are summarized in Table 37.

Table 37 Aviation fuel properties. 1 MBtu = 1,000 Btu (British thermal units).

Fuel	Avgas (100LL)	Jet-A	Jet-A1	Jet-B
Uses	Piston engines	Turbine engines (United States)	Turbine engines (international)	Turbine engines (cold climates)
Certification standard	ASTM D910	ASTM D1655	ASTM D1655	ASTM D6615
Average density at 15°C (59°F)	0.710 kg/L; 5.93 lbs/gal	0.808 kg/L; 6.74 lbs/gal	0.808 kg/L; 6.74 lbs/gal	0.777 kg/L; 6.48 lbs/gal
Density range at 15°C (59°F)	–	0.775–0.840 kg/L; 6.47–7.01 lbs/gal	0.775–0.840 kg/L; 6.47–7.01 lbs/gal	0.751–0.802 kg/L; 6.27–6.69 lbs/gal
Minimum heat of combustion	43.5 MJ/kg; 18.7 MBtu/lb	42.8 MJ/kg; 18.4 MBtu/lb	42.8 MJ/kg; 18.4 MBtu/lb	42.8 MJ/kg; 18.4 MBtu/lb
Maximum freezing point	-58°C; -72.4°F	-40°C; -40.0°F	-47°C; -52.6°F	-50°C; -58.0°F

Jet-fuel density ranges in Table 37 were obtained directly from the certification standards; average densities are the average of the upper and lower limits. However, the standard for aviation gasoline [161] does not give a density range; density is instead reported by the supplier. In lieu of such data, a typical density from Table 10.5 of Raymer [2] is provided in Table 37. Also, tabulated freezing points represent upper limits. Jet-fuel suppliers are permitted by the standards [162, 163] to produce fuel with lower freezing points.

B. Synthetic Aviation Fuel

Synthetic aviation fuel (SAF), also called sustainable aviation fuel, refers to jet fuel produced using processes other than by refining petroleum. While still a hydrocarbon-based fuel, SAF is proposed as a means of reducing aviation's impact on climate change. This is because the carbon in SAF can be obtained from atmospheric carbon dioxide (CO_2, a greenhouse gas), rather than from underground as with petroleum. Therefore, combusting SAF in an engine (releasing CO_2 back into the atmosphere) does not cause a net increase in atmospheric CO_2, since the CO_2 released was obtained from the atmosphere in the first place. Furthermore, SAF is ideally a "drop-in" solution: unlike other proposed energy carriers such as hydrogen, aircraft and engines designed for jet fuel should be able to use SAF with few or (ideally) no modifications. However, SAF is generally both more expensive and less available than petroleum-based jet fuel.

As of this writing, SAF is both an active research area and a subject of regular industrial developments. A full discussion of SAF should include the various pathways for producing it, its properties and how they differ from petroleum-based fuel, production quantities and availability limitations, life-cycle analysis (LCA) for assessing its environmental impacts, including climate and air quality, and techno-economic analysis (TEA) for assessing its cost. Such a discussion is beyond the scope of this paper; references [164–167] are recommended. Instead, a brief summary of the issues directly relevant to aircraft powertrain design is presented here.

SAF falls into two main categories depending on how the carbon is obtained:

- **Biofuels:** the carbon comes from biomass such as waste cooking oil, crops and/or plant residues. These sources in turn obtain their carbon from atmospheric CO_2 via photosynthesis. Biofuels are also called waste-based SAF, biomass-based SAF, or bio-SAF.

- **Power-to-liquid (PtL) fuels**: the carbon comes from industrial processes such as direct air capture (DAC, in which carbon is extracted directly from the atmosphere) or as waste from another process. PtL fuels are also known as electrofuels, e-fuels, or e-SAF.

All SAF must meet ASTM standard D4054 [168] to be certified as jet fuel. Table A4.1 of this standard specifies a density range of 0.730-0.880 kg/L (6.09-7.34 lbs/gal), a wider range than in Table 37 for Jet-A and Jet-A1. Therefore, larger margins for fuel-tank volume (Equation 104) may be necessary. Other properties, such as heat of combustion and freezing point, may also vary from those in Table 37, and should be checked against the specifications for a given SAF.

Aromatics are various organic compounds found in petroleum-based fuel. They are involved in the formation of particulate matter (PM, also called soot) during combustion. PM is involved in the formation of contrails: clouds which sometimes form behind aircraft engines and contribute to climate change. PM also has negative effects on human health. SAF can be produced with little or no aromatics, potentially mitigating both issues. However, running an engine on fuel without aromatics may cause issues with engine seals: aromatics cause the seals to swell; without the aromatics, the seals may fail due to the lack of swelling [167]. For this reason, SAF, as of this writing, can only be used on commercial aircraft if blended up to 50% with petroleum-based jet fuel; 100% SAF in a certified commercial aircraft remains a goal. Therefore, when selecting an engine, it is essential to check its compatibility with the envisaged SAFs.

C. Fuel Volume

Fuel volume is needed to compute fuel-tank volume, which is in turn required to ensure that the fuel tanks are sufficiently large. Therefore, a model for fuel-tank volume is developed in this section. The external volume of a given fuel tank Q_{tank} is estimated using a model adapted from Raymer [2] as

$$Q_{\text{tank}} = K_{\text{tank}} K_{\text{temp}} \frac{m_f}{\rho_f} \tag{104}$$

where m_f is the fuel mass including "trapped fuel" which cannot be accessed during the mission, even for reserves (typically about 6% of accessible fuel). ρ_f is the fuel density (Table 37). The constant $K_{\text{temp}} \sim 1.03$-$1.05$ accounts for the fact that fuel is generally less dense at higher temperatures, requiring a greater tank volume than at 15°C [2]. The constant K_{tank} accounts for the difference between a fuel tank's external and internal volume; it varies depending upon the type of fuel tank[18] and on where the tank is mounted. Values for K_{tank} for integral and bladder tanks calculated from data in Chapter 10 of Raymer [2] are provided in Table 38. For discrete tanks, using $K_{\text{tank}} = 1$ in Equation 104 yields the tank internal volume; adding the tank wall thickness gives the tank external volume.

Tank type	Wing	Fuselage
Discrete	1.00	
Integral	1.18	1.09
Bladder	1.30	1.20

Table 38 Values for the fuel-tank internal volume constant K_{tank}.

D. Battery Volume

In addition to the mass estimation of the battery, volume considerations are important. Unlike fuel, typically stored in conformal wing tanks, battery cells need to be arranged to fit the required number of cells and add overhead for the battery pack and thermal management system. The volume required for batteries can actively determine the size of the fuselage, wing, nacelle, or whatever component they are stored in. Heit and Liscouët-Hanke [62] provide a method for estimating volume build-up. For a first-order estimate, a volumetric efficiency of 0.27 (cell-to-pack) can be assumed. For example, for a Li-Ion cell with a volumetric density of 740 Wh/L, a pack-level energy density of 200 Wh/L must be assumed. Hence, it will be essential to check if enough space is available to install the battery in the aircraft.

[18] Commercial airliners typically use integral fuel tanks, which are created by sealing part of an aircraft's existing structure [2]. Other types of fuel tanks include discrete tanks (in which the fuel tank is built and mounted separately from the aircraft's structure) or bladder tanks (in which a rubber bag is inserted into a space in the aircraft). A single aircraft may have multiple different types of fuel tanks.

E. Appendix E: Generalized Powertrain Sizing

If the designer wants to evaluate more complex powertrain architectures with two types of propulsors, or use a systematic set of equations to relate component powers to propulsive powers, then a matrix-based approach with a more comprehensive parameterization of the powertrain is preferable. In that case, to size each powertrain component:

1) Select the desired powertrain architecture such as all-electric, parallel hybrid, series hybrid, or series–parallel (mixed) hybrid. Sources such as [7, 23] provide a basis for various configurations. Figure 17 illustrates a generic series–parallel hybrid architecture. Components are grouped into "primary" (mechanically coupled to the thermal engine) and "secondary" (serving electrically-driven propulsion). The primary branch comprises the fuel tank (F), thermal engine (TE), gearbox (GB), and the first propulsor (P1), which may be a propeller or a fan. The secondary branch includes the batteries (B), connected to the primary branch via a power management device (PM). The batteries can be recharged by a generator (GEN) coupled to the GB and GT, or can supply power to other electric motors (EM) that spin electrically-driven propulsors (P2). This generic architecture enables the use of a single set of equations to compute component powers, eliminating the need for architecture-specific formulations.

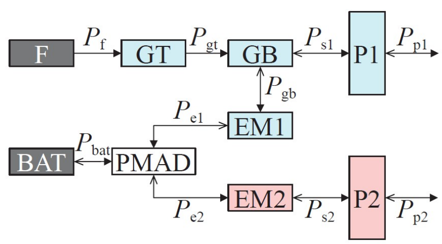

Fig. 17 Serial/Parallel partial hybrid architecture example. Adapted from [23].

2) Identify how power is distributed through the selected architecture for each flight phase and operating mode. Define the source hybridization ratio (or *supplied power ratio*)

$$\Phi = \frac{P_{\mathrm{bat}}}{P_{\mathrm{bat}} + P_{\mathrm{f}}}, \tag{105}$$

where P_{bat} is battery power supplied to propulsion and P_{f} is fuel/engine power.
Define the *shaft power ratio*

$$\varphi = \frac{P_{\mathrm{s2}}}{P_{\mathrm{s2}} + P_{\mathrm{s1}}}, \tag{106}$$

where P_{s1} and P_{s2} are the shaft power contributions for the two propulsors.
Apply Φ and φ consistently across components and branches to map the power paths for each flight phase (takeoff, climb, cruise, etc.) and operating condition (e.g., battery recharge, emergency power). The hybridization schedules $\Phi(t)$ and $\varphi(t)$ may vary over the mission and can be treated as design/optimization variables for component sizing and energy management (e.g., to minimize mass, fuel/energy use, or thermal load subject to power and state-of-charge constraints). However, when evaluating a specific wing-loading/power-loading constraint, hold $\Phi(t)$ and $\varphi(t)$ constant to represent that operating point. You may choose different constant values for different flight phases, but keep them fixed while computing any single constraint.
3) Model efficiency chains: assume conversion/transmission efficiencies η for each component. Efficiencies may vary by flight phase or operating conditions, and these variations must be considered in the modelling, but they can be considered constant during the evaluation of a specific flight phase or of wing loading/power loading constraint. The generic powertrain model described in [23] involves ten unknown power paths, requiring ten equations for a solution. The last three equations are derived from the specified supplied power ratio Φ and shaft

power ratio φ. The full system of equations can be represented as

$$\begin{bmatrix} -\eta_{\mathrm{te}} & 1 & 0 & 0 & 0 & 0 & 0 & 0 & 0 & 0 \\ 0 & -\eta_{\mathrm{gb}} & 1 & 1 & 0 & 0 & 0 & 0 & 0 & 0 \\ 0 & 0 & 0 & -\eta_{\mathrm{p1}} & 0 & 0 & 0 & 0 & 1 & 0 \\ 0 & 0 & -\eta_{\mathrm{em}} & 0 & 1 & 0 & 0 & 0 & 0 & 0 \\ 0 & 0 & 0 & 0 & -\eta_{\mathrm{pm}} & -\eta_{\mathrm{pm}} & 1 & 0 & 0 & 0 \\ 0 & 0 & 0 & 0 & 0 & 0 & -\eta_{\mathrm{gen}} & 1 & 0 & 0 \\ 0 & 0 & 0 & 0 & 0 & 0 & 0 & -\eta_{\mathrm{p2}} & 0 & 1 \\ \Phi & 0 & 0 & 0 & 0 & (\Phi-1) & 0 & 0 & 0 & 0 \\ 0 & 0 & 0 & \varphi & 0 & 0 & 0 & (\varphi-1) & 0 & 0 \\ 0 & 0 & 0 & 0 & 0 & 0 & 0 & 0 & 1 & 1 \end{bmatrix} \cdot \begin{bmatrix} P_{\mathrm{f}} \\ P_{\mathrm{te}} \\ P_{\mathrm{gb}} \\ P_{\mathrm{s1}} \\ P_{\mathrm{e1}} \\ P_{\mathrm{bat}} \\ P_{\mathrm{e2}} \\ P_{\mathrm{s2}} \\ P_{\mathrm{p1}} \\ P_{\mathrm{p2}} \end{bmatrix} = \begin{bmatrix} 0 \\ 0 \\ 0 \\ 0 \\ 0 \\ 0 \\ 0 \\ 0 \\ 0 \\ P_{\mathrm{p}} \end{bmatrix} \tag{107}$$

where $P_{\mathrm{p}} = P_{\mathrm{p1}} + P_{\mathrm{p2}}$ is the total required propulsive power. Throughout the design process, this matrix can be used instead of the equations given in Table 7.

4) Once the total required propulsive power loading W/P_{p} is derived from the SMP, this can be propagated backward to the components that need to be sized, accounting for component efficiencies at each step. For instance from Equation (107), the thermal engine power loading, electric motor power loading and battery would be respectively

$$\frac{W}{P_{\mathrm{te}}} = \left(\eta_{\mathrm{p1}} + \eta_{\mathrm{p2}} \frac{\varphi}{1+\varphi}\right) \eta_{\mathrm{gb}} \frac{W}{P_{\mathrm{p}}} \tag{108}$$

$$\frac{W}{P_{\mathrm{em}}} = \left(\eta_{\mathrm{P1}} \frac{1-\varphi}{\varphi} + \eta_{\mathrm{P2}}\right) \frac{W}{P_{\mathrm{p}}} \tag{109}$$

$$\frac{W}{P_{\mathrm{B}}} = \left(\eta_{\mathrm{P1}} \frac{1-\varphi}{\varphi} + \eta_{\mathrm{P2}}\right) \eta_{\mathrm{PM}} \eta_{\mathrm{EM}} \frac{W}{P_{\mathrm{p}}} \tag{110}$$

5) Construct component-level SMPs, using W/P_{comp} to size each unit.

F. Appendix F: Aircraft Systems Architecture considerations

Table 39 Comparison of Aircraft Systems Architectures for weight estimation, space allocation, and secondary power demand calculation - Power Consuming Systems

System / Aircraft	Small General Aviation	Regional Turboprop	Commercial / Large, High-Speed Business Aircraft
Flight Control System			
Primary flight controls	Often mechanical	Sometimes partly hydraulic, partly mechanical; hydro-mechanical actuation (with or without manual reversion)	Mostly hydraulic (FBW); more-electric actuation possible (EHA or EBHA); no EMA in civil applications
High-lift systems	Simple, mostly single flap; sometimes electrically actuated	Often flaps only; electrically or hydraulically actuated (central power drive)	Slats and flaps; hydraulically or electrically powered (central power unit)
Landing Gear Systems			
Steering	Mechanical or hydraulic	Typically hydraulic	Mostly hydraulic; more-electric actuation possible (EHA or EBHA)
Braking	Hydraulic	Hydraulic	Mostly hydraulic; more-electric actuation possible; some aircraft with electric brakes
Extension/retraction	If retractable landing gear: hydraulic actuation	Hydraulic	Mostly hydraulic; more-electric actuation possible (EHA or EBHA)
Cabin Systems	often minimal; lights	cabin lights, small galley, lavatories	cabin lights, entertainment systems, individual seat power, galleys, lavatories
Avionic Systems	Often minimal and analog;	a significant amount of functionality, often federated architecture (each function as its own avionics box)	even more functionality for long-range aircraft, tendency to have at least partly integrated avionics (so-called integrated modular avionics), saving some boxes and power consumption; might require dedicated avionics ventilation/cooling
Ice protection System	minimal (pitot anti-ice, windshield)	wing: often de-ice system	wing: mostly fully-evaporative anti-ice required
Environmental Control System	cockpit/cabin fan and heater	for pressurized cabin: integrated pressurization and cooling system using an air cycle machine and electrically powered fans	same a regional, additional equipment ventilation needs considered

Table 40 Comparison of Aircraft Systems Architectures for weight estimation, space allocation, and secondary power demand calculation - Power Distribution Systems

System / Aircraft	Small General Aviation	Regional Turboprop	Commercial / Large, High-Speed Business Aircraft
Hydraulic Power Systems	Often minimal; sometimes only for landing gear systems (often lower pressure)	Two or three independent systems, depending on level of hydraulic actuation in primary flight controls; 3000 psig standard	Three independent hydraulic systems (3000 or 5000 psig); reduced or localized hydraulics possible with significant use of EHA/EBHA in primary flight controls (two instead of three systems)
Electrical Power Systems	1 generator per engine (DC), battery for ground; 28VDC network	1 generator per engine (AC or DC), normal and essential bus, can have 115VAC generators and 28VDC for avionics; battery for essential bus, emergency, and auxiliary power generator possible depending on hydraulic/flight control architecture	1-2 generators per engine, normal and essential bus, typically 115VAC generators and 28VDC for avionics; battery for essential bus, emergency, and auxiliary power generator required; high-power DC and dual-channel system for more-electrical architectures; dedicated cooling systems for MEA
Pneumatic Power System	n/a	engine bleed air take off	engine bleed air take off, typically with large pre-cooler in nacelle or pylon

Table 41 Comparison of Aircraft Systems Architectures for weight estimation, space allocation, and secondary power demand calculation - Secondary Power Generation Systems

System / Aircraft	Small General Aviation	Regional Turboprop	Commercial / Large, High-Speed Business Aircraft
Engine-connected secondary power	Small electrical generator (also called alternator) connected to the engine shaft (work for ICE and GTE)	Typically, an engine-mounted accessory gear box (AGB) connecting the electrical generator and hydraulic pump; bleed air off-takes from the engine compressor possible	Typically engine-mounted accessory gear box (AGB) connecting electrical generator and hydraulic pump; bleed air off-takes from the engine compressor using several bleed-ports; only AGB for bleed-less engine
APU	typically, no APU; battery can be used instead for ground power or engine start	APU possible (designer choice, depends on operation), might be a ground-only APU; typically provides electrical power and bleed air	APU for ground and in-flight commonly used; bleed-air supply altitude-limited
Emergency power	Battery	Battery for avionics; if fully powered primary flight control: Ram Air Turbine (RAT) required	Battery for avionics and transient loads; if fully powered primary flight control: Ram Air Turbine (RAT) required

Acknowledgements

This white paper is a non-profit initiative of the AIAA Electrified Aircraft Technologies Technical Committee (EAT TC). The authors would like to thank the other EAT TC members for their support.

References

[1] Roskam, J., *Airplane Design Part I: Preliminary Sizing of Airplanes*, DARcorporation, 1985.

[2] Raymer, D. P., *Aircraft Design: A Conceptual Approach*, seventh ed., American Institute of Aeronautics and Astronautics, Reston, VA, 2024.

[3] Torenbeek, E., *Synthesis of Subsonic Airplane Design*, Delft University Press, 1982.

[4] Torenbeek, E., *Advanced aircraft design: conceptual design, analysis and optimization of subsonic civil airplanes*, John Wiley & Sons, 2013.

[5] Nicolai, L. M., and Carichner, G. E., *Fundamentals of Aircraft and Airship Design - Volume I - Aircraft Design*, AIAA, Reston, VA, USA, 2010.

[6] Gudmundsson, S., *General Aviation Aircraft Design: Applied Methods and Procedures*, Butterworth-Heinemann, Oxford, Great Britain, 2014.

[7] Brelje, B. J., and Martins, J. R. R. A., "Electric, hybrid, and turboelectric fixed-wing aircraft: A review of concepts, models, and design approaches," *Progress in Aerospace Sciences*, Vol. 104, 2019, pp. 1–19. https://doi.org/10.1016/j.paerosci.2018.06.004.

[8] International Civil Aviation Organization, "Annex 14 to the Convention on International Civil Aviation: Aerodromes, Volume I—Aerodrome Design and Operations, Eighth Edition, July 2018," *International Civil Aviation Organization*, Vol. I, No. AN14-1, 2018, pp. 1–14. https://doi.org/https://www.iacm.gov.mz/app/uploads/2018/12/an_14_v1_Aerodromes_8ed._2018_rev.14_01.07.18.pdf.

[9] International Civil Aviation Organization, "Annex 16 to the Convention on International Civil Aviation: Environmental Protection, Volume I—Aircraft Noise, Eighth Edition, July 2017," *International Civil Aviation Organization*, Vol. I, 2017.

[10] Federal Aviation Administration, "14 CFR Part 23: Airworthiness Standards for Normal Category Airplanes," *Code of Federal Regulations, Title 14: Aeronautics and Space*, Vol. Part 23, n.d.. https://doi.org/https://www.ecfr.gov/current/title-14/part-23.

[11] Federal Aviation Administration, "14 CFR Part 25 – Airworthiness Standards: Transport Category Airplanes," , n.d.. URL https://www.law.cornell.edu/cfr/text/14/part-25, accessed: 2026-05-12.

[12] Federal Aviation Administration, "14 CFR § 23.2005 Certification of Normal Category Airplanes," *Code of Federal Regulations, Title 14: Aeronautics and Space*, Vol. Part 23, No. § 23.2005, 2024. https://doi.org/https://www.ecfr.gov/current/title-14/chapter-I/subchapter-C/part-23/section-23.2005.

[13] European Union Aviation Safety Agency, "Special Condition E-19: Electric / Hybrid Propulsion System," Issue 1, 2021.

[14] ANAC-EASA-FAA-TCCA Certification Management Team, "Single Fault Tolerance and LOPC in Electric Engines: Level 1 and 2 Normal-Category Aeroplanes in General Aviation," Certification Management Team Decision Document, October 12 2023.

[15] "SAE AIR7130: Assessment of Electric Engine Failures Leading to LOPC," SAE International, 2024.

[16] "SAE AIR7128: Integration and Certification Considerations for Electrified Propulsion Aircraft," SAE International, 2026.

[17] "SAE ARP8676: Nomenclature and Definitions for Electrified Propulsion Aircraft," SAE International, 2022. https://doi.org/10.4271/ARP8676.

[18] "SAE ARP8678: Architecture Examples for Electrified Propulsion Aircraft," SAE International, 2022. https://doi.org/10.4271/AIR8678.

[19] NASA, "The Lifting Bodies," https://www.nasa.gov/wp-content/uploads/2021/09/171367main_fs-011-dfrc.pdf, 1998. Accessed: 2026-04-07.

[20] Wang, Z., de Breuker, R., Sodja, J., Wolleswinkel, R. E., de Vries, R., and Giuffré, A., "A study on wing structural design and sizing for a large battery-electric aircraft," *AIAA Aviation Forum & ASCEND 2025*, 2025. https://doi.org/10.2514/6.2025-3470.

[21] Reuel, F., van Wensveen, J., Lampl, D., and Weckenmann, T., “Low-Fidelity Aerostructural Wing Sizing for Battery-in-Wing Electric Commuter Aircraft,” *AIAA SCITECH 2026 Forum*, 2026. https://doi.org/10.2514/6.2026-0919.

[22] Schmidt, R. K., *The design of aircraft landing gear*, SAE International, 2021.

[23] de Vries, R., Brown, M., and Vos, R., “Preliminary Sizing Method for Hybrid-Electric Distributed-Propulsion Aircraft,” *Journal of Aircraft*, Vol. 56(6), 2019, pp. 2172–2188. https://doi.org/10.2514/1.C035388.

[24] Obert, E., *Aerodynamic Design of Transport Aircraft*, IOS Press, 2009.

[25] Chapman, J. W., Hasseeb, H., and Schnulo, S., “Thermal Management System Design for Electrified Aircraft Propulsion Concepts,” AIAA Propulsion and Energy 2020 Forum, Virtual Event, August 24-28 2020. https://doi.org/10.2514/6.2020-3571.

[26] ESDU, “Drag and pressure recovery characteristics of auxiliary air inlets at subsonic speeds,” ESDU 86002, 1986.

[27] Sovran, G., and Klomp, E. D., “Experimentally determined optimum geometries for rectilinear diffusers with rectangular, conical or annular cross-section,” *Fluid mechanics of internal flow*, 1967, pp. 270–309.

[28] Giuffré, A., Ascione, F., Colonna, P., and de Servi, C., “Integrated Design Optimization of Environmental Control Systems for Next-Generation Aircraft,” *Journal of Aircraft*, Vol. 62(3), 2025, pp. 498–516. https://doi.org/10.2514/1.C038093.

[29] Nichols, M. R., “Investigation of Flow Through an Intercooler Set at Various Angles to the Supply Duct,” NACA Wartime Report L-408, 1942.

[30] Grey, R. E., and Wilsted, H. D., “Performance of conical jet nozzles in terms of flow and velocity coefficients,” NACA Report 933, 1949.

[31] Wolleswinkel, R. E., de Vries, R., Hoogreef, M. F. M., and Vos, R., “A New Perspective on Battery-Electric Aviation, Part I: Reassessment of Achievable Range,” AIAA Scitech 2024 Forum, Orlando, FL, USA, January 8-12 2024.

[32] Sadraey, M. H., *Aircraft design: A systems engineering approach*, John Wiley & Sons, 2024.

[33] Finger, D. F., “Methodology for multidisciplinary aircraft design under consideration of hybrid-electric propulsion technology,” Phd thesis, RMIT University, Melbourne, Austrailia, 2024.

[34] De Vries, R., Hoogreef, M. F. M., and Vos, R., “Range equation for hybrid-electric aircraft with constant power split,” *Journal of Aircraft*, Vol. 57, No. 3, 2020, pp. 552–557.

[35] Ruijgrok, G. J., Voskuijl, M., and Varriale, C., *Elements of airplane performance*, TU Delft OPEN Publishing, 2025.

[36] Sadraey, M. H., *Aircraft performance: an engineering approach*, CRC Press, 2017.

[37] Lents, C. E., Hardin, L. W., Rheaume, J., and Kohlman, L., “Parallel Hybrid Gas-Electric Geared Turbofan Engine Conceptual Design and Benefits Analysis,” *52nd AIAA/SAE/ASEE Joint Propulsion Conference*, 2016. https://doi.org/10.2514/6.2016-4610, AIAA Paper 2016-4610.

[38] Seitz, A., Nickl, M., Stroh, A., and Vratny, P. C., “Conceptual Study of a Mechanically Integrated Parallel Hybrid Electric Turbofan,” *Proceedings of the Institution of Mechanical Engineers, Part G: Journal of Aerospace Engineering*, Vol. 232, No. 14, 2018, pp. 2688–2712. https://doi.org/10.1177/0954410018790141.

[39] Mokotoff, P. R., Arnson, M., Wang, Y.-C., and Cinar, G., “FAST: A Future Aircraft Sizing Tool for Conventional and Electrified Aircraft Design,” *Journal of Aircraft*, 2025. https://doi.org/10.2514/1.C038452, URL https://doi.org/10.2514/1.C038452, published online 14 October 2025.

[40] Wang, Y.-C., Stockhausen, M., Mokotoff, P. R., Arnson, M., and Cinar, G., “SUbsonic Single Aft eNgine (SUSAN) System Integration Analysis with the Future Aircraft Sizing Tool (FAST),” *AIAA SciTech 2025 Forum*, 2025. https://doi.org/10.2514/6.2025-2376, URL https://doi.org/10.2514/6.2025-2376, AIAA Paper 2025-2376.

[41] Zhao, X., Sahoo, S., Kyprianidis, K. G., Rantzer, J., and Sielemann, M., “Off-design performance analysis of hybridised aircraft gas turbine,” *The Aeronautical Journal*, Vol. 123, No. 1270, 2019, pp. 1999–2018. https://doi.org/10.1017/aer.2019.75, URL https://doi.org/10.1017/aer.2019.75.

[42] Cinar, G., Cai, Y., Bendarkar, M. V., Burrell, A. I., Denney, R. K., and Mavris, D. N., “System Analysis and Design Space Exploration of Regional Aircraft with Electrified Powertrains,” *Journal of Aircraft*, Vol. 60, No. 2, 2023, pp. 382–409. https://doi.org/10.2514/1.C036919, URL https://doi.org/10.2514/1.C036919.

[43] Molloy, A. R., Shekar, S. S., Guidotti, M., and Clarke, M. A., "Electric Aircraft Handling Qualities: Why Battery Positioning Matters," *AIAA SCITECH 2026 Forum*, 2026, p. 2808.

[44] de Vries, R., Wolleswinkel, R. E., Hoogreef, M. F. M., and Vos, R., "A New Perspective on Battery-Electric Aviation, Part II: Conceptual Design of a 90-Seater," AIAA Scitech 2024 Forum, Orlando, FL, USA, January 8-12 2024.

[45] Nguyen Van, E., Alazard, D., Döll, C., and Pastor, P., "Co-design of aircraft vertical tail and control laws with distributed electric propulsion and flight envelop constraints," *CEAS Aeronautical Journal*, Vol. 12, 2021, pp. 101–113. https://doi.org/10.1007/s13272-020-00481-8.

[46] Torenbeek, E., "Cruise performance and range prediction reconsidered," *Progress in Aerospace Sciences*, Vol. 33, No. 5-6, 1997, pp. 285–321.

[47] Arnson, M. G., Cinar, G., Waddington, E., Ansell, P. J., Clarke, M. A., de Vries, R., Salucci, F., Prabhakar, N., Gladin, J. C., Shi, M., et al., "System-level energy pack requirements for sustainable commercial aviation," *AIAA AVIATION FORUM AND ASCEND 2024*, 2024, p. 3828.

[48] Onorato, G., Proesmans, P., and Hoogreef, M. F. M., "Assessment of hydrogen transport aircraft," *CEAS Aeronautical Journal*, Vol. 13, No. 4, 2022, pp. 813–845. https://doi.org/10.1007/s13272-022-00601-6, URL https://doi.org/10.1007/s13272-022-00601-6.

[49] Adler, E. J., and Martins, J. R., "Hydrogen-powered aircraft: Fundamental concepts, key technologies, and environmental impacts," *Progress in Aerospace Sciences*, Vol. 141, 2023, p. 100922. https://doi.org/https://doi.org/10.1016/j.paerosci.2023.100922, URL https://www.sciencedirect.com/science/article/pii/S0376042123000386, special Issue on Green Aviation.

[50] Roskam, J., *Airplane Design Part V: Component Weight Estimation*, Design, Analysis and Research Corporation (DARcorporation), Lawrence, KS, 2003.

[51] Daly, M., *Jane's Aero-Engines: 2019-2020*, IHS Markit, London, UK, 2019.

[52] Filippone, A., *Advanced Aircraft Flight Performance*, Cambridge University Press, New York, NY, 2012.

[53] Hoburg, W., Kirschen, P., and Abbeel, P., "Data fitting with geometric-programming-compatible softmax functions," *Optimization and Engineering*, Vol. 17, 2016, p. 897–918. https://doi.org/10.1007/s11081-016-9332-3.

[54] Budynas, R. G., Nisbett, J. K., et al., *Shigley's mechanical engineering design*, Vol. 9, McGraw-Hill New York, 2011.

[55] Tallerico, T., Sankar, B., Nordeck, A., and Handschuh, R., "Genetic Optimization of Planetary Gearboxes Based on Analytical Gearing Equations," Tech. Rep. NASA/TM–2022-08843, NASA Glenn Research Center, 2022. URL https://ntrs.nasa.gov/api/citations/20220008843/downloads/TM-20220008843.pdf.

[56] Rodriguez, C. D., and Liscouët-Hanke, S., "Weight Estimation and Architecture Definition of Fuel Systems for Aircraft Conceptual Design," *Journal of Aircraft*, Vol. 62, No. 6, 2025, pp. 1620–1629. https://doi.org/10.2514/1.C037723.

[57] Wilson, G., Sahoo, S., Sabharwal, P., and Bindra, H., "Packed Bed Thermal Storage for LWRs," *Storage and Hybridization of Nuclear Energy*, edited by H. Bindra and S. Revankar, Academic Press, 2019. https://doi.org/10.1016/B978-0-12-813975-2.00007-7.

[58] Enersys, "Hawker Aviation Batteries," https://www.enersys.com/en/products/batteries/hawker/hawker-aviation/, Accessed 2024.

[59] Boeing, "Batteries and Advanced Airplanes," , Accessed 2024. URL http://787updates.newairplane.com/787-Electrical-Systems/Batteries-and-Advanced-Airplanes#.

[60] Hepperle, M. J., "Electric Flight - Potential and Limitations," *AVT-209 Workshop on ENERGY EFFICIENT TECHNOLOGIES AND CONCEPTS OPERATION*, 2012.

[61] McDonald, R., "Batteries are not Fuel," , 2023. https://doi.org/10.31224/2803.

[62] Heit, Z., and Liscouët-Hanke, S., "Estimation of Battery Pack Layout and Dimensions for the Conceptual Design of Hybrid-Electric Aircraft," *AIAA SciTech 2023*, AIAA, 2023, pp. 1–13. https://doi.org/10.2514/6.2023-1362.

[63] Beyers, I., Bensmann, A., and Hanke-Rauschenbach, R., "Ragone plots revisited: A review of methodology and application across energy storage technologies," *Journal of Energy Storage*, Vol. 73, 2023, p. 109097. https://doi.org/https://doi.org/10.1016/j.est.2023.109097, URL https://www.sciencedirect.com/science/article/pii/S2352152X23024957.

[64] Marín-Coca, S., Roibás-Millán, E., and Pindado, S., "Analytical modelling and sizing of supercapacitors for spacecraft hybrid energy storage systems," *Acta astronautica*, Vol. 211, 2023, pp. 382–392.

[65] Jansen, R. H., Bowman, C., Jankovsky, A., Dyson, R., and Felder, J. L., "Overview of NASA electrified aircraft propulsion (EAP) research for large subsonic transports," *53rd AIAA/SAE/ASEE Joint Propulsion Conference*, 2017. https://doi.org/10.2514/6.2017-4701.

[66] Zaghari, B., Kiran, A., Sinnige, T., Pontika, E., Enalou, H. B., Kipouros, T., and Laskaridis, P., "The impact of electric machine and propeller coupling design on electrified aircraft noise and performance," *AIAA SciTech 2023 Forum*, 2023, p. 2133.

[67] Golovanov, D., Gerada, D., Sala, G., Degano, M., Trentin, A., Connor, P. H., Xu, Z., La Rocca, A., Galassini, A., Tarisciotti, L., et al., "4-MW class high-power-density generator for future hybrid-electric aircraft," *IEEE Transactions on Transportation Electrification*, Vol. 7, No. 4, 2021, pp. 2952–2964.

[68] Haran, K., Madavan, N., and O'Connell, T. C., *Electrified Aircraft Propulsion: Powering the Future of Air Transportation*, Cambridge university press, 2022.

[69] Zhang, D., He, J., and Pan, D., "A megawatt-scale medium-voltage high-efficiency high power density "SiC+ Si" hybrid three-level ANPC inverter for aircraft hybrid-electric propulsion systems," *IEEE Transactions on Industry Applications*, Vol. 55, No. 6, 2019, pp. 5971–5980.

[70] Erickson, R. W., and Maksimovic, D., *Fundamentals of power electronics*, Springer Science & Business Media, 2007.

[71] Mohan, N., Undeland, T. M., and Robbins, W. P., *Power electronics: converters, applications, and design*, John wiley & sons, 2003.

[72] Jiang, J., Li, Z., Li, W., Ranjan, P., Wei, X., Zhang, X., and Zhang, C., "A review on insulation challenges towards electrification of aircraft," *High Voltage*, Vol. 8, No. 2, 2023, pp. 209–230.

[73] Naderi, A., Keilmann, R., Asgari, A., Mehraban, A., Mallwitz, R., Henke, M., and Terörde, M., "System-Wide Analysis of Electric Power System for a Reference Short-Range Electrified Aircraft," *IEEE Access*, 2025.

[74] Thue, W. A., *Electrical power cable engineering*, Crc Press, 2017.

[75] Azizi, A., and Ghassemi, M., "An analysis of parameters affecting ampacity in aircraft bipolar MVDC power cables via coupled electrical, thermal, and computational fluid dynamic modelling," *High Voltage*, Vol. 9, No. 6, 2024, pp. 1208–1220.

[76] Pastra, C. L., Cai, Y., Kenny, J. D., Balkas, E., and Mavris, D. N., "Modeling and Vehicle-Level Assessment of Thermal Management System for Hybrid Electric Regional Turboprop Aircraft," *AIAA SCITECH 2026 Forum*, 2026. https://doi.org/10.2514/6.2026-2130.

[77] Balkas, E., Kenny, J. D., Pastra, C. L., Cai, Y., and Mavris, D. N., "Modeling and Aircraft-Level Assessment of Thermal Management System for Battery Hybrid Electric Commercial Transport," *2025 IEEE/AIAA Transportation Electrification Conference and Electric Aircraft Technologies Symposium (ITEC+EATS)*, 2025. https://doi.org/10.1109/ITEC63604.2025.11097993.

[78] Shekar, S. S., and Clarke, M. A., "Design and in-flight analysis of an electric aircraft's battery thermal management system," *2024 IEEE Transportation Electrification Conference and Expo (ITEC)*, IEEE, 2024, pp. 1–8.

[79] Chapman, J. W., Hasseeb, H., and Schnulo, S., "Thermal management system design for electrified aircraft propulsion concepts," *2020 AIAA/IEEE Electric Aircraft Technologies Symposium (EATS)*, IEEE, 2020, pp. 1–23.

[80] Gratton, G., Delaney, T., Zaghari, B., and Kendall, G., "Take-off performance of a single engine battery-electric aeroplane," *The Aeronautical Journal*, Vol. 128, No. 1330, 2024, pp. 2781–2798.

[81] Carneiro, M. V. P., Cavicchioli, P., Tavares, M., Rolón, D. A., Oberschmidt, D., and Barbosa Jr, J. R., "Comparing spray and microchannel as evaporators of a compact refrigeration system for electronics cooling," *Applied Thermal Engineering*, 2025, p. 128526.

[82] Link, A., Staggat, M., and de Graaf, S., "Characterisation of thermal management system specific heat rejection for electric propulsion architectures," *Aerospace Europe Conference 2023–10th EUCASS–9th CEAS*, 2023.

[83] Asli, M., König, P., Sharma, D., Pontika, E., Huete, J., Konda, K. R., Mathiazhagan, A., Xie, T., Höschler, K., and Laskaridis, P., "Thermal management challenges in hybrid-electric propulsion aircraft," *Progress in Aerospace Sciences*, Vol. 144, 2024, p. 100967.

[84] Wells, D. P., Horvath, B. L., and McCullers, L. A., "The Flight Optimization System Weight Estimation Method," Technical Memorandum NASA TM-2017-219627 / Vol 1, National Aeronautics and Space Administration, 2017. URL https://ntrs.nasa.gov/citations/20170005851.

[85] Mohan, V., Jeyaraj, A. K., and Liscouët-Hanke, S., "Systems Integration Framework for Hybrid-Electric Commuter and Regional Aircraft," *Aerospace*, Vol. 10, No. 6, 2023, p. 533. https://doi.org/10.3390/aerospace10060533, URL https://www.mdpi.com/2226-4310/10/6/533.

[86] Lampl, T. S., "Integrated Design of Advanced Flight Control Configurations and System Architectures," Ph.D. thesis, Technische Universität München, 2021. URL https://mediatum.ub.tum.de/1580094.

[87] Bauer, C., Lagadec, K., Bès, C., and Mongeau, M., "Flight Control System Architecture Optimization for Fly-By-Wire Airliners," *Journal of Guidance, Control, and Dynamics*, Vol. 30, No. 4, 2007, pp. 1023–1029. https://doi.org/10.2514/1.26311, URL https://arc.aiaa.org/doi/10.2514/1.26311.

[88] Jeyaraj, A. K., "A Safety-Focused Systems Architecting Framework for Aircraft Conceptual Design," Ph.D. thesis, Concordia University, January 2025. URL https://spectrum.library.concordia.ca/id/eprint/995552/.

[89] Rodriguez, C. D., "An Architecture-Based Weight Estimation Method for Aircraft Fuel Systems," Master's thesis, Concordia University, August 2022. URL https://spectrum.library.concordia.ca/id/eprint/991221/, unpublished master's thesis.

[90] Liscouët-Hanke, S., "A Model-Based Methodology for Integrated Preliminary Sizing and Analysis of Aircraft Power System Architectures," Ph.D. thesis, Université Toulouse III - Paul Sabatier, 2008. Accessed: 2025-11-04.

[91] Chakraborty, I., "Subsystem Architecture Sizing and Analysis for Aircraft Conceptual Design," Ph.D. thesis, Georgia Institute of Technology, Atlanta, GA, USA, 2015. URL https://repository.gatech.edu/server/api/core/bitstreams/1268cd5b-0a8a-4d32-8293-1c6a3bff1e10/content, accessed: 2025-11-04.

[92] Liscouët-Hanke, S., and Huynh, K., "A Methodology for Systems Integration in Aircraft Conceptual Design – Estimation of Required Space," *SAE 2013 AeroTech Congress & Exhibition*, SAE International, 2013. https://doi.org/10.4271/2013-01-2235, paper 2013-01-2235.

[93] Vézina, J., and Liscouët-Hanke, S., "Initial Systems Layout and Safety Analysis for the Flying-V Aircraft," *2025 AIAA Regional Student Conferences*, American Institute of Aeronautics and Astronautics (AIAA), 2025. https://doi.org/10.2514/6.2025-98122, URL https://arc.aiaa.org/doi/abs/10.2514/6.2025-98122, accessed: 2025-11-04.

[94] Bamrah, P., "Zonal Safety and Particular Risk Analysis for Early Aircraft Design Using Parametric Geometric Modelling," Master's thesis, Concordia University, July 2023. URL https://spectrum.library.concordia.ca/id/eprint/992615/, unpublished master's thesis.

[95] Sobieszczanski-Sobieski, J., Morris, A., and Van Tooren, M., *Multidisciplinary design optimization supported by knowledge based engineering*, John Wiley & Sons, 2015.

[96] Martins, J. R., and Ning, A., *Engineering design optimization*, Cambridge University Press, 2021.

[97] Kaneko, S., Arnson, M. G., Hajdik, H., Cinar, G., Martins, J., and Uranga, A., "Gradient-Based MDAO Framework for Advanced Aircraft Concepts," *AIAA SCITECH 2026 Forum*, 2026, p. 1302.

[98] Kumar, P., Al-Nadawi, Y. K., and Ilak, M., "Fast real-time power splitting for hybrid electric propulsion using neural network based approximate model predictive control," *AIAA SCITECH 2024 Forum*, 2024. https://doi.org/10.2514/6.2024-2357.

[99] Doff-Sotta, M., Cannon, M., and Bacic, M., "Predictive Energy Management for Hybrid Electric Aircraft Propulsion Systems," *IEEE Transactions on Control Systems Technology*, 2023. https://doi.org/10.1109/TCST.2022.3193295.

[100] Cassidy, E., Liu, Y., Kirsch, K., Li, M. Z., and Cinar, G., "Energy and Power Management Optimization for Sequential Daily Operations in Regional Hybrid-Electric Aircraft," *2025 IEEE/AIAA Transportation Electrification Conference and Electric Aircraft Technologies Symposium (ITEC+EATS)*, 2025. https://doi.org/10.1109/ITEC63604.2025.11098014.

[101] de Vries, R., Wolleswinkel, R. E., Exalto, J. E., van den Berg, P., Vos, R., and Hoogreef, M. F. M., "Conceptual Redesign of a 90-Seater Battery-Electric Aircraft," AIAA AVIATION FORUM AND ASCEND 2025, Las Vegas, NV, USA, July 21-25 2025. https://doi.org/10.2514/6.2025-3153.

[102] Atanasov, G., van Wensveen, J., Peter, F., and Zill, T., "Electric Commuter Transport Concept Enabled by Combustion Engine Range Extender," Paper 490245, Deutscher Luft- und Raumfahrtkongress DLRK 2019, Darmstadt, Germany, September 30 - October 2 2019.

[103] Voskuijl, M., van Bogaert, J., and Rao, A. G., "Analysis and design of hybrid electric regional turboprop aircraft," *CEAS Aeronautical Journal*, Vol. 9, 2018, pp. 15–25. https://doi.org/10.1007/s13272-017-0272-1, URL https://doi.org/10.1007/s13272-017-0272-1.

[104] Cinar, G., Cai, Y., Denney, R. K., and Mavris, D. N., "Modeling and Simulation of a Parallel Hybrid Electric Regional Aircraft for the Electrified Powertrain Flight Demonstration (EPFD) Program," *2022 IEEE/AIAA Transportation Electrification Conference and Electric Aircraft Technologies Symposium (ITEC+EATS)*, 2022. https://doi.org/10.1109/ITEC53557.2022.9813832, URL https://doi.org/10.1109/ITEC53557.2022.9813832.

[105] Friedrich, C., and Robertson, P. A., "Hybrid-Electric Propulsion for Aircraft," *Journal of Aircraft*, Vol. 52, No. 1, 2015, pp. 176–189. https://doi.org/10.2514/1.C032660.

[106] Bonnin, V. O., and Hoogreef, M. F. M., "Exploration of Off-Design Performance for Hybrid Electric Regional Aircraft," *Journal of Aircraft*, Vol. 62, No. 4, 2025, pp. 876–895. https://doi.org/10.2514/1.C037893.

[107] Jansen, R. H., Brown, G. V., Felder, J. L., and Duffy, K. P., "Turboelectric Aircraft Drive Key Performance Parameters and Functional Requirements," *AIAA Propulsion and Energy Forum*, 2015. https://doi.org/10.2514/6.2015-3890, AIAA Paper 2015-3890.

[108] Jansen, R. H., Duffy, K. P., and Brown, G. V., "Partially Turboelectric Aircraft Drive Key Performance Parameters," *53rd AIAA/SAE/ASEE Joint Propulsion Conference*, 2017. https://doi.org/10.2514/6.2017-4702, AIAA Paper 2017-4702.

[109] Mokotoff, P. R., and Cinar, G., "A graph-based framework for advanced aircraft propulsion system analysis," *Aerospace Science and Technology*, Vol. 168, 2026, p. 110798. https://doi.org/10.1016/j.ast.2025.110798, URL https://doi.org/10.1016/j.ast.2025.110798.

[110] Bertrand, P., Spierling, T., and Lents, C. E., "Parallel Hybrid Propulsion System for a Regional Turboprop: Conceptual Design and Benefits Analysis," *AIAA Propulsion and Energy 2019 Forum*, 2019. https://doi.org/10.2514/6.2019-4466, AIAA Paper 2019-4466.

[111] Cinar, G., Cai, Y., Chakraborty, I., and Mavris, D. N., "Sizing and Optimization of Novel General Aviation Vehicles and Propulsion System Architectures," *2018 Aviation Technology, Integration, and Operations Conference*, 2018. https://doi.org/10.2514/6.2018-3974, URL https://doi.org/10.2514/6.2018-3974, AIAA Paper 2018-3974.

[112] Department of Defense, High Performance Computing Modernization Program, "CREATE: Computational Research and Engineering Acquisition Tools and Environments," https://centers.hpc.mil/CREATE/products.html, n.d. Accessed: 2025-11-13.

[113] NASA, "X-57 Technical Papers," https://www.nasa.gov/directorates/armd/x-57-technical-papers/, n.d.. Accessed: 2025-11-13.

[114] Airbus A^3, "Vahana Configuration Trade Study," https://acubed.airbus.com/blog/vahana/vahana-configuration-trade-study-part-ii/, n.d. Accessed: 2025-11-13.

[115] NASA Ames Research Center, "NASA Design and Analysis of Rotorcraft," https://software.nasa.gov/software/ARC-16265-1, n.d. Accessed: 2025-11-13.

[116] NASA, "Aviary: Multidisciplinary Aircraft Design Framework," https://github.com/OpenMDAO/Aviary, n.d.. Accessed: 2025-11-13.

[117] The Regents of the University of Michigan, The Integrated Design of Efficient Aerospace Systems Laboratory, "FAST: Future Aircraft Sizing Tool," https://github.com/ideas-um/FAST, 2026. GitHub repository, README last updated 2026-01-20. Accessed: 2026-04-11.

[118] Stanford University Aerospace Design Laboratory, "SUAVE: Open-Source Aircraft Design Environment," https://suave.stanford.edu/, n.d. Accessed: 2025-11-13.

[119] LEADS Research Group, "RCAIDE: Research Community Aircraft Interdisciplinary Design Environment," https://github.com/leadsgroup/RCAIDE_LEADS, n.d. Accessed: 2025-11-13.

[120] Clarke, M. A., Guidotti, M., Shekar, S., Molloy, A., Boggan, C., and Guerrero, Y. N., "RCAIDE: A Multidisciplinary Analysis Toolbox for Aircraft Design and Flight Simulation," *Aerospace Science and Technology*, 2026, p. 112328.

[121] de Vries, R., "Hybrid Electric Aircraft Sizing Tool," https://gitlab.tudelft.nl/reynardvries/heast, 2024.

[122] Saves, P., Lafage, R., Bartoli, N., Diouane, Y., Bussemaker, J., Lefebvre, T., Hwang, J. T., Morlier, J., and Martins, J. R. R. A., "SMT 2.0: A Surrogate Modeling Toolbox with a focus on Hierarchical and Mixed Variables Gaussian Processes," *Advances in Engineering Sofware*, Vol. 188, 2024, p. 103571. https://doi.org/https://doi.org/10.1016/j.advengsoft.2023.103571.

[123] NASA, "OpenMDAO," https://software.nasa.gov/software/LEW-18550-1, n.d.. Accessed: 2025-11-13.

[124] Adams, B. M., Bohnhoff, W. J., Bolstad, M. B., Dalbey, K. R., Ebeida, M. S., Eddy, J. P., Eldred, M. S., Hooper, R. W., Hough, P. D., Hu, K. T., Jakeman, J. D., Khalil, M., Maupin, K. A., Monschke, J. A., Prudencio, E. E., Ridgway, E. M., Rizzi, F., Robbe, P., Rushdi, A. A., Seidl, D. T., Stephens, J. A., Swiler, L. P., and Winokur, J. G., "Dakota 6.23.0 documentation," http://snl-dakota.github.io, 2025. Technical Report SAND2025-14179O Sandia National Laboratories.

[125] Blender Foundation, "Blender," https://www.blender.org/, n.d. Accessed: 2025-11-13.

[126] MIT Aerospace Computational Design Laboratory, "Engineering Sketch Pad (ESP)," https://acdl.mit.edu/ESP/, n.d. Accessed: 2025-11-13.

[127] FreeCAD Community, "FreeCAD," https://www.freecad.org/, n.d. Accessed: 2025-11-13.

[128] NASA, "GASP Python: Geometry and Simulation Processor in Python," Tech. rep., NASA Technical Reports Server (NTRS), n.d.. Accessed: 2025-11-13.

[129] NASA, "OpenVSP: Vehicle Sketch Pad," https://openvsp.org/, n.d.. Accessed: 2025-11-13.

[130] NASA, "VSPaero," https://www.nasa.gov/reference/openvsp-vspaero-basics/, n.d..

[131] Mark Drela and Harold Youngren, "XFOIL Subsonic Airfoil Development System," https://web.mit.edu/drela/Public/web/xfoil/, n.d.

[132] XFLR5 Development Team, "XFLR5," https://www.xflr5.tech/, n.d. Accessed: 2025-11-13.

[133] SU2 Development Team, "SU2: Open-Source CFD Code," https://su2code.github.io/, n.d. Accessed: 2025-11-13.

[134] OpenFOAM Foundation, "OpenFOAM," https://www.openfoam.com/, n.d. Accessed: 2025-11-13.

[135] U.S. Air Force, "Digital DATCOM," https://www.pdas.com/datcom.html, n.d. Accessed: 2025-11-13.

[136] Mark Drela, "Athena Vortex Lattice (AVL)," https://web.mit.edu/drela/Public/web/avl/, n.d.. Accessed: 2025-11-13.

[137] Jasa, J. P., Hwang, J. T., and Martins, J. R. R. A., "Open-source coupled aerostructural optimization using Python," *Structural and Multidisciplinary Optimization*, Vol. 57, No. 4, 2018, pp. 1815–1827. https://doi.org/10.1007/s00158-018-1912-8, URL https://mdolab-openaerostruct.readthedocs-hosted.com/en/latest/#.

[138] Ricci, S., "NeoCASS," , n.d. URL https://www.neocass.org/.

[139] NASA, "PyCycle," https://software.nasa.gov/software/LEW-19288-1, n.d.. Accessed: 2025-11-13.

[140] Visser, W., and Kogenhop, O., "GSPy," , 2026. URL https://github.com/wvisser1958/GSPy.git.

[141] NASA, "T-MATS: Toolbox for the Modeling and Analysis of Thermodynamic Systems ," https://github.com/nasa/T-MATS, 2025.

[142] NASA, "AGTF30-e: Advanced Geared Turbofan 30,000lbf - electrified," https://github.com/nasa/AGTF30-e, 2024.

[143] ESOTEC, "CROTOR," http://www.esotec.org/sw/crotor.html, n.d. Accessed: 2025-11-13.

[144] Mark Drela, "XROTOR," https://web.mit.edu/drela/Public/web/xrotor/, n.d.. Accessed: 2025-11-13.

[145] NASA, "FLOPS: Flight Optimization System," https://software.nasa.gov/software/LAR-18934-1, n.d.. Accessed: 2025-11-13.

[146] Falck, R., Gray, J. S., Ponnapalli, K., and Wright, T., "dymos: A Python package for optimal control of multidisciplinary systems," *Journal of Open Source Software*, Vol. 6, No. 59, 2021, p. 2809. https://doi.org/10.21105/joss.02809, URL https://doi.org/10.21105/joss.02809.

[147] The Boeing Company, "CASCADE," https://app.cascade.boeing.com/, n.d. Accessed: 2025-11-13.

[148] Völk, S., Yamashita, H., Megill, L., Dahlmann, K., and Grewe, V., "OpenAirClim," , Mar. 2026. https://doi.org/10.5281/zenodo.19110811, URL https://doi.org/10.5281/zenodo.19110811.

[149] MIT Laboratory for Aviation and the Environment, "Aviation Emissions Inventory Tools," https://lae.mit.edu/resources/codes/, n.d. Accessed: 2025-11-13.

[150] Espinosa-Juárez, E., Jouannet, C., Amadori, K., and Sánchez-Mata, A., "Comparative Analysis on Aircraft Direct Operating Cost Models," *AIAA Aviation Forum & ASCEND 2025*, 2025. https://doi.org/10.2514/6.2025-3499, URL https://doi.org/10.2514/6.2025-3499.

[151] Michael S. Selig, "UIUC Airfoil Coordinates Database," https://m-selig.ae.illinois.edu/ads/coord_database.html, n.d. Accessed: 2025-11-13.

[152] Public Domain Aeronautical Software, "PDAS: Public Domain Aeronautical Software," https://www.pdas.com/, n.d. Accessed: 2025-11-13.

[153] AirfoilTools.com, "AirfoilTools," http://airfoiltools.com/, n.d. Accessed: 2025-11-13.

[154] U.S. Department of Transportation, "U.S. Department of Transportation Data Hub," https://data.transportation.gov/, n.d. Accessed: 2025-11-13.

[155] OpenFlights, "OpenFlights Data," https://openflights.org/data, n.d. Accessed: 2025-11-13.

[156] OurAirports, "OurAirports Data," https://ourairports.com/data/, n.d. Accessed: 2025-11-13.

[157] Commission, E., "European Union Statistical Office," https://ec.europa.eu/eurostat, n.d. Accessed: 2026-05-08.

[158] German Aerospace Center (DLR), "CPACS: Common Parametric Aircraft Configuration Schema," https://dlr-sl.github.io/cpacs-website/, n.d. Accessed: 2025-11-13.

[159] Bruggeman, A. M. R. M., La Rocca, G., and Hoogreef, M. F. M., "Dynamic multidisciplinary design analysis and optimization workflows: Concept and implementation," *Aerospace Science and Technology*, Vol. 175, 2026, p. 111748. https://doi.org/10.1016/j.ast.2026.111748, URL https://www.sciencedirect.com/science/article/pii/S127096382600129X.

[160] van Gent, I., La Rocca, G., and Hoogreef, M. F. M., "CMDOWS: a proposed new standard to store and exchange MDO systems," *CEAS Aeronautical Journal*, Vol. 9, No. 4, 2018, pp. 607–627. https://gitlab.tudelft.nl/lr-fpp-mdo/cmdows.

[161] "ASTM D910: Standard Specification for Aviation Gasolines," ASTM International, 2024. https://doi.org/10.1520/D0910-21.

[162] "ASTM D1655: Standard Specification for Aviation Turbine Fuels," ASTM International, 2023. https://doi.org/10.1520/D1655-22A.

[163] "ASTM D6615: Standard Specification for Jet B Wide-Cut Aviation Turbine Fuel," ASTM International, 2025. https://doi.org/10.1520/D6615-22.

[164] Holladay, J., Abdullah, Z., and Heyne, J., "Sustainable Aviation Fuel: Review of Technical Pathways," Tech. Rep. DOE/EE-2041, U.S. Department of Energy, Office of Energy Efficiency and Renewable Energy, Bioenergy Technologies Office, Washington, DC, 2020. https://doi.org/10.2172/1660415.

[165] Bergero, C., Gosnell, G., Gielen, D., Kang, S., Bazilian, M., and Davis, S. J., "Pathways to net-zero emissions from aviation," *Nature Sustainability*, Vol. 6, No. 4, 2023, pp. 404–414. https://doi.org/10.1038/s41893-022-01046-9.

[166] Ueckerdt, F., Bauer, C., Dirnaichner, A., Everall, J., Sacchi, R., and Luderer, G., "Potential and risks of hydrogen-based e-fuels in climate change mitigation," *Nature Climate Change*, Vol. 11, No. 5, 2021, pp. 384–393. https://doi.org/10.1038/s41558-021-01032-7.

[167] Undavalli, V. K., Gbadamosi Olatunde, O. B., Boylu, R., Wei, C., Haeker, J., Hamilton, J., and Khandelwal, B., "Recent advancements in sustainable aviation fuels," *Progress in Aerospace Sciences*, Vol. 136, 2023, p. 100876. https://doi.org/10.1016/j.paerosci.2022.100876.

[168] "ASTM D4054: Standard Practice for Evaluation of New Aviation Turbine Fuels and Fuel Additives," ASTM International, 2023. https://doi.org/10.1520/D4054-22.